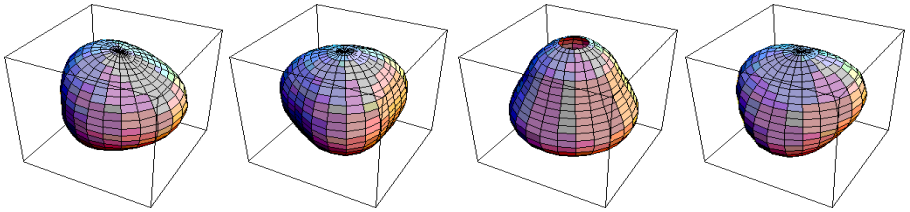

Non-radial pulsations in Be stars. Preparation of the COROT space mission

PhD Thesis presented by

Juan Gutiérrez-Soto

December 2006

Dr. Juan Fabregat Llueca,
titular de la Universidad de Valencia,

CERTIFICA:

Que la presente memoria, "Non-radial pulsations in Be stars. Preparation of the COROT space mission", ha sido realizada bajo su dirección, por Juan Gutiérrez Soto, y que constituye su tesis doctoral para optar al grado de Doctor en Físicas.

Y para que quede constancia y tenga los efectos que corresponda, firma el presente certificado en Valencia, a 7 de Noviembre de 2006.

Firmado: Juan Fabregat Llueca

Agradecimientos

Esta tesis se ha desarrollado en el contexto de una amplia colaboración internacional. Varios de sus miembros han aportado importantes contribuciones al trabajo que aqui presentamos. A ellos les quiero manifestar mi mas sincero agradecimiento.

A mi director Juan por todo lo que me ha enseñado y por su paciencia y disponibilidad en los momentos más difíciles y a mi jefa Julia por su apoyo, ánimo y estímulo durante estos cuatro años.

A Rafa Garrido, otra persona fundamental en el desarrollo de esta tesis y que gracias a él entiendo mucho más de periodogramas.

A Anne-Marie Hubert y Michelle Floquet por su amable acogida durante mis estancias en Paris, asi como su atención y disponibilidad para aclararme dudas en todo momento.

A Coralie Neiner por su gran aportación en el trabajo de espectroscopía (cap. 4) y por ser tan paciente con mi inglés.

A Yves Frémat por su participación en la determinación de parámetros físicos (cap. 4) y por estar siempre dispuesto a ayudarme.

A Slobodan Jankov por haberme proporcionado los resultados del analisis del FDI (cap. 4) y por nuestras discusiones por email que tanto han contribuido a la mejora científica de esta tesis.

A Christophe Martayan que gracias a su colaboración he obtenido tan buenos resultados en el capítulo de la SMC (cap. 6).

A Christian Buil por permitirme utilizar sus datos de espectroscopía para la estrella NW Ser (cap. 4).

A Slavek Rucinski por darme la oportunidad de observar en el DDO de Toronto.

A Juan Carlos Suárez y Andy Moya por su ayuda en la interpretación teórica de los datos de fotometría y por ser tan divertidos.

A Mariana por estar siempre dispuesta a realizar observaciones en el OSN.

A los evaluadores Rafa Garrido, Anne-Marie Hubert y Pablo Reig por haber aceptado corregir y juzgar este trabajo, así como por la celeridad con la que lo han realizado.

A todos los colegas del GACE y del Observatorio Astronómico con los que he compartido ratos de trabajo y de ocio. Siempre me acordaré de los buenos cafés que nos tomamos en mi etapa de becario.

A mis amigos y a mi familia que son los que realmente me han soportado, que siempre han estado a mi lado y que sin ellos no hubiera podido terminar este trabajo, a veces tan duro y a veces tan gratificante.

Y por último, a la música heavy por acompañarme durante las largas noches de escritura.

Seguramente hay muchas más personas a las que debería agradecer, a todos ellos, gracias.

Acknowledgements

This thesis has been developed within the framework of an international collaboration. Several of their members have provided significant contributions to the work we present here. I would like to express to them my most sincere gratitude.

To my supervisor Juan for all he taught me and for his patience and availability in the most difficult moments and to Julia for her support and encouragement during these four years.

To Rafa Garrido, another fundamental person in the development of this thesis and thanks to whom I have learned all that I know about periodograms.

To Anne-Marie Hubert and Michelle Floquet for their friendly welcome during my stays in Paris, as well as their attention and availability to clarify all my doubts in any moment.

To Coralie Neiner for her great contribution to the spectroscopic work (Chapt. 4) and for being so patient with my English.

To Yves Frémat for the spectroscopic determination of the physical parameters (Chapt. 4) and for always being willing to help me.

To Slobodan Jankov for providing me the results of the FDI analysis (Chapt. 4) and for the fruitful email discussions which improved the scientific quality of this work.

To Christophe Martayan, thanks to whose collaboration I found such good results in the chapter of the SMC (Chapt. 6).

To Christian Buil for allowing me to use his spectroscopic data of the star NW Ser.

To Slavek Rucinski for giving me the opportunity of observing at the DDO in Toronto.

To Juan Carlos Suárez and Andy Moya for their help in the theoretical interpretation of the photometric data and for being so funny.

To Mariana for always being willing to making observations at the OSN.

To the referees of this thesis, Rafa Garrido, Anne-Marie Hubert and Pablo Reig, for having accepted to correct and assess this work, as well as for the swiftness with which they made it.

To all my colleagues from the GACE and the Observatorio Astronómico with whom I have shared great moments of work and leisure. I will always remember the very good coffees that we enjoyed together in my PhD student's stage.

To my friends and family, who have really supported me and have always been by my side and without whom I would not have completed this work, sometimes so hard and sometimes so gratifying.

And finally to heavy metal sharing all these long writing nights with me.

Certainly, there are more people to whom I should thank. To all of them, thanks.

Contents

Chapter 1

Introduction

The general objective of the present work is to contribute to the knowledge of the physics of Be stars. In particular, we are interested in studying and characterising their pulsational properties. A very suitable tool to reach this goal is the study and analysis of photometric time series with the maximum time baseline, density and photometric accuracy.

The space mission COROT scheduled to be launched in December 2006, will provide ultra high precision, relative stellar photometry for very long continuous observing runs. Up to ten stars will be observed in the seismology fields with a photometric accuracy of 1 ppm, and several thousands in the exoplanet fields with an accuracy of a few 10^{-4} and colour information.

The observations of Be stars with COROT will provide photometric time series with unprecedented quality. Their analysis will allow us to qualitatively improve our knowledge and understanding of the pulsational characteristics of Be stars. In consequence, we have started a research project aimed at observing Be stars both in the seismology and exoplanet fields of COROT.

In this thesis we present the first step of this project, which is the preparation and study of the sample of Be stars that will be observed by COROT. We have performed photometric analysis of all Be stars located in the seismology fields (Chapt. 2). Special emphasis has been given to two Be stars (NW Ser and V1446 Aql) in which we have detected multiperiodic variability and which we have modelled in terms of stellar

pulsations (Chapt. 3). We have also performed an in-depth spectroscopic study of NW Ser and modelled the non-radial pulsations taking into account the rotational effects (Chapt. 4). A technique to search for faint Be stars based on CCD photometry has been developed and is presented in Chapt. 5. In the same chapter, we present a list of faint Be stars located in the exoplanet fields of COROT detected with this technique and which we propose as targets for COROT. In addition, we have proven that our period-analysis techniques are suitable to detect multiperiodicity in large temporal baseline data (see Chapt. 6). In particular, we have detected non-radial pulsations in some Be stars in the low-metallicity galaxy SMC.

1.1 Be stars

Be stars are main sequence or slightly evolved, rapidly rotating stars showing near infrared excess and Balmer emission lines produced by an equatorially concentrated disk, fed by discrete mass loss events. The causes of non-regular mass loss in these stars is yet unknown. The centrifugal force produced by the high rotation rates of these stars (an average value of 88% of the critical velocity at which the centrifugal force balances gravitation at the equator, Frémat et al. 2005) is inadequate to explain by itself the formation of a disk around these stars. Non-radial pulsations (*nrp*) and stellar activity of magnetic origin combined to the near break-up rotational velocity have been proposed as mechanisms that could give rise to the additional amount of momentum needed to cause mass ejection. Rivinius et al. (2001) found that the beating produced by the *nrp* modes with low, identical degree ℓ and identical azimuthal order m determine the times of mass loss events in the Be star μ Cen. The question is: is this fact valid for all Be stars?

Be stars show two different types of photometric variability, with different origin and time scale:

- Long-term variability due to variations in the size and density of the circumstellar envelope. Variations are irregular and sometimes quasi-periodic, with time scales of weeks or months. In some stars variations are in form of outbursts with total duration of weeks or months.

- In early Be stars, short periodic light and line profile variability (*lpv*) are nearly omnipresent. Periods are in the range of 0.1 to 2 days. Hubert and Floquet (1998), based on Hipparcos observations, found that this short-term variability is present in 86% of early Be stars, in 40% of intermediate sub-spectral types (B4e-B5e) and in only 18% of late Be stars. This fact could be due to the variability detection level of current instrumentation, since the amplitude of pulsations in late sub-types is expected to be lower from theory.

Baade (1982) attributed the short periodic *lpv* to non-radial pulsations (*nrp*). Further detailed studies of a few well-observed objects led to a complete and consistent multimode modelling of the observed variations (Rivinius et al. 2001; Maintz et al. 2003; Neiner et al. 2005a). In addition, high-precision photometric data obtained with MOST satellite showed the presence of multiple periods in the Be stars ζ-Oph (Walker et al. 2005b) and HD 163 868 (Walker et al. 2005a). They modelled the detected frequencies as *nrp* in terms of p-modes in the case of ζ-Oph, and g- and r-modes in the case of HD 163 868.

In the HR diagram, early Be stars are located at the lower border of the instability domain of the β Cephei stars, while mild and late Be stars are mixed with Slowly Pulsating B (SPB) stars. Short-period p-modes are expected in early Be stars and long-period g-modes in mid to late Be stars. Currently, observational results disagree somewhat with theoretical computations. Nevertheless, up to now, the available predictions for instability regions of B stars are restricted to non or slowly-rotating models (Balona 1999). Recently, Townsend (2005) in a theoretical study of the pulsational stability of rotating B-type stars, proposed that Be stars might correspond to a class of retrograde mixed mode pulsators. If that is the case, observations might be reconciled, since retrograde mixed modes have prograde group velocities which are required for mass ejection to occur.

The observation of classical Be stars by COROT will provide important keys to understand the physics of these objects and the nature of the Be phenomenon. COROT observations will allow the study of the beating phenomenon of *nrp* modes and its relation with recurrent outbursts and the building of a circumstellar disk.

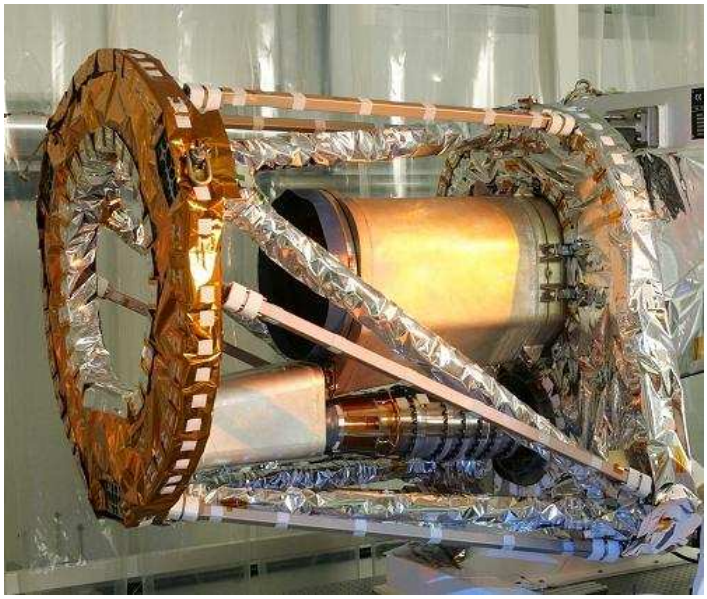

Figure 1.1: The COROT telescope. Copyrights 2006 - © CNES.

1.2 COROT

1.2.1 Definition and objectives

COROT[1], which stands for COnvection, ROtation and planetary Transits, is dedicated to ultra high precision, wide field, relative stellar photometry for very long continuous observing runs on the same field of view. The two main goals of the mission are the study of the stellar interiors by looking at their oscillations and to search for extrasolar planets by means of the transit method (see Baglin et al. 2002).

For both programmes a very high photometric precision is needed. An accuracy of less than 1 ppm is expected for 6th magnitude stars and of a few 10^{-4} for stars with magnitude ranging from 11.5 to 16. On the other hand, the major characteristic of COROT, with respect to the other space projects devoted to high precision photometry, is the possibility to perform very long observations of the same field (up to 150 days). In

[1] http://corot.oamp.fr/

addition, the expected duty cycle excluding short and long interruptions is $\sim 94\%$, which is much better than what can be obtained for ground-based data.

It is expected that COROT will be launched in December 2006 with a mission lifetime of nominally three years.

COROT is developed under the leadership of the French space agency CNES, with participations by Spain, Germany, Austria, RSSD/ESTEC, the European Space Agency (ESA), Belgium, Brazil, Italy, Hungary and Romania.

The telescope

The telescope design is constrained by the need to minimise straylight from Earth entering the telescope. The best protection is reached with an off-axis afocal parabolic system. The light is collected by a $f/4$ telescope of 27 cm entrance pupil to achieve the goal of a 2.8×2.8 deg FOV. The beam of the output of the telescope is re-imaged on the local plane by dioptric optics. In Fig. 1.1 we display a recent picture of the COROT telescope.

The observable sky

The telescope of COROT will monitor selected targets towards the Galactic Centre and Anticentre directions. These two cones of observations (Fig. 1.2) centred at $\alpha = 18^{\mathrm{h}}50^{\mathrm{m}}$, $\delta = 0^{\circ}$ and $6^{\mathrm{h}}50^{\mathrm{m}}$, $\delta = 0^{\circ}$, each having a radius of 10°, are the pointing limits for the CCDs. A small drift of the plane of the orbit will optimise the observing conditions with respect to straylight, and transform these circles in slightly elongated ellipses.

When the Sun reaches the orbital plane, the satellite is turned in the opposite direction to keep the Sun in its back. As shown in Fig. 1.3, each year period contains two long runs (150 days each, *Core programme*) and a 4 short runs (20 to 30 days each, *Exploratory programme*).

The camera

The focal plane is composed of four 2048×2048 Marconi MPP CCDs, working in frame transfer, at -40° C. Two are dedicated to the seismology

Figure 1.2: The two observing cones of COROT, towards the Galactic Centre (**left**) and Anticentre (**right**) directions. Copyrights 2006 - © CNES.

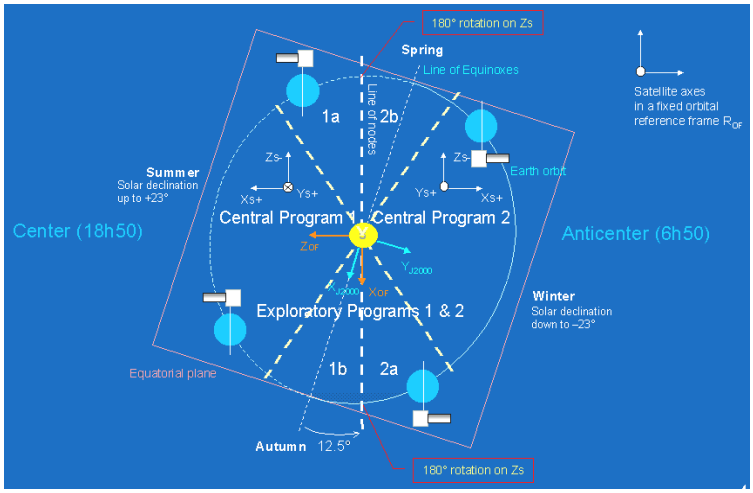

Figure 1.3: The relative positions of COROT and the Sun during a year. The two long runs (Core Programme) and the four short runs (Exploratory Programme) are marked in the Figure. Copyrights 2006 - © CNES.

Table 1.1: Number of targets that will be observed in the seismology and exoplanet CCDs and the range of magnitudes.

	# targets/run	V magnitude
Seismology	10	5.7-9.5
Exoplanet	12 000	11.5-16

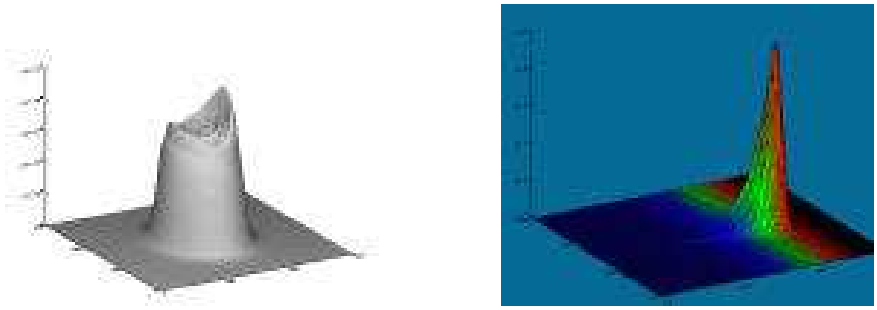

Figure 1.4: Point spread function (PSF) for the seismology (**left**), and exoplanet cameras (**right**). See the text for more details. Copyrights 2006 - © CNES.

programme (stars with $5.7 \leq m_v \leq 9.5$) and the other two to the exoplanet programme (stars with $11.5 \leq m_v \leq 16$).

In order to collect the largest number of photons per star, the seismology channel must be defocused (see left panel of Fig. 1.4); in this way the spot image covers more than 250 pixels and a bright star can be observed without saturation. A maximum of 5 defocused stars per CCD and 5 sky reference windows should be readout every 32 seconds.

In the exoplanet channel, a prism is placed in the optical beam and a low-dispersion spectrum is focused in the CCD (see right panel of Fig. 1.4). Approximately 12 000 stars per run will be recorded as well as few dark reference windows. In order to avoid saturation of stars of about 12th mag, the exposure time is 32 seconds for 500 windows per CCD and 512 seconds for the rest. Since the planetary transit is essentially achromatic, the colour information is required to resolve the ambiguity between stellar activity and planet occultation. The output will be the time series in

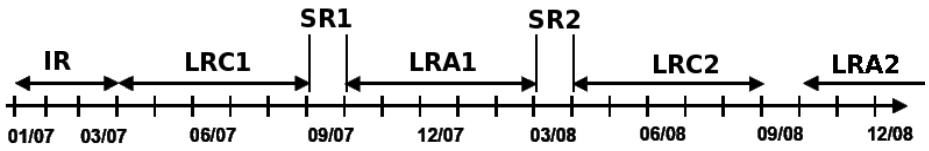

Figure 1.5: Observing runs in a chronological order.

different colours for $\sim$ 5000 stars with magnitudes $V < 15$ and in one filter for the rest. Due to the heavy data processing required, the time resolution in this channel will be $\sim$ 17 minutes.

Observation scheduling

The observation scheduling is represented in Fig. 1.5. The COROT satellite will be launched in December 2006. A period of approximately two months will be used for the commissioning, where all the calibrations and engineering assessment has to be made. Then, an *initial run* (IR) will monitor the first targets observed by COROT until April 2007. From that moment, at least five long runs will be performed with a duration of 150 days each, pointing alternatively towards the Galactic Centre (LRC1, LRC2, ...) and the Anticentre (LRA1, LRA2, ...) directions. In addition, short observing runs (SR1, SR2, ...) with a duration of 20-30 days each will be performed on specific targets in order to cover the HR diagram as much as possible .

1.2.2 Seismology programme

COROT will perform an *exploratory programme*, to detect oscillations in a large variety of stars and to classify the asteroseismologic properties in the HR diagram, and a more specific programme, the *Core programme*, centred on a detailed study of a few stars, specially chosen to test the hydrodynamics of the internal layers and the physical state of stellar cores.

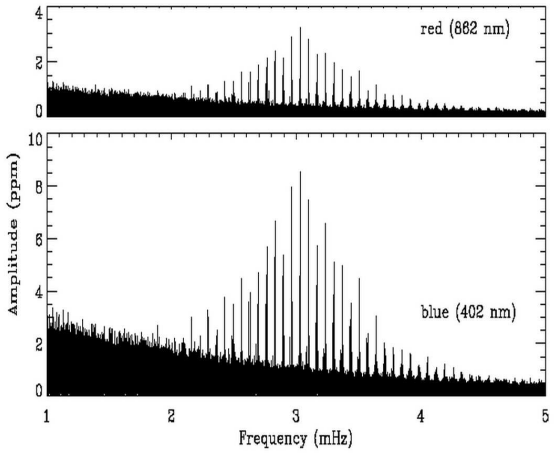

Figure 1.6: The spectrum of the Sun derived from the experiment VIRGO on board SOHO (from Frohlich et al. 1997; Bedding and Kjeldsen 2003).

The Core programme

Its objective is to observe very precisely a small set of objects during 150 days. The general problem addressed by the COROT seismology Core programme is the nature of transport processes in stellar interiors during the Main Sequence evolution stage and around it. This covers several aspects of transport, from convective heat transport to angular momentum transport, including overshooting, transport of chemical species, etc. Through these phenomena, COROT will decipher the main sources of uncertainty in the modelling of intermediate and moderate mass stars during a stage of evolution which represent about 90% of their life-time and has crucial consequences on their further evolution.

In the case of solar-like pulsators, it is well known that the characteristic features of the internal structure induce signatures in the oscillation frequencies at the level of $0.1\mu Hz$ (1 cycle in about 100 days). COROT needs this accuracy in frequency to have access to the profile of the modes and the rotational divisions, and for a precise measurement of the modal frequencies. In Fig. 1.6 we show the oscillation spectrum of the Sun derived from the VIRGO experiment onboard SOHO.

For A and F stars close to the main sequence, it will then be possible to measure the size of the convective cores, the size of the outer convective zones and their helium content. For moderate-mass stars as δ-Scuti stars, a 150 days run will provide accurate enough frequencies to tackle precise inversion of the rotational profile.

At least 5 long runs are planned, during which one or two bright stars (primary targets) and several fainter ones ($5.7 \leq m_v \leq 9.5$) in the surrounding field of view (secondary targets) will be surveyed by the satellite.

The Exploratory programme

The principal objective of the exploratory programme is to determine the domain of stellar parameters for which stellar oscillations can be detected. In consequence, one needs to observe a sample of objects with a large variety of stellar parameters, as mass, age, chemical composition, rotational state etc, for which only a modest signal to noise ratio is needed. COROT will study all the different types of pulsating stars in the HR diagram, depicted in Fig. 1.7, and probably find new ones.

A frequency resolution of 0.5 μHz will be sufficient, corresponding to observations that last 20-30 days. Stars with magnitudes less than about 9 will be bright enough for these studies.

1.2.3 Exoplanet programme

Since the discovery of the first extrasolar planet (51 Peg b in 1995 by Mayor and Queloz), the understanding of the formation of planetary systems has improved drastically. After the study of the giant exoplanet class, the challenge is now to characterise the telluric exoplanet class. COROT is planned to take up the challenge with a planet finding programme whose main goal is to detect the first telluric extra-solar planet with the transit method.

The transit method is the only one which allows the precise determination of the orbital period and the size of the planet. The problem is to detect the small luminosity decrease of a star when occulted by one of its planets, either a giant with a Jupiter mass or a small telluric one (see Fig. 1.8).

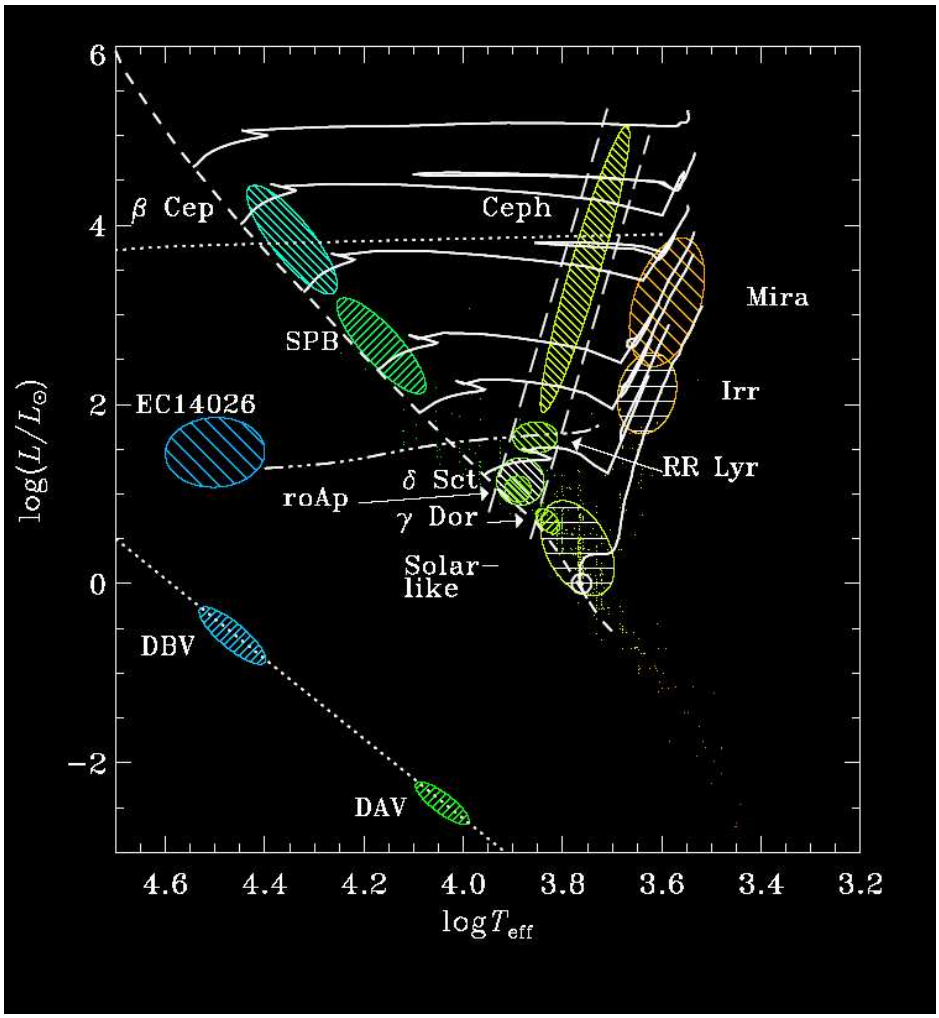

Figure 1.7: The different types of pulsating stars across the HR diagram. which will be studied by the exploratory programme (Image courtesy of Prof. Christensen-Dalsgaard, J. Aarhus University, Denmark).

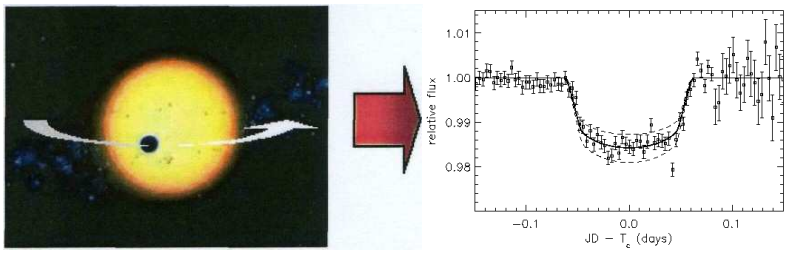

Figure 1.8: The transit method for detecting planets. A decrease in the light of the star is observed when the planet is on the line of sight between us and the star. © Hans Deeg.

A transit event is characterised by a relative amplitude of 10^{-2} for a Jupiter-like planet and only 8.10^{-5} for an Earth-like one and a periodicity which ranges from a few days to several months. This implies a great necessity of high precision photometry and continuous observations during a long period.

Furthermore, this event may be observed only when the line of sight lies within the orbital plane of the planet. The associated geometrical probability is very low (0.5% for the Earth-like planets and 16% for 51 Peg b, Bordé et al. 2001), so that a large number of stars must be monitored to have a chance to find a planet. For this reason, an amount of 12 000 stars per run, with a magnitude $V = 11.5$ to 16 will be monitored continuously during 5 months on the two exoplanet CCDs of COROT .

The major difficulty in the detection of planetary transit is to identify the false alarms due to photometric variations of stellar origin, as stellar activity. Projects like STARE (Alonso et al. 2004) are studying the strategies to recognise these false alarms. To do so a bi-prism has been included in the COROT exoplanet field providing a short spectrum. It has been shown that the coloured information decreases the false-alarm probability.

1.2.4 Additional Scientific Programme

COROT will provide long, continuous and highly accurate photometric data of more than 60 000 stars. These data can be used for other purposes than the primary science goals.

The Additional programme (AP) addresses any science case outside of

the Core Programme with the goal to maximise the scientific results of the mission. Seismology in the exoplanet field and exoplanet studies in the seismology field belong to the Additional Programmes.

There are three possibilities to request COROT data within the AP:

- Half of the short runs scheduled for COROT will be devoted to the AP. During these short runs data from a specific target field will be obtained and they need not be devoted to asteroseismology or planet search.
- A few hundred windows of the exoplanet field during each long run will be available within the AP.
- Archival data obtained within the Core Programme or the Additional programmes can be requested.

Announcements of Opportunity for observations within the COROT-AP will be issued each year. This programme is open to the entire astronomical community.

In April 2005, the first AO (AO-1) for the Additional Programme of the COROT Mission was sent to the scientific community. Observations during the first two long runs (centred on HD 49933 and HD 181555) and various short runs (number not yet decided) were subject of a proposal. Responses to the official AO have been examined by the Scientific Committee and authors of accepted proposals have become Guest Investigators (GIs) and will have exclusive rights for the science of their project during the proprietary period (1 year).

1.2.5 Targets

The list of principal and secondary targets has changed since the first "COROT week" conference held in 2001. The ground-based observations performed in the last years by the COROT scientific working groups have given some constraints in the determination of the primary targets, including a β Cephei star or taking out some stars from the list due to the high $V \sin i$. At the moment, the position of the CCDs of the initial run and the two first long runs are fixed (see Table 1.2). The primary targets, the coordinates of the centre of the four CCDs and the roll angle are also

Table 1.2: List of observing runs to be performed by COROT in a chronological order. Notes: 1.- fixed position; 2.- proposed position to be confirmed by the scientific committee; 3.- Position to be proposed.

Run	Primary Target(s)	Coordinates RA	DEC	Roll Angle	Notes
IR01		$6^h50^m25^s$	$-10^\circ\,42'\,00''$	$+9^\circ.60$	1
LRC1	HD 181555 HD 180642	$19^h23^m33^s$	$+00^\circ\,27'\,36''$	$+18^\circ.88$	1
LRA1	HD 49933 HD 49434	$6^h46^m52.8^s$	$-00^\circ\,12'\,00''$	$+7^\circ.28$	1
LRC2	HD 171834	$18^h29^m03^s$	$+06^\circ\,16'\,12''$	$+23^\circ.60$	2
LRA2	HD 52265	$6^h54^m20^s$	$-04^\circ\,23'\,24''$	$+4^\circ.64$	2
LRC3	HD 170580				3
LRA3	HD 43587				3

shown in the table. The positions of the two next long runs (*LRA2* and *LRC2*) are proposed but not confirmed yet by the scientific committee and, finally, stars HD 170580 and HD 43587 are likely to be observed at the end of the mission, but positions of the CCDs are not yet proposed.

The list of the proposed primary and secondary targets to be observed by COROT in the long run towards the Galactic Centre (*LRC1*) and Anticentre (*LRA1*) directions are given in Tables 1.3 and 1.4. Note that several Be stars (in bold) have been selected as secondary targets. Only five stars will be observed per CCD.

1.3 The study of Be stars with COROT

Due to the interest of observing Be stars with COROT, illustrated in the previous sections, a vigorous international collaboration (The COROT Be stars team[2]) has been established to propose such observations and to study and analyse the data of Be stars which COROT will produce. The group is a collaboration between 11 scientists of several European and

[2]http://www.ster.kuleuven.ac.be/∼coralie/corotbe.html

Table 1.3: List of proposed primary and secondary targets in the LRC1 in order of priority. Selected Be stars are shown in bold. Only the first five stars for each CCD will be observed.

Targets	log T_{eff}	V	$V \sin i$	Sp. Type	Comments
			CCDA1		
181420	3.82	6.57	21	F2	solar-like
181907	3.64	5.83		G8III	
182198	4.06	7.94	25	B9V	
181231	4.14	8.58	250	B5IV	Be
181390	3.88	8.64		A0	
			complementary targets		
181991	3.86	8.86		A2	solar-like
181690	3.92	9.03		B9V	
181440	4.05	5.49	56	B9III	
			CCDA2		
181555	3.81	7.52		A5	δ Scuti; Primary
180642	4.42	8.27		B1.5II-III	β Cephei; Primary
181906	3.81	7.65	18	F8	
181072	3.84	9.14		A2	
181973	3.81	6.74	130	F0	
			complementary targets		
181439	3.88	8.97	45	F0	
181732	3.70	7.66		F5	
180622	3.68	7.63		K2	

Table 1.4: The same as Fig. 1.3, but for the LRA1.

Targets	log T_{eff}	V	$V \sin i$	Sp. Type	Comments
			CCDA1		
49330	4.43	8.95	270	B0.5IV	Be
49385	3.79	7.89	7.5	G0	
49294	3.91	7.00	111	A2	
49808	3.85	7.98	114	F0	
50064	3.71	8.29	41	B6I	
			complementary targets		
49585	4.41	9.13	310	B0.5IV	Be
49431	3.92	9.35		A2	
49567	4.23	6.15	72	B3III	Be
			CCDA2		
49933	3.81	5.77	11	F2V	Primary
49434	3.87	5.75	89	F1V	γ Dor; Primary
50209	4.09	8.36	200	B8IV	Be
50230	4.03	8.95	23	B3	
49862	3.86	9.47	130	A5	Ap
			complementary targets		
49432	3.82	9.47		A5	
49433	3.96	9.13		A0	
49713	4.09	7.32	50	B9	Ap

Brazilian institutes with great expertise in the domain of Be stars. The French-Belgian team led by A.-M. Hubert has a large expertise in the study of Be stars in spectroscopy, as well as in photometry. The Spanish team led by J. Fabregat is composed of experts on photometry from ground-based observations and the Brazilian team, led by E. Janot-Pacheco are experts on spectroscopy of Be stars.

The COROT Be stars team has proposed to the scientific committee to observe Be stars with COROT in two ways:

- Observations of bright Be stars as secondary targets in the seismology fields. This proposal has been accepted by the scientific committee as part of the core programme, and several Be stars are included in the list of targets of the two first long runs already decided (Tables 1.3 and 1.4). Several others are being considered to be included in successive long runs and in the short runs still to be fixed. In Figs. 1.9 and 1.10 we display the position of the bright Be stars (crosses) and the main targets (circles) of COROT in the seismology fields in the Galactic Anticentre and Centre directions respectively. The CoIs of COROT for the Be stars programme are Anne-Marie Hubert, Coralie Neiner and Eduardo Janot-Pacheco.

- Observations of faint Be stars in the exoplanet fields. These observations will be part of the Additional science Programme. We have proposed this observations to answer the first Announcement of Opportunity for additional science issued in 2005. Our proposal has been accepted and thus the faint Be stars we are proposing will be actually observed and the data reduction and exploitation will be our responsibility. Coralie Neiner is GI of this project.

During the last years, our team has been working on the preparation of the proposal for COROT described above. The French-Belgian group led by A.-M. Hubert have published several papers related to the Be stars and the COROT mission: Neiner et al. (2005b) identified new Be stars in GAUDI database; Frémat et al. (2006) determined the fundamental parameters of 64 Be stars, based on high-resolution spectroscopic data.

Our group is responsible for the photometric study of the bright Be stars to be proposed as secondary targets for the asteroseismology fields

and for the detection of faint Be stars in the exoplanet fields. The work done up to now on this topic is presented in this thesis.

In general, the main objectives of our study of Be stars with COROT are the following:

- Detect new pulsation periods, especially beating periods. The long-time coverage is needed for the detection of a beat phenomenon of *nrp* modes in relation with recurrent outbursts.
- Perform a seismic modelling of their interior structure.
- Disentangle stable periods due to pulsations from transient periods due to rotational modulation of temporary, possibly magnetic, corotating structures.
- Better understand how the circumstellar disk is generated.
- Detect high degree p-modes of low amplitude in main sequence or slightly evolved early Be stars: Balona and Kambe (1999) have shown that predicted light amplitudes in V band for spherical harmonic degrees $\ell = 4 \ldots 8$ are less than 1 mmag if the pulsational velocity amplitude is less than 20 $\mathrm{km\,s^{-1}}$.
- Detect low amplitude g-modes in late Be stars
- Detect rotation and associated modulation.
- Study the influence of a magnetic field on pulsational characteristics.

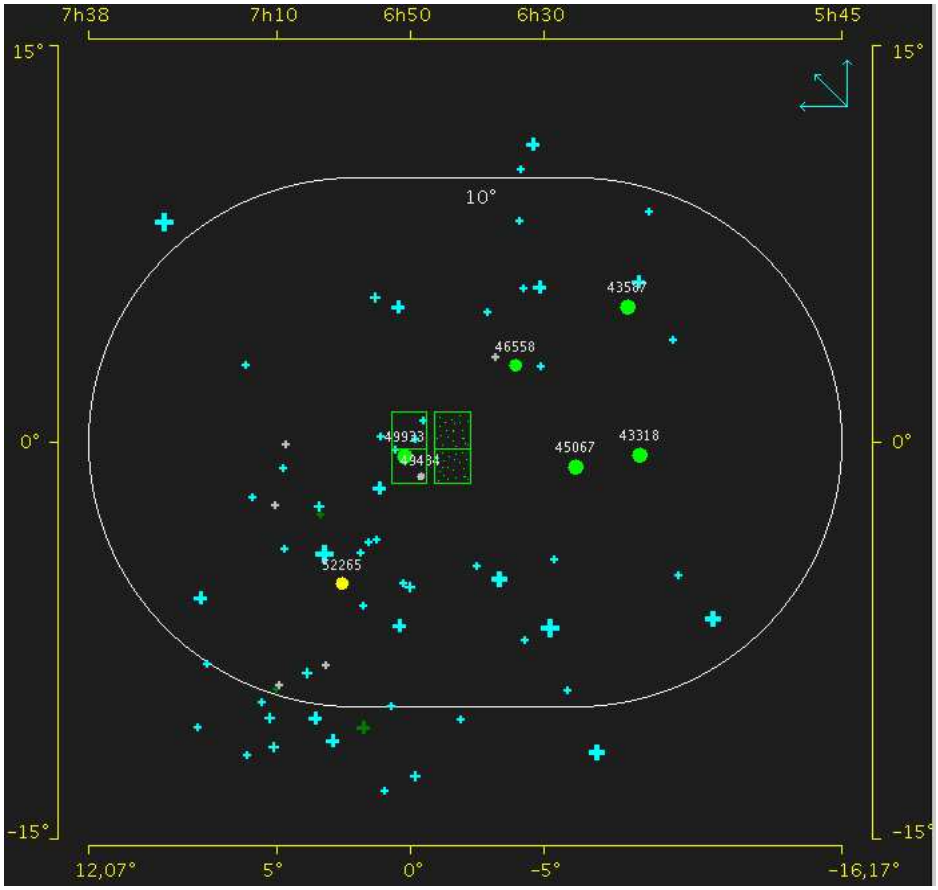

Figure 1.9: The position of the primary targets (circles) and Be stars (crosses) for the seismology fields towards the Galactic Anticentre direction. The ellipse corresponds to the cone of COROT in this direction while the four green squares are the field of view of the four CCDs. Image extracted from COROTSKY.

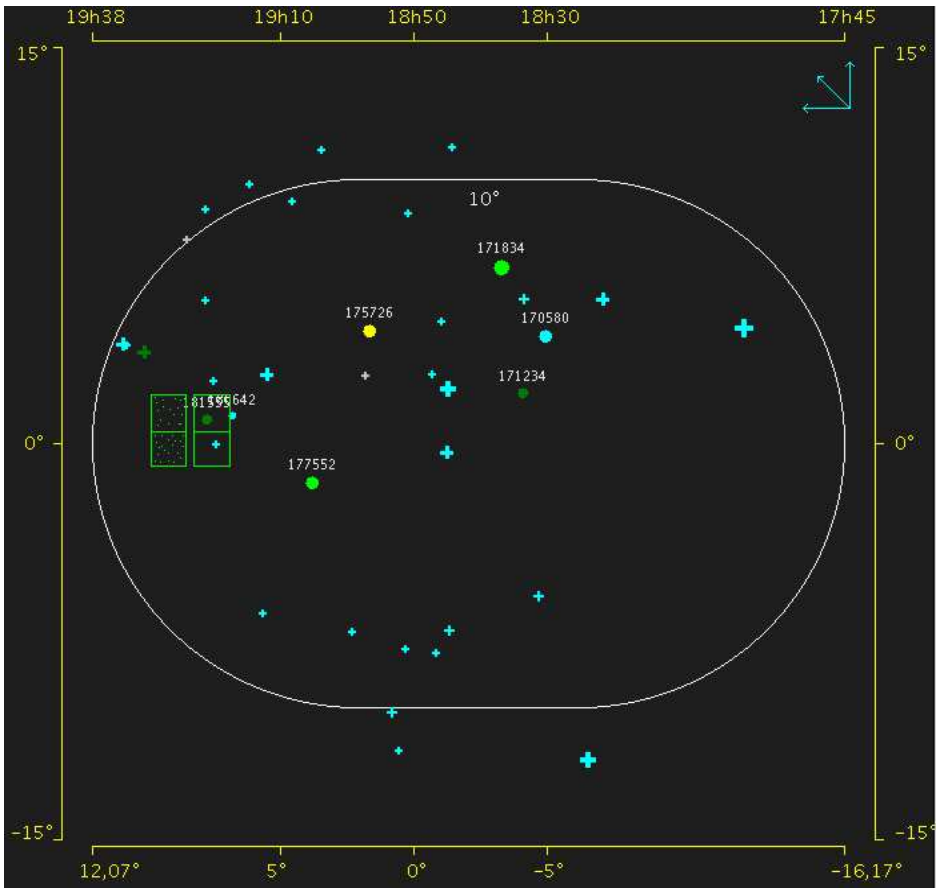

Figure 1.10: The same as Fig. 1.9, but for the seismology fields towards the Galactic Centre direction.

Bibliography

Alonso, R., Deeg, H. J., Brown, T. M., and Belmonte, J. A.: 2004, in F. Favata, S. Aigrain, and A. Wilson (eds.), *ESA SP-538: Stellar Structure and Habitable Planet Finding*, pp 255–259

Baade, D.: 1982, *A&A* **105**, 65

Baglin, A., Auvergne, M., Catala, C., Michel, E., Goupil, M. J., Samadi, R., Popielsky, B., and The COROT Team: 2002, in C. Aerts, T. R. Bedding, and J. Christensen-Dalsgaard (eds.), *ASP Conf. Ser. 259: IAU Colloq. 185: Radial and Nonradial Pulsations as Probes of Stellar Physics*, p. 626

Balona, L. A.: 1999, *MNRAS* **306**, 407

Balona, L. A. and Kambe, E.: 1999, *MNRAS* **308**, 1117

Bedding, T. R. and Kjeldsen, H.: 2003, *Publications of the Astronomical Society of Australia* **20**, 203

Bordé, P., Rouan, D., and Léger, A.: 2001, *Academie des Sciences Paris Comptes Rendus Serie Physique Astrophysique* **7**, 1049

Frémat, Y., Neiner, C., Hubert, A.-M., Floquet, M., Zorec, J., Janot-Pacheco, E., and Renan de Medeiros, J.: 2006, *A&A* **451**, 1053

Frémat, Y., Zorec, J., Hubert, A.-M., and Floquet, M.: 2005, *A&A* **440**, 305

Frohlich, C., Andersen, B. N., Appourchaux, T., Berthomieu, G., Crommelynck, D. A., Domingo, V., Fichot, A., Finsterle, W., Gomez, M. F., Gough, D., Jimenez, A., Leifsen, T., Lombaerts, M., Pap, J. M., Provost, J., Cortes, T. R., Romero, J., Roth, H., Sekii, T., Telljohann, U., Toutain, T., and Wehrli, C.: 1997, *Sol. Phys.* **170**, 1

Hubert, A. M. and Floquet, M.: 1998, *A&A* **335**, 565

Maintz, M., Rivinius, T., Štefl, S., Baade, D., Wolf, B., and Townsend, R. H. D.: 2003, *A&A* **411**, 181

Mayor, M. and Queloz, D.: 1995, *Nat* **378**, 355

Neiner, C., Floquet, M., Hubert, A. M., Frémat, Y., Hirata, R., Masuda, S., Gies, D., Buil, C., and Martayan, C.: 2005a, *A&A* **437**, 257

Neiner, C., Hubert, A.-M., and Catala, C.: 2005b, *ApJS* **156**, 237

Rivinius, T., Baade, D., Štefl, S., Townsend, R. H. D., Stahl, O., Wolf, B., and Kaufer, A.: 2001, *A&A* **369**, 1058

Townsend, R. H. D.: 2005, *MNRAS* **364**, 573

Walker, G. A. H., Kuschnig, R., Matthews, J. M., Cameron, C., Saio, H., Lee, U., Kambe, E., Masuda, S., Guenther, D. B., Moffat, A. F. J., Rucinski, S. M., Sasselov, D., and Weiss, W. W.: 2005a, *ApJ Lett.* **635**, L77

Walker, G. A. H., Kuschnig, R., Matthews, J. M., Reegen, P., Kallinger, T., Kambe, E., Saio, H., Harmanec, P., Guenther, D. B., Moffat, A. F. J., Rucinski, S. M., Sasselov, D., Weiss, W. W., Bohlender, D. A., Božić, H., Hashimoto, O., Koubský, P., Mann, R., Ruždjak, D., Škoda, P., Šlechta, M., Sudar, D., Wolf, M., and Yang, S.: 2005b, *ApJ Lett.* **623**, L145

Chapter 2

A photometric study of Be stars located in the seismology fields of COROT

2.1 Introduction

The aim of this chapter is to characterise the short-term photometric variability of all bright Be stars located in the COROT cones, which are suitable to be observed in the seismology fields.

A total of 84 Be stars have been found in the observing cones of COROT with magnitudes ranging from 5.5 to 9.4. The list has been taken from Jaschek and Egret (1982), complemented with the new Be stars identified by Neiner et al. (2005). Two Be stars (NW Ser and V1446 Aql), which have shown multiperiodic behaviour and have been modelled in terms of non-radial pulsations are excluded from this study (see Chapt. 3). Therefore, a sample of 82 Be stars has been considered, 49 and 33 towards the Galactic Anticentre and Centre directions respectively.

Due to the high number of stars to be analysed, a selection criterion has been made. As a first step, all the stars close to the primary targets of COROT have been observed during a 4-year campaign at the Observatorio de Sierra Nevada (OSN). They were firstly selected as they have the highest probability to be observed by the satellite. As the decision of the exact position of the CCDs has been finally taken by the scientific

committee of COROT in 2006, we observed some Be stars which are not located near the actual primary targets. Be stars whose results did not lead to a convincing period determination during the observing run were re-observed at the OSN and re-analysed. Finally, Hipparcos and ASAS-3 light curves of the total number of Be stars have been analysed in order to complement the study performed with the OSN data.

2.2 Observations and data analysis

The photometric data presented in this chapter have been obtained with three instruments with different properties. The studied stars are reported in Tables 2.2 and 2.3. The spectral type and the $V \sin i$ were taken from Frémat et al. (2006) and from the Simbad database[1].

2.2.1 Hipparcos

Hipparcos (High Precision Parallax Collecting Satellite, Perryman et al. 1997) was an astrometric mission of the European Space Agency dedicated to the measurement of positions, parallaxes and proper motions of stars. As a by-product of the astrometric mission, stellar magnitudes were repeatedly measured for each star on numerous occasions throughout the mission, resulting in an enormous collection of light curves. Hubert and Floquet (1998) has shown that Hipparcos is a useful tool for the study of variability of bright Be stars. A total of 62 stars located in the observing cones of COROT have been observed by Hipparcos. An average of 100 datapoints spanning 1000 - 1100 days are provided for each observed star. The standard error of a measurement ranges from 6 mmag at magnitude 6 to about 17 mmag at magnitude 9.

2.2.2 Observatorio de Sierra Nevada (OSN)

Ground-based observations have been obtained at the 0.9 m telescope of the Observatorio de Sierra Nevada in Granada, Spain, from 2002 to 2006. The instrument used is the automatic four-channel spectrophotometer which allows simultaneous observations through the four *uvby* filters of

[1] http://simbad.u-strasbg.fr/Simbad

Table 2.1: Summary of observing nights at the OSN. The mean accuracy of each dataset is also provide (see text for details).

Dates	Observing	Accuracy (mmag)			
	nights	u	v	b	y
20-29 May 2002	10	10	6	6	7
8-14 Jan 2003	4	9	4	3	4
1-13 July 2003	9	8	4	4	6
30 Jan - 8 Feb 2004	4	10	5	5	6
13 - 24 Jul 2005	6	10	5	5	5
16 - 30 Jan 2006	5	7	4	4	5

the Strömgren system. Obtaining photometric light curves in four filters at the same time allows us to confirm or reject uncertain periods. Only frequencies detected simultaneously in the *vby* filters are considered as certain. As the signal to noise is significantly lower, the u filter is noisier and less reliable.

Dates of the observing runs and observing nights are reported in Table 2.1. We have applied the three-star differential photometry, similar to the one described by Lampens et al. (2005). The variable star, a comparison and check stars and the appropriate sky background were measured successively (sky - var - comp - check - sky - var ...). Usually we observed up to 8 target stars every night and we repeated the measurements for each night. Only in the winter 2003 we devoted each clear night to survey an individual star.

Sky level and mean extinction coefficients were obtained for each night. An amount of 22 Be stars were observed at the OSN in the Anticentre and the Centre directions. These Be stars with the corresponding comparison and check stars are presented in Tables 2.2 and 2.3 respectively. A few comparison stars were found to be low-amplitude variables, as for example HD 171 305 and HD 182 786.

The mean accuracy of the differential photometry, measured as the rms of the difference between the comparison and check values, is, in all cases, less than 10 mmag in u and 7 in *vby*, as shown in Table 2.1.

2.2.3 ASAS-3

The All Sky Automated Survey (Pojmanski 2002) is a project whose final goal is photometric monitoring of approximately 10^7 stars brighter than 14 magnitude all over the sky. ASAS-3 is the third stage of the ASAS project, which has surveyed the whole of the southern and part of the northern sky. In this work, we have benefited from the huge amount of data gathered by ASAS-3. We have analysed the light curve of 50 stars fainter than 7.8 located in the observing cones of COROT. Stars brighter than 7.8 were eliminated from the list for being saturated. The studied stars taken from ASAS-3 are listed in Tables 2.2 and 2.3. An average of 200 datapoints spanned over 1700 days are provided for each star. Since five different magnitudes depending on the aperture radius are provided, we have selected the one which produces less error, usually the 4th and 5th aperture in our case. Only measurements with quality grade A have been analysed. A photometric error between 10 to 25 mmag is provided in the ASAS-3 database for the studied stars.

2.2.4 Spectral analysis

Spectral analysis is then applied to the time series of each star in the three datasets separately.

Period analysis is performed by means of standard Fourier analysis and least-square fitting. We have used Period04 (Lenz and Breger 2005) which is especially designed for the analysis of time series containing gaps. This program finds the frequencies one by one by computing the Fourier Transform and then adjusts the parameters of a sinusoidal function using a least-square fitting. Then this frequency is removed (prewhitened) and a new step is started finding a new frequency, the subsequent least-square fitting is made allowing the two frequencies to move in order to get the minimum variance. The method is iterative ending when removing of a new frequency is not statistically significant.

We have also used a non-linear multi-parameter fitting code which scans a wide range in frequency based on Vaníček (1971) and explained in detail in Zerbi et al. (1997). This code is also well-suited for the OSN and ASAS-3 data, for which daily aliases are present in the periodogram, due to the fact that the observations have been obtained at only one site.

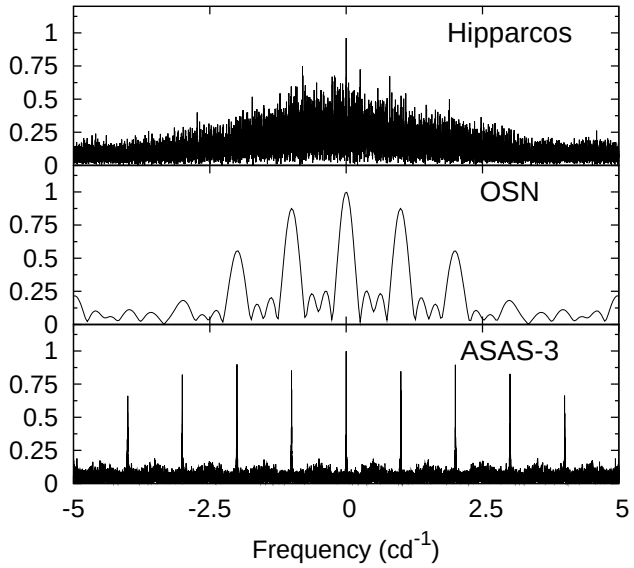

Figure 2.1: Examples of spectral window for the three instruments studied in this chapter.

In Fig. 2.1 we show examples of spectral windows for Hipparcos, OSN and ASAS datasets. The non-random distribution in time of the Hipparcos photometry produces a spectral window which is not very satisfying. In the case of OSN and ASAS-3 observations, a typical 1-day alias pattern is present in the spectral window. Note the different widths of the sidelobes, depending on the time length of the observations.

The way in which we determine whether the frequencies are statistically significant or not is described in Breger et al. (1993) and basically consists in the calculation of the *signal to noise ratio* (SNR), the noise being the average amplitude, within a 5 c d^{-1} frequency interval, of the residual periodogram after the prewhitening as previously explained around a frequency and the signal being the corresponding amplitude of that frequency. Breger et al. (1993) showed that this value must be greater than 4.

Following Montgomery and O'Donoghue (1999), the expected error in frequency for uncorrelated observations can be derived from the equation

$$\sigma_F = \frac{\sqrt{6}}{\pi} \cdot \frac{\sigma_n}{A \cdot \sqrt{N} \cdot T}$$

where A/σ_n indicates the signal to noise ratio, N is the number of observations and T the time elapsed between the first and the last data point. As noted by Schwarzenberg-Czerny (1991), correlations in the residuals of the fitting have to be taken into account multiplying the error frequency by $\sqrt{D}$, where D is the correlation length. D can be estimated by performing an autocorrelation analysis of the final residuals. We have obtained a formal error in frequency of $2-4\times10^{-3}$, $3-4\times10^{-5}$ and $1-2\times10^{-5}$ c d^{-1} for the OSN, Hipparcos and ASAS-3 datasets respectively. The frequency resolution is given by $1/T$. In our case, we estimate 0.1, 0.001 and 0.0006 c d^{-1} for the OSN, Hipparcos and ASAS observations respectively.

Table 2.2: Studied Be stars in the Galactic Anticentre direction. ID numbers and SIMBAD V magnitudes are given for each target in cols. 1 and 2. The spectral type and $V \sin i$ are gathered in cols. 3 and 4. Comparison and check stars used for the differential photometry are given in cols. 5 and 6. References of the spectral type and $V \sin i$ are given in col. 7. Notes: 1 - Frémat et al. (2006); 2 - Simbad database; 3 - Only ASAS-3 and/or Hipparcos observations have been used in the analysis.

Be star	V	Sp.Type	$V \sin i$ $\mathrm{km\,s^{-1}}$	Comp.	Check	Notes
HD 42259	8.89	B0V	-	HD 294788	HD 42369	2
HD 42406	8.0	B4IV	300			1,3
HD 43264	6.05	B9III	284			1,3
HD 43285	6.05	B5IV	260	HD 44783	HD 43526	1
HD 43777	7.8	B5				2,3
HD 43913	7.88	A0				2,3
HD 44783	6.23	B9II	227			1,3
HD 45260	9.04	B8				2,3
HD 45626	9.25	B7				2,3
HD 45901	8.85	B0.5IV	164			1,3
HD 45910	6.74	B2III				2,3
HD 46380	8.05	B1.5IV	300	HD 46541	HD 46519	1
HD 46484	7.65	B0.5IV	120	HD 46106	HD 46748	1
HD 47054	5.52	B7III				1,3
HD 47160	7.10	B8IV	158			1,3
HD 47359	8.87	B0IV	443			1,3
HD 47761	8.72	B2V	50			2,3
HD 48282	8.79	B3V	188			2,3
HD 49330	8.95	B0.5IV	270	HD 50086	HD 50230	1
HD 49567	6.15	B3III				1,3
HD 49585	9.13	B0.5IV	310	HD 50086	HD 50230	1
HD 49787	7.55	B1V	169			1,3
HD 49992	8.98	B1				2,3
HD 50083	6.91	B2III	193			1,3
HD 50087	9.08	B8III	-	HD 50086	HD 50230	2
HD 50209	8.36	B8IV	200	HD 50086	HD 50230	1
HD 50424	8.92	B9				2,3
HD 50581	7.54	A0IV				1,3
HD 50696	8.87	B1.5III	350	HD 50086	HD 50230	1

Continued...

Table 2.2: Continued.

Be star	V	Sp.Type	$V \sin i$ km s^{-1}	Comp.	Check	Notes
HD 50820	6.27	B3IV				2,3
HD 50868	7.87	B1.5V				1,3
HD 50891	8.88	B0.5V	220	HD 50348	HD 51150	1
HD 51193	8.06	B1.5IV	215	HD 50348	HD 51150	1
HD 51404	9.30	B1.5V	335	HD 50348	HD 51150	1
HD 51452	8.08	B0IV	298	HD 50348	HD 51150	1
HD 51506	7.68	B2.5IV	186			1,3
HD 53085	7.21	B4IV	222			1,3
HD 53367	6.97	B0IV	70			2,3
HD 54464	8.4	B2.5III	160			1,3
HD 55135	7.34	B2.5V	264			1,3
HD 55439	8.47	B2				2,3
HD 55606	9.04	B0.5V	350			1,3
HD 55806	9.11	B7III	202			1,3
HD 57386	8.0	B1.5V				2,3
HD 57539	6.6	B5III	155			1,3
HD 259431	8.71	B6	95			2,3
HD 259440	9.12	B0	430			2,3
HD 259597	9.33	B1V				2,3
HD 293396	8.59	B1V				2,3

Table 2.3: The same as for Table 2.2, but for studied stars in the Galactic Centre direction

Be star	V	Sp.Type	$V \sin i$ km s^{-1}	Comp.	Check	Notes
HD 166917	6.69	B8III	-			1,3
HD 170009	8.00	B2.5III	-			1,3
HD 170714	7.38	B1.5IV	264	HD 171305	HD 169581	1
HD 171219	7.65	B5III	300	HD 170200	SAO 123607	1
HD 173219	7.82	B0.5IV	-			1,3
HD 173292	8.60	B8	-			2,3
HD 173371	6.89	B7IV	-			1,3

Continued...

Table 2.3: Continued.

Be star	V	Sp.Type	$V \sin i$ $\mathrm{km\,s^{-1}}$	Comp.	Check	Notes
HD 173530	8.87	B7III	250			1,3
HD 173637	9.29	B1IV	197	HD 173693	HD 173850	1
HD 173817	8.65	B6IV	270	HD 172868	HD 173422	1
HD 174512	8	B8				2,3
HD 174513	8.70	B1.5IV	251	HD 174395	HD 174650	1
HD 174571	8.89	B1.5V	240			1,3
HD 174705	8.34	B1.5IV	331			1,3
HD 174886	7.77	B4III	-			1,3
HD 175869	5.56	B8III	-			1,3
HD 176159	8.98	B5IV	227			1,3
HD 176630	7.70	B3III	-			1,3
HD 178479	8.92	B3V	99			1,3
HD 179343	6.94	B8III	155			1,3
HD 180126	8.00	B2IV	243			1,3
HD 181231	8.58	B5IV	250	HD 182198	HD 182786	1
HD 181308	8.70	B5IV	246			1,3
HD 181367	9.36	B6IV	279	HD 182198	HD 182786	1
HD 181709	8.79	B6III	249			1,3
HD 181803	9.10	B7III	185			1,3
HD 183656	6.09	B6V	270	HD 183227	HD 183563	2
HD 184203	9.16	B9				2,3
HD 184279	6.98	B0V	230	HD 183227	HD 183563	1
HD 184767	7.18	A0III	49			1,3
HD 194244	6.14	B9III	-			1,3
HD 230579	9.10	B1IV	320			1,3
BD -094858	8.84	B1.5V	108			1,3

2.3 Notes on individual stars

Here we present some notes on all the Be stars observed at the OSN and stars observed by ASAS-3 that have shown periodicity in their light curve. We have divided the sample in stars located in the Galactic Centre and Anticentre directions.

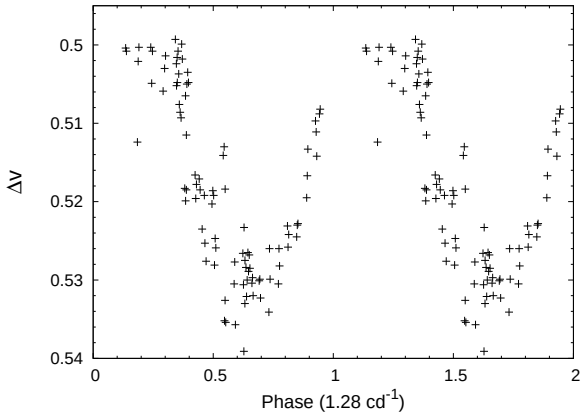

Figure 2.2: Light curve of the star HD 42259 folded in phase with the frequency 1.28 c d^{-1}, for the OSN data in the v filter.

2.3.1 Stars in the Galactic Anticentre Direction

HD 42259

The Hipparcos light curve shows variability with an amplitude from peak to peak of 6 hundredths of magnitude.

We have observed this star in 2006 at the OSN. The amplitude of the light curve varies from night to night, suggesting the presence of multi-periodicity. Strong peaks appear in the periodogram of the v filter at frequency 1.28 c d^{-1} and its one-day aliases. Results with the by filters are similar within errors. A phase plot with this frequency is displayed in Fig. 2.2. A frequency at 1.41 c d^{-1} also has a good fit and good phase diagram. The time span of the observations does not allow us to distinguish between these two frequencies. However, a frequency similar to 1.28 c d^{-1} within errors has been found in the ASAS-3 database (see below).

No long-term trend is present in the ASAS-3 light curve. Thanks to the large time span of the observations, we are able to refine the frequency found at the OSN to F1 = 1.3223 c d^{-1}(Fig. 2.3, upper panel). After prewhitening for F1, we find another significant frequency which has not been detected at the OSN, at F2 = 0.7401 c d^{-1}. The 1-day alias F2′ = 1.2626 c d^{-1} gives also a similar fit, although F2 has a less scattered phase

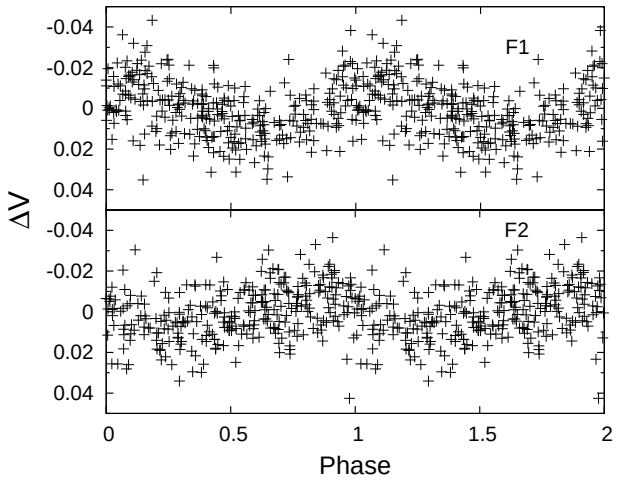

Figure 2.3: Light curve of the star HD 42259 folded in phase with the frequency F1 = 1.3223 c d^{-1} for the ASAS-3 dataset (**top**) and with the frequency F2 = 0.7401 c d^{-1} for the residuals after prewhitening for F1 (**bottom**).

diagram (Fig. 2.3, bottom panel). Note that the frequency detected at the OSN (1.28 c d^{-1}) is between F1 = 1.3223 c d^{-1} and F2$'$ = 1.2626 c d^{-1}. Therefore, we conclude that HD 42259 is multiperiodic with frequencies F1 = 1.3223 c d^{-1} and F2 = 0.7401 c d^{-1}.

HD 43285

A frequency at 2.203 c d^{-1} is detected in the Hipparcos data, although the resulting phase diagram is not very convincing.

We observed this star during only one season in 2003 at the OSN. Our light curve spanning 9 hours does not show any sign of variation at any frequency with an amplitude exceeding 2 mmag in the *vby* filters and 3 mmag in the *u* filter.

This star is saturated in the ASAS-3 database.

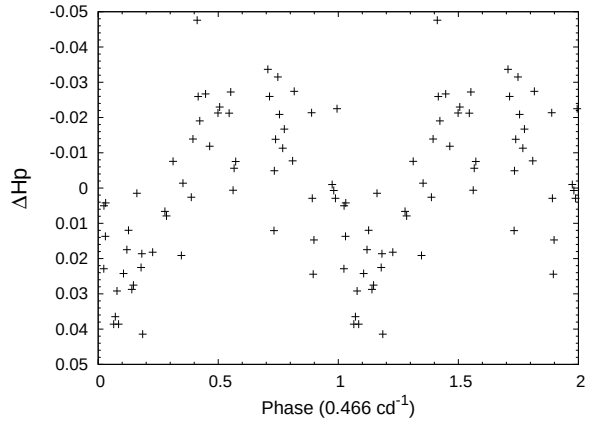

Figure 2.4: Light curve of the star HD 45901 folded in phase with the frequency 0.466 c d^{-1} for the Hipparcos dataset.

HD 45901

This star has only been observed with Hipparcos and ASAS-3.

A long-term trend is present in the Hipparcos light curve. After prewhitening for this trend, significant peaks at frequencies 0.548 c d^{-1} and 0.466 c d^{-1} are clearly detected in the periodogram. The most convincing phase diagram is obtained with frequency 0.466 c d^{-1}, which is shown in Fig. 2.4.

The ASAS-3 data show a long-term variation which we are not able to model and thus we have not searched for short-term variability in this dataset.

HD 46380

The Hipparcos light curve shows short-term variability with a frequency at 1.22 c d^{-1}.

The photometric observations collected at the OSN extend over two seasons, 2003 and 2006. The 2003 dataset confirms the variability of the star. A frequency of 3.49 c d^{-1} appears clearly in the periodogram, although it is very uncertain, due to the short time coverage (6 hours).

The light curve obtained in 2006 shows clear variability at frequency

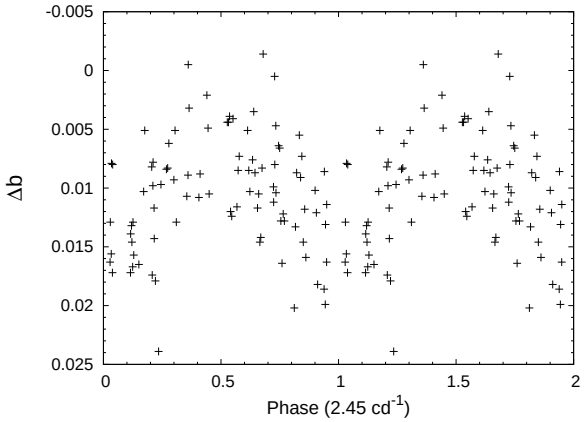

Figure 2.5: Phase diagram of HD 46484 folded with the frequency 2.45 c d^{-1} for the OSN data in the *b* filter.

1.75 c d^{-1} in all filters. The phase diagram for this frequency is very scattered, due to the fact that the semi-amplitude of the signal is 3 mmag, which is similar to the photometric precision in this season. Therefore, more observations are required to confirm this frequency.

Note that the frequency obtained in 2003 is twice the frequency found in 2006. The light curve obtained in 2006 has been folded in phase with the frequency 3.49 c d^{-1}, with a negative result.

The ASAS-3 light curve shows a long-term trend which does not allow us to search for short periods.

HD 46484

This star has been detected as spectroscopic variable by Hubert (priv. comm.). No results have been obtained with Hipparcos data, due to the bad sampling of the data and the few observed points.

Our 4-day light curve obtained in 2004 at the OSN shows variability with an amplitude from peak to peak of less than 10 mmag. A frequency at 2.45 c d^{-1} and its one-day aliases appear in the periodogram of the *vby* light curves. On the other hand, a frequency at 1.02 c d^{-1} is found in the *u* filter, which is noisier and less reliable.

The phase diagram of the *b* light curve folded with the frequency 2.45

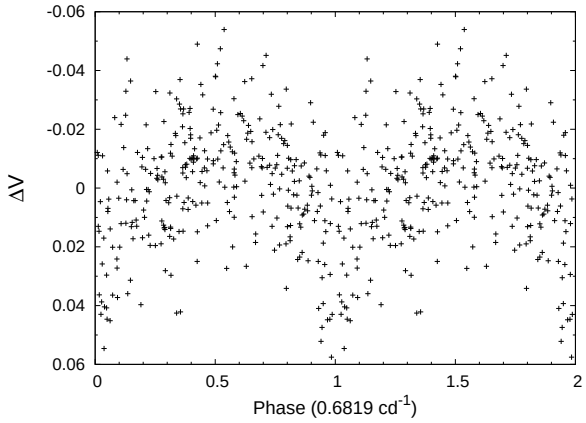

Figure 2.6: Phase diagram of HD 48282 folded with the frequency 0.6819 c d^{-1} for the ASAS-3 data.

c d^{-1} is presented in Fig. 2.5. The semi-amplitude corresponding to this frequency is of the order of 4 mmag.

This star is saturated in the ASAS-3 database.

HD 48282

A long-term trend is present in the light curve of Hipparcos and ASAS-3, which has been removed with a low-order polynomial. No results have been found with Hipparcos data. The frequency analysis of the ASAS-3 dataset yields a main variation at 0.6819 c d^{-1}. The corresponding phase diagram is very scattered, probably due to the presence of the long-term trend (Fig. 2.6). This frequency is considered as uncertain and more precise photometric data will be required to confirm it.

Unfortunately, no OSN data have been collected for this star.

HD 49330

The Hipparcos data show a clear periodicity of 0.283 d, i.e. at frequency 3.534 c d^{-1}.

This star has been observed at the OSN during three observing runs, in 2003, 2004 and 2006. In 2003, our 8.5-hour light curve presents clear

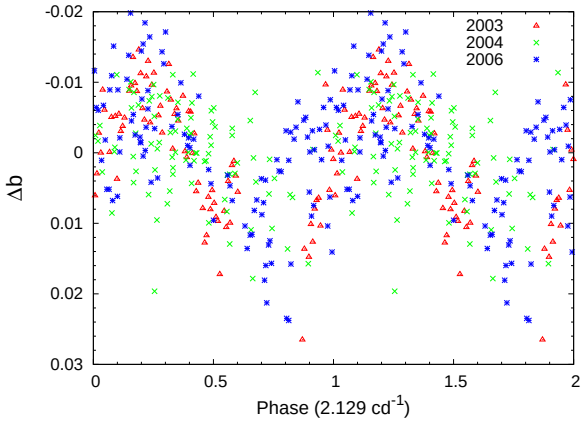

Figure 2.7: Phase diagram of the combined dataset obtained at the OSN of the star HD 49330 folded with the frequency 2.129 c d^{-1}. Triangles in red, crosses in green and asterisks in blue correspond to the 2003, 2004 and 2006 observations respectively.

variability. The short-time coverage did not allow us to perform a period search.

In 2004, our 4-day light curve did not show this variation. Only peaks at $1, 2, \ldots$ c d^{-1} are present in the periodograms of each filter, with an incoherent phase diagram.

In 2006, a frequency at 1.15 c d^{-1} and its one-day aliases strongly appear in the periodogram.

As a final check, we combined the data of the three seasons, which allowed us to detect a frequency at $f = 2.129$ c d^{-1}. This frequency is a 1-day alias of the frequency found in the 2006 data. In Fig. 2.7 we show the light curve in phase with this frequency for the three seasons with different symbols and colours. Note that this frequency has been present in the light curve over the three years, but its amplitude has changed dramatically, from 13 mmag in 2003 to 4 mmag in 2004 and 8 mmag in 2006 in the v filter. Errors in the amplitude are of the order of 1 mmag in this filter.

The light curve of ASAS-3 shows a quasi-cyclical variation of about 1600 days, disturbed by an outburst of shorter duration of about 200 days.

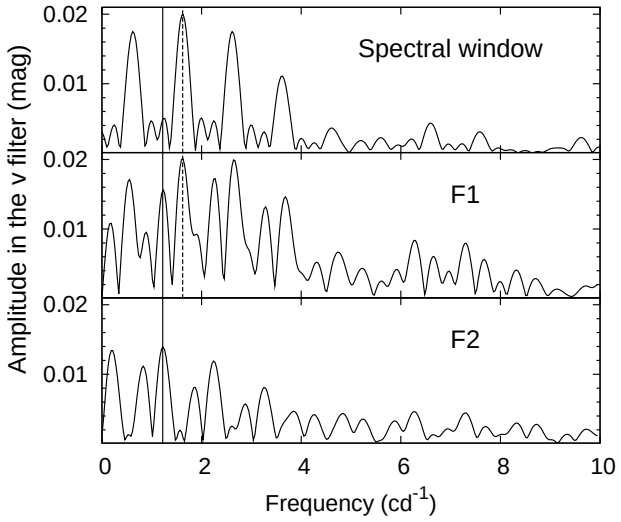

Figure 2.8: Successive periodograms and spectral window of the light curve of HD 49585 in the v filter. The dashed and solid vertical arrows stand for the position of frequencies F1 = 1.647 c d^{-1} and F2 = 1.218 c d^{-1} respectively.

We noticed that the OSN data obtained in 2003 was observed during this short outburst. In addition, this star has been included in the variable database of ASAS-3 (Pojmanski 2002). A long-period of 1676.5 d has been found, but according to the authors, this value has to be checked.

HD 49585

There are no Hipparcos data for this faint star. This star has been observed during one season at the OSN in 2004. Only detailed analysis for the v filter is provided here, since results with other filters are similar within errors. The periodogram shows strong peaks in frequency F1 = 1.647 c d^{-1} and its one-day aliases (see middle panel of Fig. 2.8). In the top panel of Fig. 2.8, we represent the spectral window of the light curve shifted at frequency F1. Another peak is present in the data at frequency

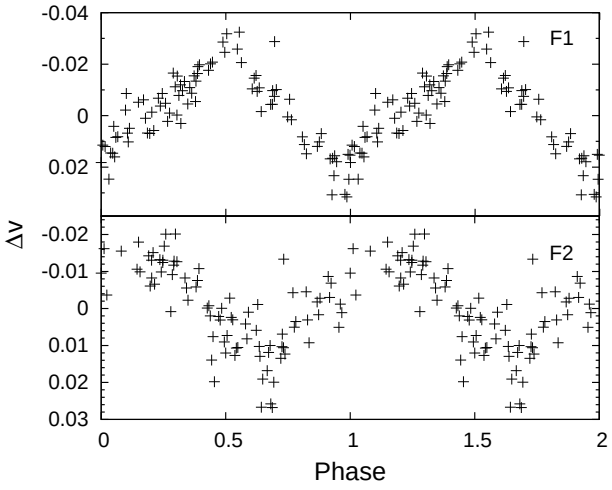

Figure 2.9: Phase plots of HD 49585 folded with the frequency F1 = 1.647 c d^{-1}, after prewhitening for F2 = 1.218 c d^{-1}(**top**) and with the frequency F2 = 1.218 c d^{-1}(**bottom**), after prewhitening for F1 = 1.647 c d^{-1}.

F2 = 1.218 c d^{-1} which is not seen in the spectral window. Periodogram of the residuals after prewhitening for frequency F1 is depicted in the lower panel of Fig. 2.8. The 1-day alias of F2 (0.21 c d^{-1}), gives a similar fit, although phase diagram for F2 is much better. The phase plots for frequencies F1 and F2 are displayed in Fig. 2.9.

In addition, this star has been included in the ASAS-3 catalogue of variable stars (Pojmanski 2002). A long-term trend is apparent in the light curve, which, according to the authors, corresponds to a period of 452.14 d. We have not been able to model this long-term trend, and thus, we have not been able to search for short-term periodicity.

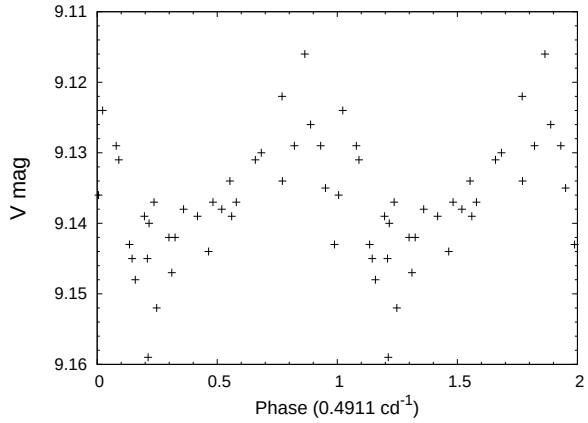

Figure 2.10: Phase diagram of HD 50087 folded with the frequency 0.4911 c d^{-1} for the ASAS-3 subset.

HD 50087

We have observed this star in 2006 at the OSN. Different frequencies are detected in the four filters with very low signal-to-noise ratio, and thus these frequencies are probably artifacts.

Using the ASAS-3 database, a frequency has been found at 0.4911 c d^{-1}. However, this frequency is detected only from JD = 2452621.7574 to 2452784.45463. The light curve does not show any significant variation before and after this range of time. In Fig. 2.10 we display the phase diagram with frequency 0.4911 c d^{-1} only for the range mentioned above for the ASAS-3 dataset. The phase diagram of the OSN data folded with this frequency is very scattered.

HD 50209

The Hipparcos data analysis yields to a frequency of 1.689 c d^{-1}, considered as uncertain. Another peak at frequency 1.47 c d^{-1} is also present, although with less amplitude.

This star has been observed during three observing runs at the OSN. The 2003 dataset shows clear variability, but the time span of 9 hours does not allow us to perform a spectral analysis. In 2004, a frequency at 1.52

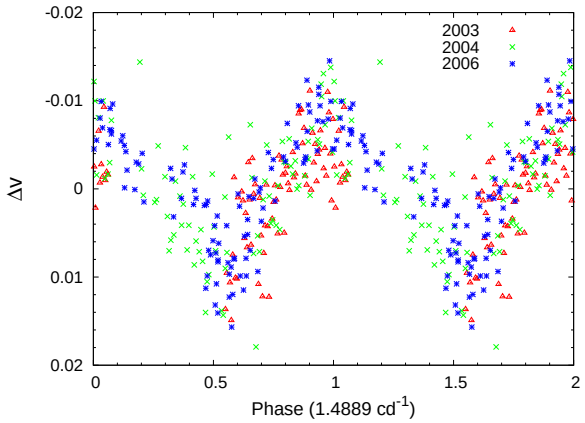

Figure 2.11: Phase plot of HD 50209 folded with the frequency 1.4889 c d^{-1} for the combined data obtained at the OSN. Triangles in red, crosses in green and asterisks in blue correspond to the 2003, 2004 and 2006 observations respectively.

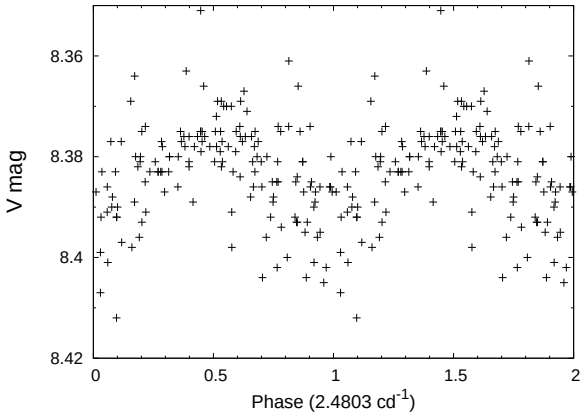

Figure 2.12: Phase plot of HD 50209 folded with the frequency 2.4803 c d^{-1} for the ASAS-3 dataset.

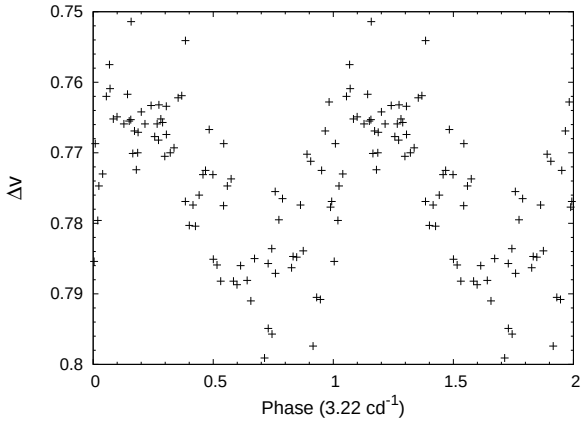

Figure 2.13: Phase plot of HD 50696 folded with the frequency 3.22 c d^{-1} for the OSN data obtained in 2004.

c d^{-1} is clearly found in all filters, while in 2006 a similar frequency at 1.48 c d^{-1} is also detected in all filters. The combined data of the three seasons allowed us to refine the frequency to 1.4889 c d^{-1}(see Fig. 2.11). Note that we removed the average magnitude of each year before combining the datasets.

The periodogram of the ASAS-3 dataset shows significant peaks at frequency 2.4803 c d^{-1} and its daily aliases. The phase plot with this frequency is depicted in Fig. 2.12. This frequency is probably a one-day alias of the frequency detected at the OSN. However, the phase diagram of the ASAS-3 dataset with the frequency 1.4889 c d^{-1} and the light curve obtained at the OSN folded with the frequency 2.4803 c d^{-1} are very scattered. This could be due to the fact that the ASAS-3 dataset contains long- and mid-term trends or to the presence of multiple periods. After prewhitening for the frequency 2.4803 c d^{-1} in the ASAS-3 dataset, a frequency at 1.4749 c d^{-1} appears in the periodogram, but the phase diagram with this frequency is not very convincing. More observational data is required to confirm the presence of multiperiodicity of this star.

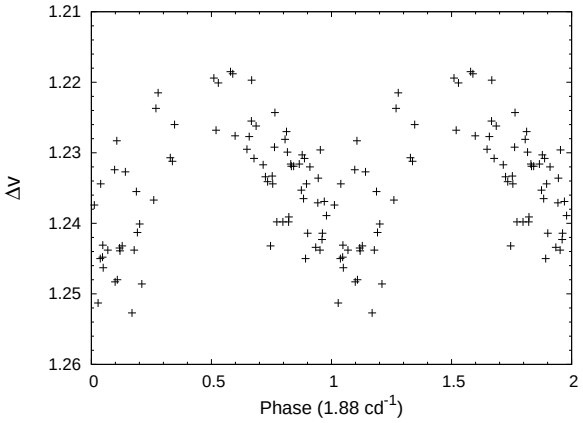

Figure 2.14: Phase plot of HD 50891 folded with the frequency 1.88 c d^{-1} for the OSN data obtained in 2004.

HD 50696

There are no Hipparcos data for this faint star. We have observed this source during two seasons at the OSN. The 2003 dataset shows clear variability, but the time span does not allow us to perform any period analysis. A clear frequency at 3.22 c d^{-1} is detected in the 2004 photometry through the four filters. We present the phase diagram, only with the v filter for clarity, in Fig. 2.13. The semi-amplitude is of the order of 12 mmag. The phase diagram of the data obtained in 2003 is compatible with this frequency.

A long-term variation is found in the ASAS-3 dataset, which stops us from searching for short-term variability.

HD 50891

There are no Hipparcos data for this star. This star has been observed only in 2004 at the OSN. The periodogram shows significant peaks at frequency 1.88 c d^{-1} and its one-day aliases for all the filters. We present the phase curve with this frequency in Fig. 2.14.

In addition, this star has been included in the ASAS-3 catalogue of variable stars (Pojmanski 2002). The authors found a long-period of 67.25

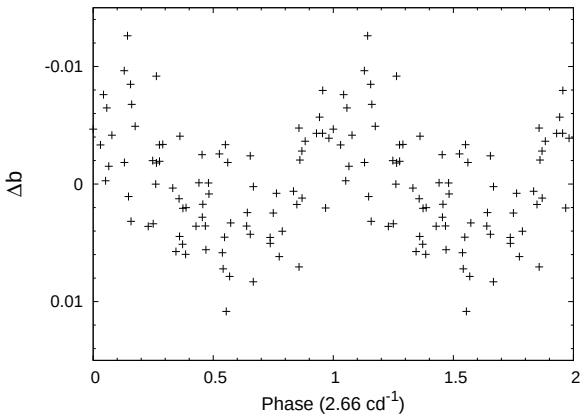

Figure 2.15: Phase plot of HD 51193 folded with the frequency 2.66 c d^{-1} in the *b* filter for the OSN data obtained in 2004.

days. We have not been able to model this long-term variation, and thus, we have not performed an analysis to detect short-term periodicity.

HD 51193

The Hipparcos light curve shows variability at frequency 1.639 c d^{-1}.

This star has been observed at the OSN in 2004 and 2006. A long-term trend is present in the light curve of 2004, which we have removed with a low-order polynomial function. We have found a frequency at 2.66 c d^{-1} in the *vby* filters, which is similar to a one-day alias of the Hipparcos frequency. Both frequencies have a similar fit, although the phase diagram with the frequency 2.66 c d^{-1} is much better (see Fig. 2.15).

In 2006, the amplitude seems to vary from night to night, as shown in Fig. 2.16. Unfortunately, we could not find any significant frequency with a coherent phase diagram.

The light curve obtained with the ASAS-3 project shows a long-term trend. After prewhitening for this trend with a low-order polynomial, a peak at frequency 1.6060 c d^{-1} and its daily aliases appear in the periodogram. The frequency fulfils the SNR criterion, but the phase diagram is very scattered. Note that this frequency is similar to the frequency detected in the Hipparcos data.

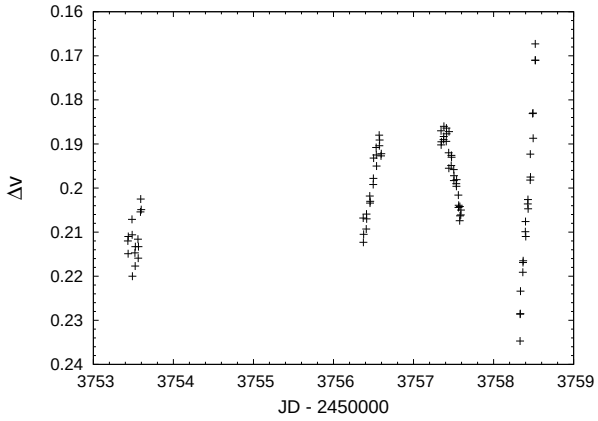

Figure 2.16: Light curve of HD 51193 for the OSN data obtained in 2006. Note the variation of the amplitude from night to night.

More photometric data are required to confirm the frequencies obtained in this chapter.

HD 51404

There are no Hipparcos data for this star. This star has only been observed in 2004 at the OSN. It is clearly variable with an amplitude from peak to peak of 0.04 mag. Strong peaks appear in the periodogram of the *vby* filters at frequency F1 = 2.68 c d^{-1} and its daily aliases. The light curve folded with this frequency is depicted in Fig. 2.17 (upper panel). After prewhitening for this frequency, another significant frequency at F2 = 5.99 c d^{-1} is detected, also in the *vby* filters. The phase plot with this frequency is displayed in the lower panel of Fig. 2.17, only for the *v* filter for clarity.

The ASAS-3 light curve shows short- and long-term variability with a rms of the observations of 24 mmag. However, no frequency is found with a convincing phase diagram.

HD 51452

There are no Hipparcos data for this star. We observed this star at the OSN in 2004. The light curve shows variability with the frequency 1.58

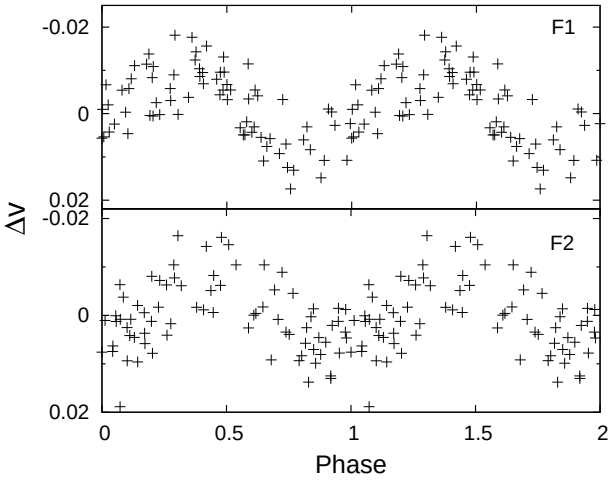

Figure 2.17: Phase plots of HD 51404 folded with the frequency F1 = 2.68 c d^{-1} after prewhitening for F2 = 5.99 c d^{-1}(**top**) and with the frequency F2 = 5.99 c d^{-1} after prewhitening for F1 = 2.68 c d^{-1} (**bottom**) in the v filter of the 2004 dataset.

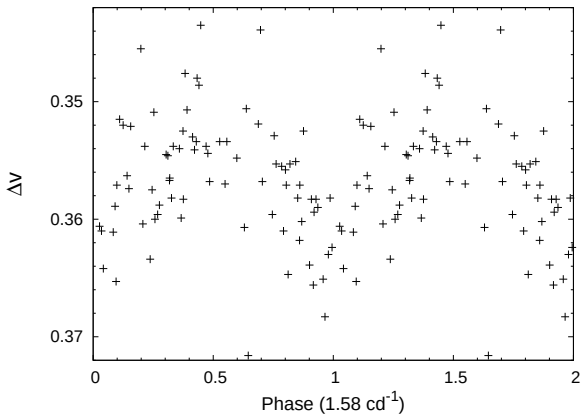

Figure 2.18: Phase plot of HD 51452 folded with the frequency 1.58 c d^{-1} in the v filter for the OSN data.

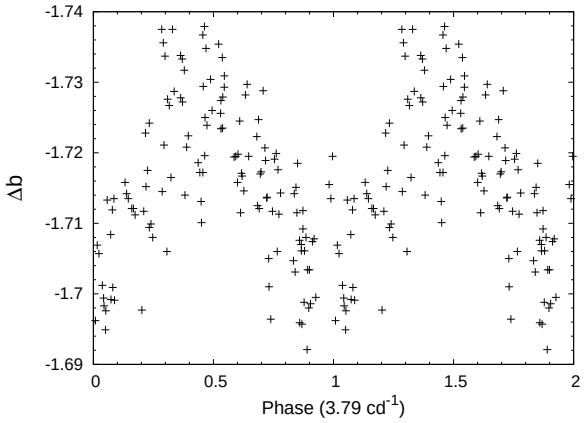

Figure 2.19: Phase plot of HD 170 714 folded with the frequency 3.79 c d^{-1} in the b filter for the OSN data.

c d^{-1}, but only in the v filter, and thus, this frequency is considered as uncertain. The phase diagram with this frequency is displayed in Fig. 2.18.

2.3.2 Stars in the Galactic Centre Direction

HD 170 714

The few datapoints collected by the Hipparcos mission for this star do not allow us to search for short-term variability.

This star was observed at the OSN in 2005. Strong peaks at frequency 3.79 c d^{-1} and its one-day aliases appear in the periodogram of all the filters. The semi-amplitude corresponding to this frequency is 10 mmag for the *vby* filters (±1 mmag) and 13 for the u filter (±2 mmag). In Fig. 2.19 we represent the light curve folded in phase with the detected frequency for the b filter.

This star is saturated in the ASAS-3 dataset.

HD 171 219

This star is classified as constant in the Hipparcos catalogue. We have re-analysed the light curve and no short-term variability has been found. We have observed this star at the OSN during two seasons, in 2002 and

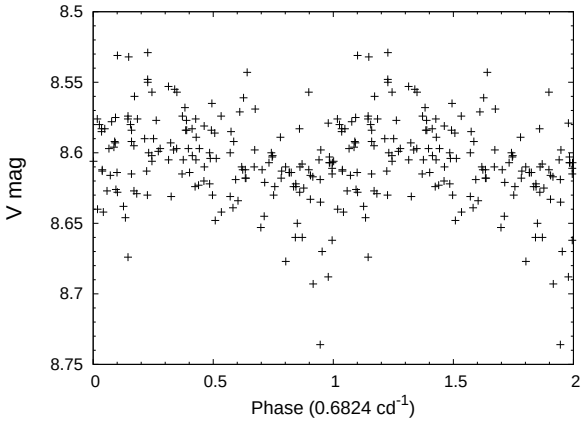

Figure 2.20: Phase plot of HD 173 292 folded with the frequency 0.6824 c d^{-1} for the ASAS-3 dataset.

2003. The periodograms of both datasets do not show any significant peak greater than 2 mmag. We conclude that the star is not variable at our detection level.

HD 173 292

The Hipparcos data show short-term variability with an amplitude of 0.1 magnitude from peak to peak. However, no frequency has been detected in the Fourier analysis.

The spectral analysis of the ASAS-3 dataset shows peaks at frequency 0.6824 c d^{-1} and its daily aliases. A phase diagram with this frequency is depicted in Fig. 2.20.

This star has not been observed at the OSN.

HD 173 530

There are no Hipparcos data for this faint star. A significant peak at frequency 1.3703 c d^{-1} appears in the periodogram of the ASAS-3 light curve with a semi-amplitude of 6 mmag. A phase diagram for this frequency is plotted in Fig. 2.21.

This star has not been observed at the OSN.

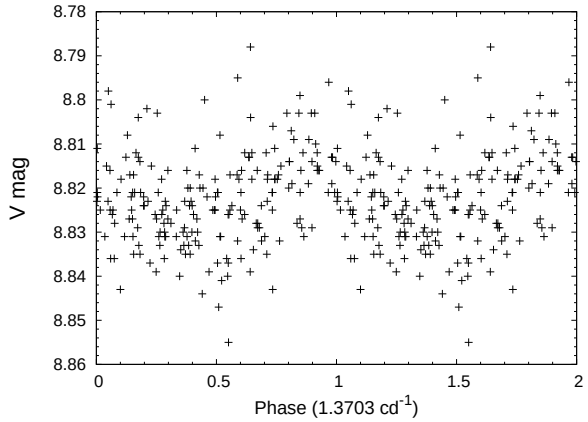

Figure 2.21: Phase plot of HD 173 530 with the frequency 1.3703 c d^{-1} for the ASAS-3 dataset.

HD 173 637

The Hipparcos data show a long-term variation, which does not allow us to search for short-term periodicity.

This star has been observed at the OSN during two seasons, in 2003 and 2005. However, only 19 datapoints has been obtained in 2005 and therefore no result can be achieved with this dataset.

Short-term variability is found in the 2003 dataset. We detect significant peaks in the frequency domain: 1.87 c d^{-1} and its one-day aliases. The semi-amplitude of this frequency is of the order of 5 mmag in the *vby* filters and the SNR is 4.80. In Fig. 2.22 we display the phase diagram with this frequency in the *b* filter.

This star is included in the ASAS-3 catalogue of variable stars (Pojmanski 2002). A long-term trend is present in the light curve (Fig. 2.23), superimposed on which we see several outburst (at least 3) with an amplitude of 0.1 mag and a time difference of around 360 to 380 days. We have not searched for short-term periodicity because of the complexity of the light curve.

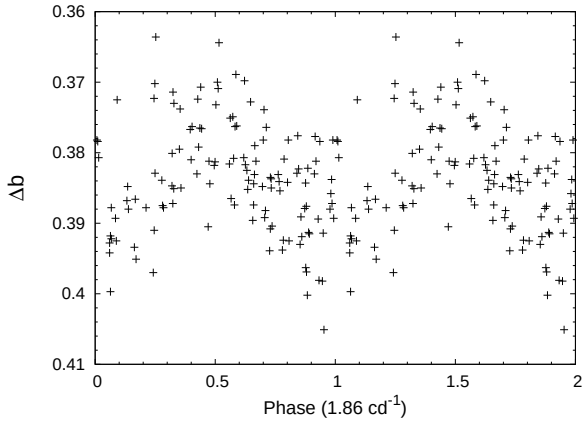

Figure 2.22: Phase plot of HD 173 637 folded with the frequency 1.87 c d^{-1} in the *b* filter for the OSN data.

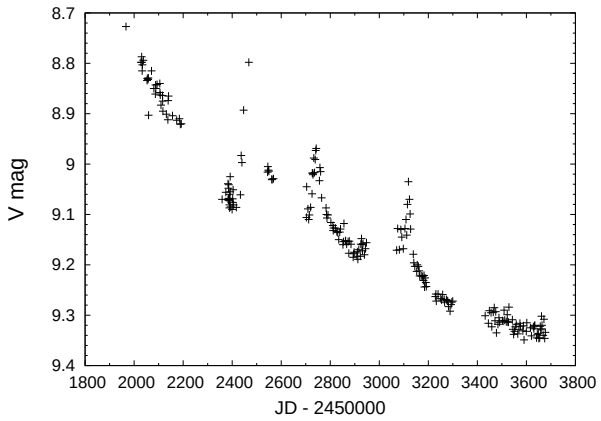

Figure 2.23: Light curve of HD 173 637 for the ASAS-3 dataset.

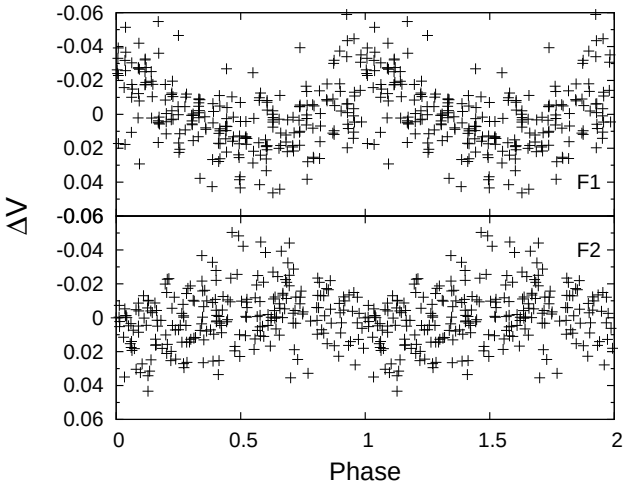

Figure 2.24: Phase plot of HD 174 513 folded with the frequency F1 = 0.0271 c d^{-1}, after prewhitening for F2 = 5.293 c d^{-1}(**top**) and with the frequency F2 = 5.293 c d^{-1}, after prewhitening for F1 = 0.0271 c d^{-1}(**top**) for the ASAS-3 dataset.

HD 173 817

The Hipparcos light curve does not show any sign of variability.

This star has been observed at the OSN in 2003. The light curve shows short-term variability with the frequency 3.51 c d^{-1} in the *vby* filters, which fulfils the SNR criterion. However, the semi-amplitude is of the order of 3 mmag and thus, the phase curve is very scattered.

A long-term trend is present in the ASAS-3 light curve. We do not find short-term variability after removing the long-term variation. The frequency found at the OSN is not detected in the ASAS-3 dataset, probably due to the fact that the ASAS-3 data have lower precision. More observational data are required to confirm the periodicity of this star.

HD 174 513

Long- and short-term variations are found in the Hipparcos light curve. However, the frequency analysis does not yield to any frequency with a coherent phase diagram.

The analysis of the dataset obtained at the OSN in 2002 confirms its variability with frequencies at 3.34 c d^{-1} and its one-day aliases. However, this frequency is very uncertain due to the low amplitude (4 mmag) and the few observed datapoints.

In the ASAS-3 dataset, a long-term trend is present, which we removed with a low-order polynomial. The periodogram of the residual shows a strong peak at the low-frequency F1 = 0.0271 c d^{-1}(i.e. 36.90 d) and its daily aliases. A phase plot for this frequency is displayed in the upper panel of Fig. 2.24. This frequency is too short to be produced by pulsations and so it is probably caused by a binary component. Prewhitening for this frequency, we found an additional significant high-frequency at F2 = 5.293 c d^{-1}, which is similar to a 1-day alias of frequency found at the OSN (3.34 c d^{-1}). A phase diagram of this frequency is plotted in the lower panel of Fig. 2.24. More photometric data are required to confirm the frequency F2.

HD 174705

Neither Hipparcos nor OSN data for this star. The ASAS-3 light curve contains individual subsets with different mean magnitudes due to the fact that the star has been observed in several different fields, as pointed out by the authors of the catalogue. Therefore, the mean magnitude has first been subtracted from each subset and then the subsets have been combined. In the periodogram of the combined dataset, a significant peak appears at frequency 2.3164 c d^{-1}. The light curve folded in phase with this frequency is displayed in Fig. 2.25.

HD 181231

The Hipparcos data do not show any indication of variability.

We observed this star at the OSN in 2003. Unfortunately, the comparison star HD 182 786 showed variability during the observing run, and thus no reliable result can be obtained with this comparison star. Using the

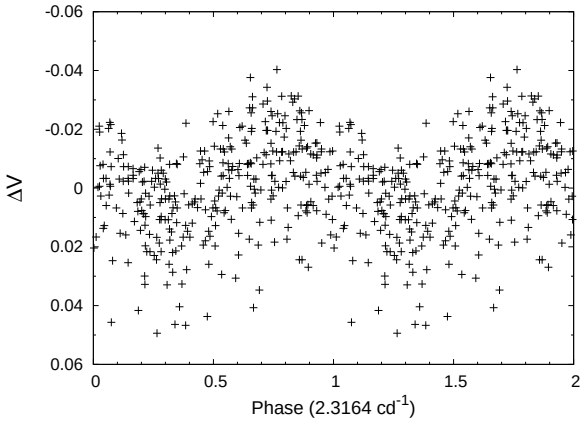

Figure 2.25: Phase plot of HD 174 705 folded with the frequency 2.3164 c d^{-1} for the ASAS-3 dataset.

check star HD 182 198, a significant peak appears in the periodogram of all filters at frequency 0.67 c d^{-1}, but the phase coverage is not complete. In addition, we have analysed photometric data obtained by Ennio Poretti at San Pedro Martir (SPM). HD 181414 was used in the differential photometry as the comparison star. Frequency 0.67 c d^{-1} is also detected in the *vby* filters. The semi-amplitude associated to this frequency is 4 and 3 mmag at the OSN and SPM respectively.

We also performed a detailed analysis of the ASAS-3 light curve, which shows short-term variability with the frequency 3.4304 c d^{-1}. However, this frequency is considered as uncertain due to the low value of the associated semi-amplitude (5 mmag). The ASAS-3 dataset has also been plotted in phase with the frequency 0.67 c d^{-1}, resulting in a scattered diagram.

The periodogram of the combined data (OSN, SPM, ASAS-3) yields a frequency of 0.6425 c d^{-1}. However, the phase diagram has a large scatter and therefore, we cannot confirm this frequency.

HD 181 367

There are no Hipparcos data for this star. No short variability is found in the light curve obtained at the OSN in 2003 with a semi-amplitude

exceeding 4 mmag. The same conclusions have been reached by Ennio Poretti (priv. comm.) in the analysis of SPM data for this star.

The ASAS-3 light curve shows a long-term trend, which has been removed with a low-order polynomial. A frequency at 1.22 c d^{-1} is detected, although with very low amplitude and with a SNR of 3.6. We conclude that this frequency is probably an artifact and further observations are required to confirm the periodicity of the star.

HD 183 656

HD 183 656 is a spectroscopic binary shell star (SB1) with an orbital period of 214.75 d (Koubsky et al. 1989). This star was found variable by Lynds (1960), who proposed a period of 0.8518 d (i.e. 1.1740 c d^{-1}). Short-term variability with a period of 0.652 d (i.e. 1.534 c d^{-1}) was obtained from the Hipparcos photometry (Hubert and Floquet 1998).

We observed this star at the OSN in 2003 and 2005. In the periodogram of the 2003 light curve, the most powerful peak appears at frequency 2.19 c d^{-1}. The phase diagram folded with the frequency 2.19 c d^{-1} is not very convincing. Note that the 1-day alias of this frequency is Lynds' period. However, the Hipparcos data appear very noisy when folded with any of the two frequencies.

The 10-day light curve obtained in 2005 shows a long-term trend, which has been removed by a low-order polynomial function. After prewhitening for this trend, a significant peak appears at frequency 3.63 c d^{-1} in the periodogram of the light curve in the *vby* filters with a semi-amplitude of 7 mmag (Fig. 2.26). The 2.19 c d^{-1} frequency is not detected in the 2005 data. More observations with a longer timescale are needed to confirm this frequency.

This star is saturated in the ASAS-3 database.

HD 184 279

Percy et al. (2002) performed an autocorrelation analysis of the Hipparcos data for this star and found a period of 0.6 days (i.e. 1.667 c d^{-1}), which they presented as uncertain. A re-analysis of the Hipparcos data with the methods explained above yields a period of 0.156 d (i.e. 6.410 c d^{-1}), although the phase diagram is not very convincing.

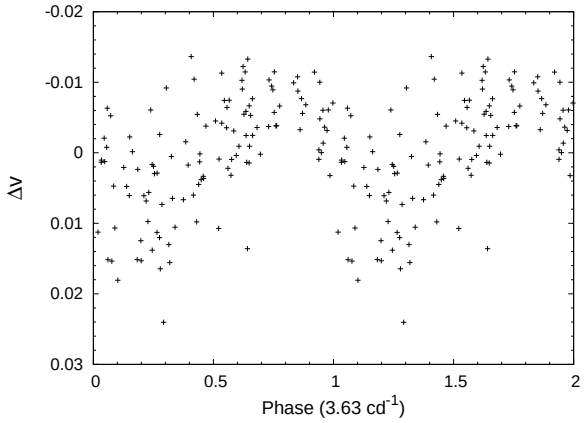

Figure 2.26: Residuals of HD 183 656 in phase with the frequency 3.63 c d^{-1}, after removing the long-term trend.

We observed this star at the OSN in 2003 and 2005. The periodogram of the 2003 dataset shows a peak at frequency 1.38 c d^{-1}, but due to the few points of the sample, we cannot confirm this frequency. The 3-night light curve obtained in 2005 confirms the presence of short-term variability for this star. However, frequencies found in the spectral analysis have very scattered phase diagrams and thus are very uncertain.

This star is included in the ASAS-3 catalogue of variable stars (Pojmanski 2002). A long period of 332.16 d has been found. Unfortunately, the long-term trend does not allow us to search for short-period variability. In Fig. 2.27 we show the light curve for the ASAS-3 data.

We conclude that this star is variable, but more observations are needed to confirm the periodicity.

2.4 Discussion

A summary of the results obtained in this chapter is given in Tables 2.4 and 2.5. These tables show that the results obtained with the three datasets are compatible in most cases. When different results have been found, the higher precision of the instrument, the more reliable the detection. Therefore, results obtained with OSN data are the most reliable

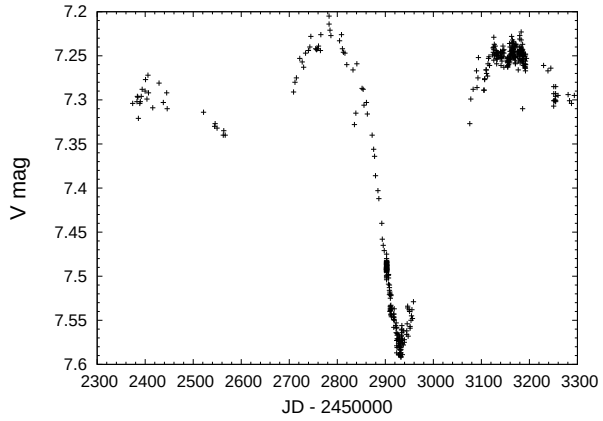

Figure 2.27: Light curve of HD 184 279 for the ASAS-3 data.

ones, followed by frequencies found with Hipparcos and ASAS-3 datasets.

Stars showing short-term variability with an amplitude from peak to peak of more than 0.04 magnitudes during several days, are considered as variable, even if we have not found a frequency with a convincing phase diagram.

Mid- and long-term variability is often present in the light curves of Be stars, and this fact makes the detection of short-term variability more difficult. In the Hipparcos and ASAS-3 datasets, the long-term variations have been removed by fitting low-order polynomial functions when possible, but we have not been able to prewhiten for the mid-term trends (for e.g. outbursts). For some of these stars we have not been able to perform a short-period analysis due to the mid or long-term variation, to the bad sampling or few datapoints of the light curve have been labelled with a '-' symbol in Tables 2.4 and 2.5.

HD 46380, HD 50087, HD 51452, HD 173817, HD 181231 and HD 184279 would require more observations to confirm the frequency presented in this work and are marked in Tables 2.4 and 2.5 with a '?'.

Table 2.4: Results of the photometric study for stars in the Galactic Anticentre direction. Frequencies in c d^{-1} are shown for the Hipparcos, OSN and ASAS-3 datasets. The '-' stands for stars for which a short-period analysis could not be performed. The '*' stands for stars that have not been observed with this instrument. The '**' stands for stars that are saturated in the ASAS-3 database. The 'var' stands for stars showing short-term variability but not periodicity. The 'no var' stands for stars that do not show short-term variations at the detection level of the instrument. The '?' stands for frequencies which are uncertain. For details, see text. Notes: (1) - Star included in the ASAS-3 catalogue of variable stars (Pojmanski 2002); (2) - Lynds (1960); (3) - Percy et al. (2002) ; (4) - Neiner et al. (2005)

Be star	Hipparcos	OSN	ASAS-3	Notes
HD 42259	var	1.28	1.3223 + 0.7401	
HD 42406	-	*	no var	
HD 43264	-	*	**	
HD 43285	2.203	no var	**	
HD 43777	-	*	no var	
HD 43913	-	*	no var	
HD 44783	-	*	**	
HD 45260	var	*	-	long-term
HD 45626	*	*	-	
HD 45901	0.548/0.466	*	-	long-term
HD 45910	-	*	**	
HD 46380	1.22	1.75 ?	-	
HD 46484	-	2.45	**	
HD 47054	no var	*	**	
HD 47160	-	*	**	
HD 47359	*	*	-	
HD 47761	-	*	-	outbursts
HD 48282	-	*	0.6819	long-term
HD 49330	3.534	2.129	-	(1)
HD 49567	0.39	*	**	0.39 (4)
HD 49585	*	1.65 + 1.21	-	(1)
HD 49787	-	*	**	
HD 49992	*	*	var	
HD 50083	-	*	**	long-term
HD 50087	-	no var	0.4911 ?	
HD 50209	1.689/1.47	1.4889	2.4803+1.4749 ?	
HD 50424	*	*	-	long-term

Continued...

Table 2.4: Continued.

Be star	Hipparcos	OSN	ASAS-3	Notes
HD 50581	no var	*	**	
HD 50696	*	3.22	-	long-term
HD 50820	no var	*	**	
HD 50868	-	*	no var	long-term
HD 50891	*	1.88	-	(1)
HD 51193	1.639	2.66	1.606	
HD 51404	*	2.68 + 5.99	var	
HD 51452	*	1.58 ?	no var	
HD 51506	-	*	**	
HD 53085	-	*	**	long-term
HD 53367	-	*	**	long-term
HD 54464	*	*	-	long-term
HD 55135	-	*	**	
HD 55439	-	*	-	outbursts
HD 55606	*	*	no var	
HD 55806	-	*	no var	long-term
HD 57386	-	*	no var	
HD 57539	-	*	**	long-term
HD 259431	-	*	no var	
HD 259440	*	*	no var	
HD 259597	*	*	no var	
HD 293396	*	*	-	long-term

Table 2.5: Same as for Table 2.4, but for stars in the Galactic Centre direction.

Be star	Hipparcos	OSN	ASAS-3	Notes
HD 166 917	no var	*	**	
HD 170 009	no var	*	*	
HD 170 714	-	3.79	**	
HD 171 219	no var	no var	**	
HD 173 219	var	*	**	
HD 173 292	var	*	0.6824	
HD 173 371	no var	*	**	
HD 173 530	*	*	1.3703	

Continued...

Table 2.5: Continued.

Be star	Hipparcos	OSN	ASAS-3	Notes
HD 173 637	-	1.87	-	(1)
HD 173 817	no var	3.51 ?	no var	
HD 174 512	0.82	*	no var	0.82 (4)
HD 174 513	-	3.34 ?	0.0271 + 5.293	long-term
HD 174 571	-	*	-	
HD 174 705	*	*	2.3164	
HD 174 886	no var	*	**	
HD 175 869	no var	*	**	
HD 176 159	-	*	no var	long-term
HD 176 630	1.59	*	**	1.59 (4)
HD 178 479	-	*	-	long-term
HD 179 343	-	*	**	
HD 180 126	-	*	-	outbursts
HD 181 231	no var	0.67?	3.4304?	
HD 181 308	*	*	-	
HD 181 367	*	no var	-	
HD 181 709	no var	*	no var	
HD 181 803	-	*	-	
HD 183 656	1.534	3.63	**	1.1739 (2)
HD 184 203	*	*	-	
HD 184 279	6.410 ?	var	**	(1); 1.667 (3)
HD 184 767	-	*	**	
HD 194 244	no var	*	**	
HD 230 579	*	*	no var	
BD -094858	*	*	-	

2.4.1 Degree of variability

We have investigated the degree of short-term variability, as Hubert and Floquet (1998) did with a larger sample of Be stars based on Hipparcos data. As Hubert and Floquet (1998) claimed, the degree of variability depends on the temperature of the star. In our case, we only distinguished between early (B0-B3) and mid- to late-type Be stars (B4-B9), due to the smaller number of star included in the sample. It has been found that short-term variability is present in 77% of early-type Be stars and 26% of

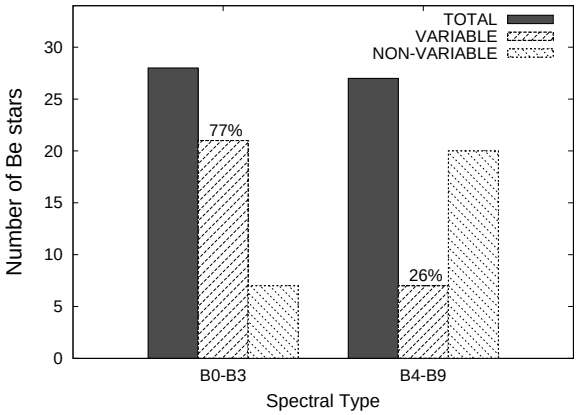

Figure 2.28: Distribution of short-term variability as a function of spectral type for stars in our sample.

mid- to late-type Be stars (see Fig. 2.28). The results presented here are compatible with those obtained by Hubert and Floquet (1998).

2.4.2 Location in the HR diagram

The theoretical HR diagram constructed with results obtained in this work is shown in Fig. 2.29. Only 39 Be stars of our sample have their fundamental parameters determined. Values of $\log L/L_{\odot}$ and $T_{\rm eff}$ of the majority of the stars are taken from Frémat et al. (2006), assuming $\Omega/\Omega_{\rm c}$= 0.90, which is the average angular velocity rate of galactic field Be stars (Frémat et al. 2005). Only for the star HD 48282, the spectral parameters are taken from the paper by Levenhagen and Leister (2004), in which the authors did not take into account high rotational effects. We have adopted the theoretical boundaries of the β Cephei and SPB instability strips from the work by Pamyatnykh (1999).

Two different symbols have been used to distinguish between variable (filled square) and non-variable stars (asterisk). The diagram clearly shows two separated groups, corresponding to early (<B3) and to mid- to late-type Be stars, which are located close or inside the β Cephei and SPB instability strips respectively. Observations and theoretical models are compatible in most of the cases: the majority of the variable stars are

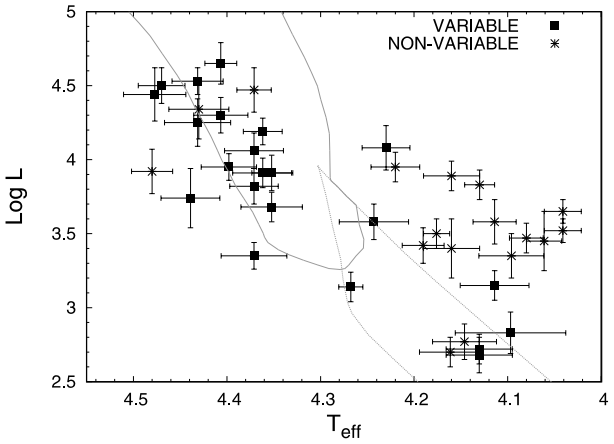

Figure 2.29: Location of the studied Be stars in the theoretical HR diagram. Filled squares correspond to variable stars and asterisks to non-variable stars. The solid and dashed lines describe the theoretical β Cephei and SPB instability strips for $Z = 0.02$ respectively, computed by Pamyatnykh (1999).

inside the instability strips (18 of 22) and the majority of the non-variable stars are outside the instability strips (12 of 17). This points towards the interpretation that Be stars are the fast-rotator counterparts of β Cephei and SPB stars.

In addition, the majority of the studied early Be stars are inside the β Cep instability strip as late Be stars are generally outside the SPB region. It would indicate that *nrp* are not efficient in mass-loss events for late Be stars. Therefore, the mechanism responsible for the formation of the circumstellar envelope could be different for early and late Be stars.

We have investigated the average frequency of the two groups of Be stars, the β Cephei-like and the SPB-like ones. A value of 2.22 ± 1.3 c d^{-1} is found for early-type Be stars, and a value of 1.44 ± 1.1 c d^{-1} for mid- to late-type Be stars.

2.4.3 Selected Be stars in the seismology fields

Fields which will be observed with COROT have already been selected based on the parameters of the potential targets. Only Be stars located in these fields can still be chosen as secondary targets and would then be observed by COROT. Table 2.6 summarises the Be stars that are candidates as secondary targets for being in the seismology fields close to the selected primary targets. In bold we show the Be stars which have high probability to be selected. Six early Be stars and one mid-type Be stars are included in the list.

Be stars that will not be observed as secondary targets in a long run can be proposed as targets for short runs.

2.5 Conclusions

We studied the short-term variability of all the Be stars located in the seismology fields of COROT. Light curves gathered by Hipparcos and ASAS-3 projects and observed at the OSN have been analysed in detail. An amount of 28 stars have been detected as variable and 27 are considered as non-variable at the detection level of the instruments. Moreover, among the 28 variable stars, four are found to be bi-periodic.

As shown in Table 2.4 and 2.5, results with the three datasets are compatible in most cases. ASAS-3 has been demonstrated as a useful tool to find periodicity, and in some cases, multiperiodicity. Recently, Pigulski (2005) found 14 β Cephei stars using the ASAS-3 database, detecting in some cases up to 4 modes.

We have detected short-term variability in 77% of the early Be stars and in only 26% of mid- to late-type Be stars, which is compatible with the results obtained by Hubert and Floquet (1998). In addition, the majority of variable stars are located in the instability strips computed by Pamyatnykh (1999). This would confirm that Be stars are the fast-rotator counterparts of β Cephei and SPB stars.

Finally, we give a list of Be stars that have high probability to be selected as secondary targets for the COROT mission. Seven of eight of these stars are considered variable in this chapter. In particular, HD 49330 shows a frequency with variable amplitude, HD 50209 is probably bi-periodic and the light curve of HD 51193 shows variable amplitude from

Table 2.6: Be stars close to primary COROT target candidates, which could be selected as secondary targets. Stars in bold have high probability to be observed by COROT.

Be Star	V	Sp. Type	COROT Field
Galactic Anticentre direction			
HD 43285	6.05	B5 IV	*LRA3* HD 43587
HD 43913	7.88	A0	*LRA3* HD 43587
HD 49330	8.95	B0.5 IV	*LRA1* HD 49933 & HD 49434
HD 49567	6.15	B3 III	*LRA1* HD 49933 & HD 49434
HD 49585	9.13	B0.5 IV	*LRA1* HD 49933 & HD 49434
HD 50087	9.08	B8 III	*LRA1* HD 49933 & HD 49434
HD 50209	8.36	B8 IV	*LRA1* HD 49933 & HD 49434
HD 50820	6.27	B3 IV	*IR01*
HD 50891	8.88	B0.5 V	*LRA2* HD 52265
HD 51193	8.06	B1.5 IV	*LRA2* HD 52265
HD 51404	9.30	B1.5 V	*LRA2* HD 52265
HD 51452	8.08	B0 IV	*LRA2* HD 52265
Galactic Centre direction			
HD 171 219	7.65	B5 III	*LRC3* HD 170 580
HD 171 219	7.65	B5 III	*LRC2* HD 171 834
HD 181 231	8.58	B5 IV	*LRC1* HD 181555 & HD 180642

night to night. The longer timescale, the larger duty cycle over the whole observing time, and the high precision of COROT will allow us to refine the actual periods and to detect many more.

Bibliography

Breger, M., Stich, J., Garrido, R., Martin, B., Jiang, S. Y., Li, Z. P., Hube, D. P., Ostermann, W., Paparo, M., and Scheck, M.: 1993, *A&A* **271**, 482

Frémat, Y., Neiner, C., Hubert, A.-M., Floquet, M., Zorec, J., Janot-Pacheco, E., and Renan de Medeiros, J.: 2006, *A&A* **451**, 1053

Frémat, Y., Zorec, J., Hubert, A.-M., and Floquet, M.: 2005, *A&A* **440**, 305

Hubert, A. M. and Floquet, M.: 1998, *A&A* **335**, 565

Jaschek, M. and Egret, D.: 1982, in M. Jaschek and H.-G. Groth (eds.), *IAU Symp. 98: Be Stars*, p. 261

Koubsky, P., Harmanec, P., Gulliver, A. F., Ballereau, D., and Chauville, J.: 1989, *Bulletin of the Astronomical Institutes of Czechoslovakia* **40**, 31

Lampens, P., Frémat, Y., Garrido, R., Peña, J. H., Parrao, L., van Cauteren, P., Cuypers, J., de Cat, P., Uytterhoeven, K., Arentoft, T., and Hobart, M.: 2005, *A&A* **438**, 201

Lenz, P. and Breger, M.: 2005, *Communications in Asteroseismology* **146**, 53

Levenhagen, R. S. and Leister, N. V.: 2004, *AJ* **127**, 1176

Lynds, C. R.: 1960, *ApJ* **131**, 390

Montgomery, M. and O'Donoghue, D.: 1999, *Delta Scuti Newsletter* **13**, p28

Neiner, C., Hubert, A.-M., and Catala, C.: 2005, *ApJS* **156**, 237

Pamyatnykh, A. A.: 1999, *Acta Astronomica* **49**, 119

Percy, J. R., Hosick, J., Kincaide, H., and Pang, C.: 2002, *PASP* **114**, 551

Perryman, M. A. C., Lindegren, L., Kovalevsky, J., Hoeg, E., Bastian, U., Bernacca, P. L., Crézé, M., Donati, F., Grenon, M., van Leeuwen, F., van der Marel, H., Mignard, F., Murray, C. A., Le Poole, R. S., Schrijver, H., Turon, C., Arenou, F., Froeschlé, M., and Petersen, C. S.: 1997, *A&A* **323**, L49

Pigulski, A.: 2005, *Acta Astronomica* **55**, 219

Pojmanski, G.: 2002, *Acta Astronomica* **52**, 397

Schwarzenberg-Czerny, A.: 1991, *MNRAS* **253**, 198

Vaníček, P.: 1971, *Ap&SS* **12**, 10

Zerbi, F. M., Garrido, R., Rodriguez, E., Krisciunas, K., Crowe, R. A., Roberts, M., Guinan, E. F., McCook, G. P., Sperauskas, J., Griffin, R. F., and Luedeke, K. D.: 1997, *MNRAS* **290**, 401

Chapter 3

Multiperiodic Pulsations in the Be Stars NW Ser and V1446 Aql

3.1 Introduction

Short-term variability is present in a large fraction of Be stars. Baade (1982) attributed the short periodic *lpv* to non-radial pulsations (*nrp*), whereas Balona (1990) argued that periods are better explained as rotational modulation. The detection of photospheric multiperiodicity, and in particular, the detection of multiperiodicity in a photometric light curve, constitutes an evidence of the non-radial pulsations hypothesis. During last few years, Walker et al. (2005a,b) have found multiple periods in some Be stars thanks to the analysis of the high-precision photometric data of the MOST satellite. These results point towards the *nrp* model.

In a similar manner, COROT will provide ultra high precision photometric data which will allow us to conclude on this issue. In preparation for the COROT mission, a sample of Be stars have been photometrically studied in order to select the most suitable candidates (see Chapt. 2). It is important to note that several multiperiodic Be stars have already been detected and are presented in Chapt. 2.

In the two following chapters, we present an in-depth analysis of two Be stars, namely NW Ser and V1446 Aql, which have shown evidence of

multiperiodicity in their light curves.

NW Ser (HR 6873, HD 168797, V=6.14) is a bright and extensively observed B2.5IIIe star, which has been photometrically monitored for over two decades. From the analysis of the Hipparcos photometric data, several authors have obtained similar results: Hubert and Floquet (1998) found short-term variability with a period of 0.488 days; Percy et al. (1999) reanalysed the Hipparcos data together with ground-based photometry finding a similar period of 0.46 days, as well as a longer period of 5.5 days; and finally, two periods (0.475 and 0.406 days) have been detected by Aerts (2000) using only Hipparcos data, although the author claimed that this finding should be confirmed by means of ground-based observations.

V1446 Aql (HD 179405, B2IVe) has been observed to be an emission-line star in the Mount Wilson objective prism all-sky survey. It appears as an irregular variable star from the Hipparcos data, which led to its inclusion in the GCVS (Kazarovets et al. 1999), although no short-term periodic variability had been detected so far.

3.2 Observations and frequency analysis

Observations have been obtained with the 0.9 m telescope of the Observatorio de Sierra Nevada (OSN, Granada, Spain) between July 1 and 9 in 2003. The instrument used is an automatic four-channel photometer, which allows simultaneous observations through the four *uvby* filters of the Strömgren photometric system. The data discussed here are the differential magnitude in the instrumental system between the variable and the comparison star of Table 3.1. A check star was also observed in order to check possible intrinsic variations of the comparison star. Data have been corrected for sky background and atmospheric extinction. Table 3.2 shows the photometric precision as given by the standard deviation of the difference between the comparison and check stars for the whole campaign for each filter. The light curves of the stars are depicted in Figs. 3.1 and 3.3, only the v filter is shown for clarity.

A period analysis has been performed by means of standard Fourier analysis and least-square fitting. We have employed the same techniques as those explained in Chapt. 2. It is important to highlight the use of the non-linear multi-parameter fitting code based on Vaníček (1971), since

Table 3.1: Comparison and check stars for differential photometry.

	Star	V	Spectral Type
variable	NW Ser	6.14	B2.5IIIe
comparison	HD 170 200	5.71	B8III-IV
check	SAO 123 607	8.6	B8
variable	V1446 Aql	9.12	B2IVe
comparison	HD 179 846	8.29	B8
check	HD 178 598	9.45	B8

Table 3.2: Photometric precision.

Star	filter u	filter v	filter b	filter y
NW Ser	0.010	0.005	0.005	0.005
V1446 Aql	0.011	0.007	0.007	0.008

this code is very well-suited for our case, with daily aliases present in the periodogram. We have to note here that the final frequency solution can be contaminated by 1 c d^{-1} aliases.

The way in which we determine whether the frequencies are statistically significant or not is also described in Chapt. 2.

Frequencies, amplitudes and phases obtained for NW Ser and V1446 Aql are presented in Tables 3.3 and 3.4 respectively and for the four Strömgren bands. We also show the total fraction of the variance removed from the signal (R), the signal to noise ratio and the σ of the final residual σ_{res}. In Figs. 3.2 and 3.4 we display the successive periodograms and the spectral window for NW Ser and V1446 Aql respectively, results are shown only for the v filter for clarity.

For the determination of the error in frequencies, we follow equations given by Montgomery and O'Donoghue (1999), taking into account the correlations in the residuals of the fitting (Schwarzenberg-Czerny 1991). In our case the correlation length is 4. Therefore, we derive a formal error in frequency of $6 - 20 \times 10^{-4}$ c d^{-1} on frequencies F1 to F4 respectively

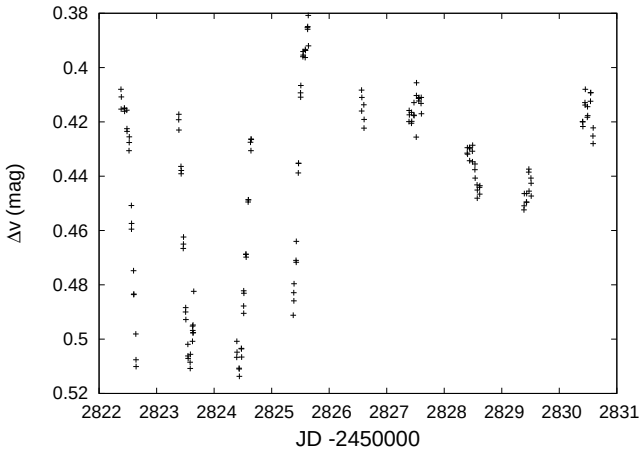

Figure 3.1: Light curve of NW Ser in the v filter.

for NW Ser and $8 - 16 \times 10^{-4}$ c d^{-1} for V1446 Aql.

3.2.1 NW Ser

The rapid amplitude variation over the short timescale spanned by our observations strongly suggests the presence of a beating phenomenon. This would explain why after prewhitening for the first peak (seen at F1 = 1.197 c d^{-1} in Fig. 3.2, together with its aliases at 1,2,... c d^{-1}) a second peak appears at a very close position corresponding to a frequency at F2 = 1.126 c d^{-1}(together with its daily aliases). Note that the width of the sidelobe is almost twice the one calculated for the spectral window. This would mean that another frequency close to 1.197 c d^{-1} is also present. Following Loumos and Deeming (1978), this occurs when the true frequencies differ by less than the half-width of the sidelobe and, in our case, a peak at the midpoint of the true frequencies would appear in the periodogram, as it is seen in Fig. 3.2. F1 and F2 have comparable amplitudes, which would produce the rapid amplitude variability in terms of a beating phenomenon.

These two frequencies differ by less than the Rayleigh resolution, which is in our case 0.11 c d^{-1}. This could indicate that the value we calculate for these frequencies might not be the real ones. However, the rapid amplitude variation present in the light curve, could hardly be explained

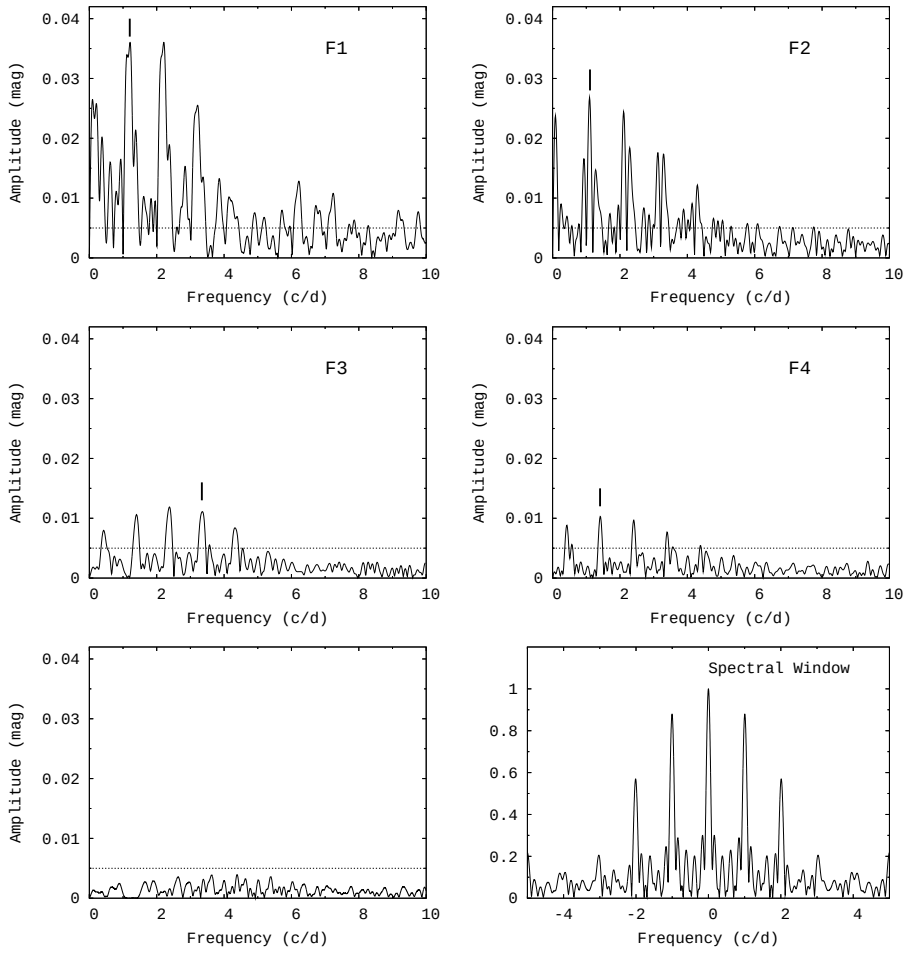

Figure 3.2: Successive periodograms for NW Ser for the v filter. The ticks indicate the positions of the detected frequencies and the dashed horizontal line indicates the level of 4σ level after the final prewhitening.

Table 3.3: Results of the frequency analysis for NW Ser.

No.	Freq. c d^{-1}	Amp. mmag	Phase 2πrad	S/N	σ_{res} mmag	R %
	Filter y		N=162	σ_{init} = 34.8 mmag		
F1	1.190	38.1	0.84	25	20.8	
F2	1.119	21.8	0.88	15	12.1	
F3	3.294	13.6	0.38	7	8.7	
F4	1.415	7.8	0.29	5	7.1	96
	Filter b		N=162	σ_{init} = 34.9 mmag		
F1	1.196	36.6	0.85	25	22.0	
F2	1.127	26.9	0.86	19	11.7	
F3	3.301	11.6	0.36	7	8.7	
F4	1.414	9.5	0.28	6	6.2	97
	Filter v		N=162	σ_{init} = 35.1 mmag		
F1	1.197	36.4	0.86	28	22.6	
F2	1.126	27.7	0.88	22	12.1	
F3	3.304	11.3	0.30	7	8.5	
F4	1.412	10.5	0.36	7	6.2	97
	Filter u		N=162	σ_{init} = 44.4 mmag		
F1	1.159	55.6	0.95	38	26.2	
F2	1.103	33.3	0.83	23	14.2	
F3	2.274	17.5	0.49	11	10.5	
F4	2.387	12.9	0.34	8	7.4	97

by any other origin than the presence of two closely spaced frequencies, even if their real values are not exactly those given in Table 3.3. Therefore we conclude that two close frequencies do actually exist, although their exact values might differ from those given here. In any case, Loumos and Deeming noticed that the true frequencies always fall at the same midpoint as those found when the resolution is not enough.

Residuals after prewhitening for these two frequencies have been analysed for additional periodic components. Frequencies F3 = 3.304 c d^{-1} and F4 = 1.412 c d^{-1} and their daily aliases have been detected in succes-

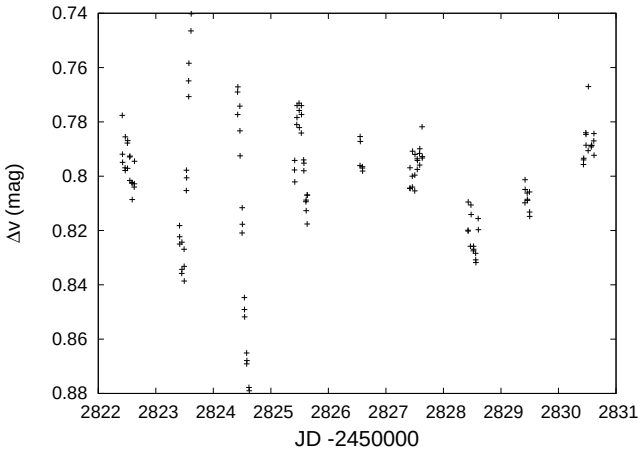

Figure 3.3: Light curve of V1446 Aql in the v filter.

sive periodograms. These new frequencies have much less amplitude than F1 and F2, although they have a SNR greater than 4, as it is shown in Fig. 3.2. Note that F3 = 3.304 c d^{-1} could be a combination of the two high-amplitude frequencies F1 and F2, since F3 = 3.304 $\sim$ F1 + F2 + 1. Finally, the 4 frequencies which minimise the residuals are those shown in Table 3.3 for the four Strömgren bands. No other significant peak appeared in the periodogram after the final prewhitening.

It is important to note that the four frequencies obtained independently for the different *vby* filters are the same within the error boxes. For the u filter we found the 1 c d^{-1} alias of the lower amplitude frequencies F3 and F4. This is due to the low SNR of the data at that wavelength. As seen in the tables the percentage of the total fraction of the variance that is removed (R-values) for all filters is very high.

It is also to be noted here that the first frequency detected by Aerts (2000) (f1 = 2.11 c d^{-1}) is a 1-day alias of F2, and her second frequency f2 = 2.46 c d^{-1} is very close to the 1-day alias of F4. In addition, the frequency (0.46 c d^{-1}) obtained by Percy et al. (1999) is a 1-day alias of F1. In any case, the multiperiodic behaviour of NW Ser, first suggested by Aerts (2000), can be confirmed by these observations.

3.2.2 V1446 Aql

The light curve of V1446 Aql, presented in Fig. 3.3, also shows rapid variation which are also probably caused by the presence of a beating phenomenon between two close frequencies. As the frequencies found for the four Strömgren filters for V1446 Aql are basically the same, we only discuss the detailed analysis for the v filter, since it shows the highest SNR. Frequencies at 1.617 c d^{-1} and at 2.783 c d^{-1} and their daily aliases appear clearly in the periodogram. Note that these two frequencies have similar amplitude. The amplitude of the first frequency (1.617 c d^{-1}) fulfilled the signal to noise criterion, as it is shown in Fig. 3.4, and it has been prewhitened from the data. Then the second frequency at 2.783 c d^{-1}, and its daily aliases, appeared clearly. After prewhitening for these two frequencies other component have been found. Either a frequency at 2.557 c d^{-1} or its 1-day alias at 1.557 c d^{-1} can be considered as the third frequency, although 1.557 c d^{-1} is so close to F1 that the fitting algorithm does not converge and we obtained unrealistic values for this solution. Therefore we proceeded to remove the frequency at F3 = 2.557 c d^{-1} and we found the fourth component F4 = 1.269 c d^{-1}, or one of its aliases.

The final set of frequencies, displayed in Table 3.4, fulfilled the signal to noise requirement in the *vby* filters. However, for the u filter daily alias solutions have been found, the reason being the higher noise present for this filter. We stop the frequency search at this point because the new peaks do not fulfil the SNR criterion mentioned above.

3.3 Theoretical modelling

In order to know whether the observed frequencies are predicted unstable or not by the current models of stellar pulsation we performed a preliminary theoretical study. The physical parameters of NW Ser and V1446 Aql have been obtained from the analysis of high resolution spectra (Frémat et al. 2006), taking into account the effects of gravitational darkening and assuming both stars are rotating at 88% of their critical break-up velocity (Frémat et al. 2005). The obtained values and associated errors are depicted in Fig. 3.5. Note that both error boxes are located in the overlapping region of the β Cephei and SPB instability strips (Pamyatnykh 1999).

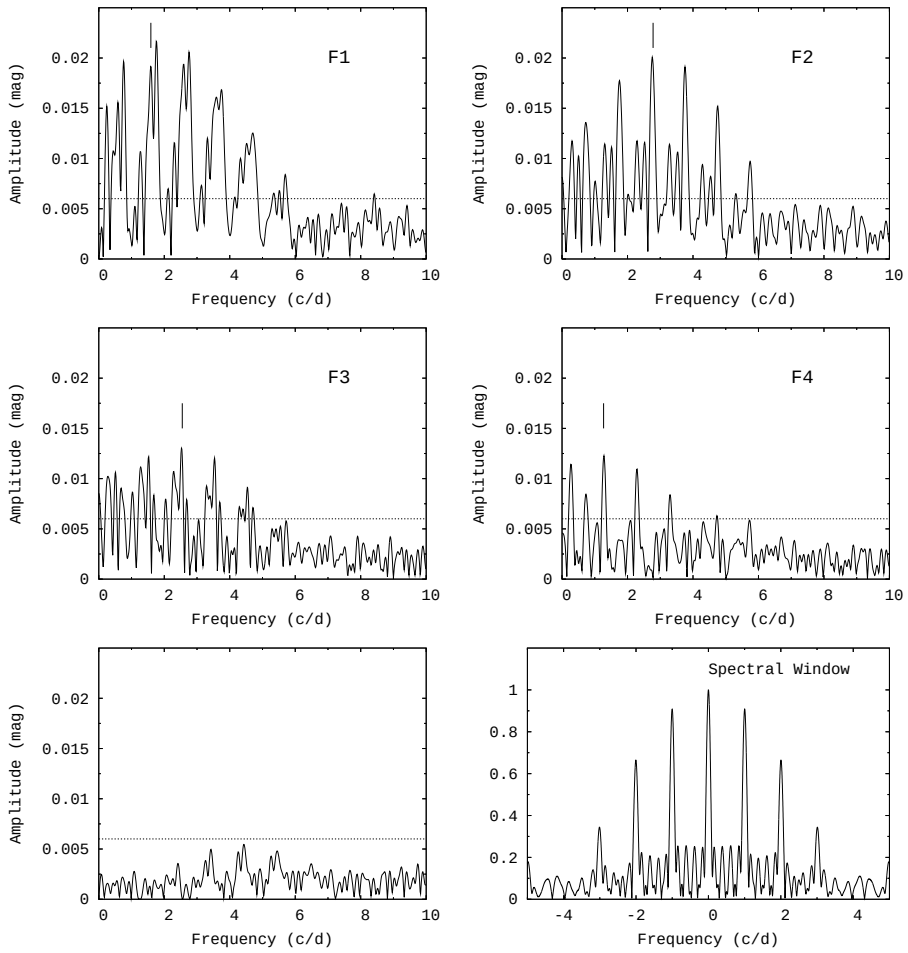

Figure 3.4: Successive periodograms for V1446 Aql for the v filter. Symbols are the same as for Fig. 3.2.

Table 3.4: Results of the frequency analysis for V1446 Aql.

No.	Freq. c d^{-1}	Amp. mmag	Phase 2πrad	S/N	σ_{res} mmag	R %
	Filter y		N=136	σ_{init} = 23.89 mmag		
F1	1.631	21.1	0.76	17	19.6	
F2	2.792	18.8	0.21	11	15.3	
F3	2.559	18.7	0.66	12	12.3	
F4	1.264	13.0	0.32	11	8.8	87
	Filter b		N=136	σ_{init} = 24.85 mmag		
F1	1.622	21.7	0.78	14	20.4	
F2	2.783	20.9	0.22	11	15.1	
F3	2.555	17.7	0.65	10	12.3	
F4	1.266	12.9	0.33	8	8.9	87
	Filter v		N=136	σ_{init} = 24.84 mmag		
F1	1.617	22.1	0.79	15	19.9	
F2	2.783	20.9	0.23	11	14.3	
F3	2.557	17.5	0.64	10	11.7	
F4	1.269	12.4	0.32	8	8.3	89
	Filter u		N=136	σ_{init} = 29.10 mmag		
F1	1.601	27.0	0.77	13	22.6	
F2	2.759	25.5	0.32	11	17.4	
F3	2.514	11.1	0.67	5	14.6	
F4	1.187	15.5	0.62	8	11.1	85

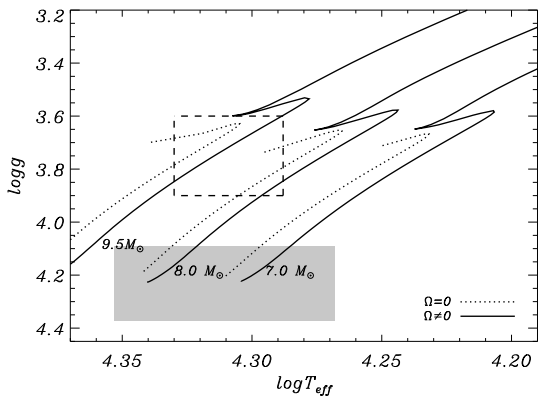

Figure 3.5: Hertzsprung-Russel diagram showing the two Be stars considered in this study and some relevant evolutionary tracks selected for the modelling. The empty and shaded regions represent the error boxes for NW Ser and V1446 Aql respectively. Continuous and dotted lines represent evolutionary tracks of 7, 8 and 9.5 $M_\odot$ for rotating models and non-rotating models respectively.

In Fig. 3.5, evolutionary tracks are shown, which have been computed with the numerical code CESAM (Morel 1997). Rotation effects have been taken into account by considering the spherically symmetric contribution of the centrifugal acceleration (Kippenhahn and Weigert 1990). During evolution, models are assumed to conserve their total angular momentum and to rotate rigidly (*pseudo*-rotating models). Considering the corresponding error boxes, masses in the range of 8.5–9.5 $M_\odot$ are found to be representative of NW Ser. Rotational velocities are in the range of 250 to 270 $km\,s^{-1}$, radii from 5.8 to 7.9 $R_\odot$ and ages around 20 Myr. In the same way, for V1446 Aql, a mass range of 7–7.5 $M_\odot$ is found, with rotational velocities ranging from 238 to 331 $km\,s^{-1}$, radii from 4 to 4.5 $R_\odot$ and an age that brings the star close to the ZAMS (Zero Age Main Sequence).

The instability analysis is then performed using the GraCo code (Moya et al. 2004, for more details), which is based on the non-adiabatic equations derived by Unno et al. (1989). Unfortunately, this code does not

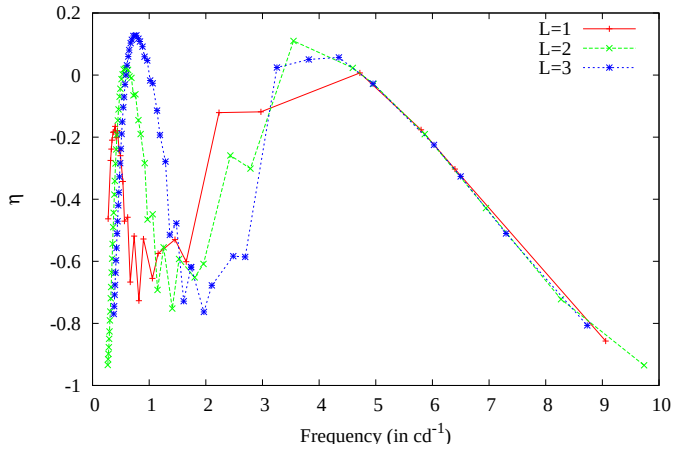

Figure 3.6: Growth rates diagram for NW Ser: positive values indicate unstable modes and vice versa.

take into account the effects of rapid rotation, needed for better characterisation of these stars. We have to note that the perturbative theory is only valid for a rotational frequency much lower than the pulsational period. In our case, the rotational frequency is larger than the pulsational frequencies and thus a non-perturbative theory is needed. Therefore, the instability analysis presented here is performed for the frequencies in the observer frame.

For both stars, the $\ell = 2$ and $\ell = 3$ modes are predicted to be unstables. In the case of NW Ser, the SPB and β Cephei instability ranges are very close (see Fig. 3.6), and this suggests that NW Ser may be a hybrid pulsator. In addition, its observed frequencies lie in the range of the g modes (SPB-like) and p modes (β Cephei-like) respectively. This result is consistent with its location in the HR diagram region where the instability strips of SPB and β Cephei overlap. In the case of V1446 Aql, only high-order g modes with $\ell = 2$ and 3 are predicted to be unstable close to the observed frequencies, as shown in Fig. 3.7.

In order to have an idea of what spherical degree ℓ is excited in these stars we have applied the photometric mode identification as described in Watson (1988) and used for δ Scuti stars in Garrido (2000). We have

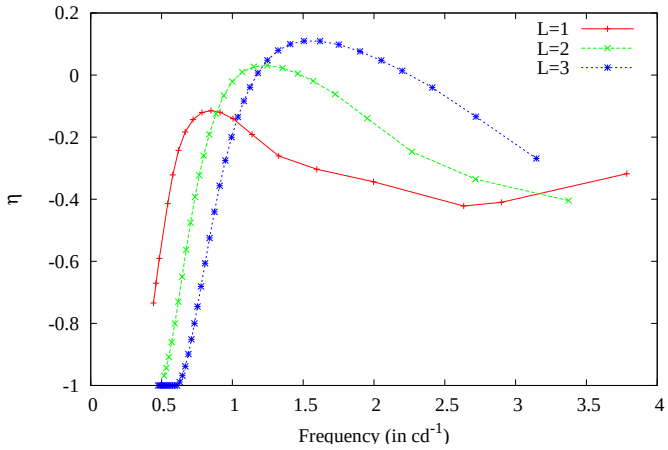

Figure 3.7: Growth rates diagram for V1446 Aql.

computed the amplitude ratios for each pulsational frequency and compare them with those predicted for stellar models using different ℓ-degrees. In Fig. 3.8 and 3.9 we show the amplitude ratios for both stars. In the case of NW Ser, pulsation mode of degree $\ell = 3$ appear to be more probable for frequencies F2 and F4, whereas for F1 and F3 the more probable degrees seem to be $\ell = 1$ and $\ell = 2$. For V1446 Aql all the detected frequencies seem to be associated to dipoles and quadrupoles. The u amplitude for frequency F3 is very low and probably due to the noise of the data at this wavelength.

At this point only spectroscopic observations can supply an unambiguous mode identification for these rapidly rotating objects.

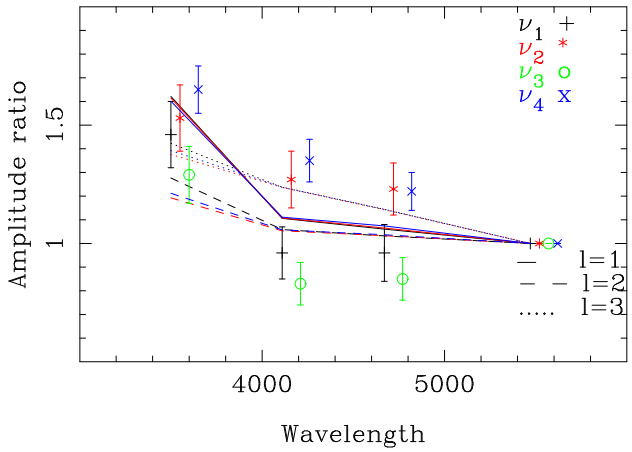

Figure 3.8: Observed amplitude ratios A_X/A_y and their error boxes for the detected frequencies of NW Ser. A_X stands for any of the amplitudes in the four Strömgren filters. The lines represent the theoretical non-adiabatic predictions of the stellar models explained in the text.

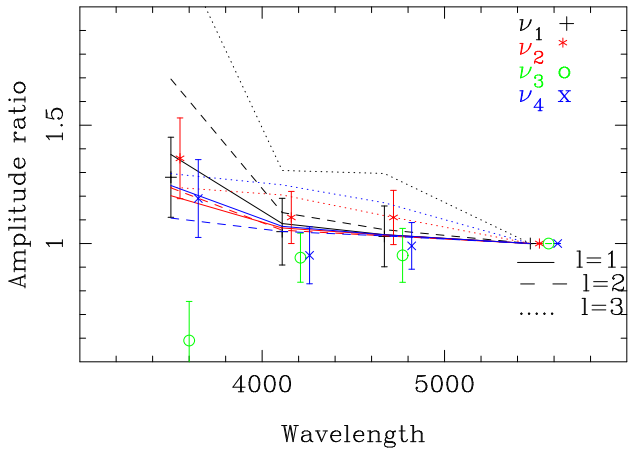

Figure 3.9: Same as Fig. 3.8, but for V1446 Aql.

3.4 Conclusions

Accurate photometric light curves of the Be stars NW Ser and V1446 Aql obtained during a preparatory program for the COROT space mission have been analysed. Our spectral analysis reveals the presence of four statistically significant frequencies in each star. Together with the multiperiodicity of HD 163 868 and ζ-Oph recently observed from space (Walker et al. 2005a,b), the present results point towards the interpretation of short-period variability of Be stars in terms of *nrp*, as suggested by spectroscopic observations obtained in the last decade. In this framework, a theoretical instability analysis of the observed frequencies has been performed. It is found that NW Ser could be an hybrid pulsator, since its observed frequencies lie in the range of g modes (SPB-like) and p modes (β Cephei-like) respectively. This would thus imply that NW Ser is one of the very few stars detected so far showing such pulsational characteristic. In the case of V1446 Aql, only frequencies corresponding to predicted g modes have been detected.

Longer timebase spectroscopic and photometric observations are thus required in order to confirm these results.

Bibliography

Aerts, C.: 2000, in *ASP Conf. Ser. 214: IAU Colloq. 175: The Be Phenomenon in Early-Type Stars*, p. 192

Baade, D.: 1982, *A&A* **105**, 65

Balona, L. A.: 1990, *MNRAS* **245**, 92

Frémat, Y., Neiner, C., Hubert, A.-M., Floquet, M., Zorec, J., Janot-Pacheco, E., and Renan de Medeiros, J.: 2006, *A&A* **451**, 1053

Frémat, Y., Zorec, J., Hubert, A.-M., and Floquet, M.: 2005, *A&A* **440**, 305

Garrido, R.: 2000, in *ASP Conf. Ser. 210: Delta Scuti and Related Stars*, p. 67

Hubert, A. M. and Floquet, M.: 1998, *A&A* **335**, 565

Kazarovets, A. V., Samus, N. N., Durlevich, O. V., Frolov, M. S., Antipin, S. V., Kireeva, N. N., and Pastukhova, E. N.: 1999, *Informational Bulletin on Variable Stars* **4659**, 1

Kippenhahn, R. and Weigert, A.: 1990, *"Stellar structure and evolution"*, Astronomy and Astrophysics library, Springer-Verlag

Loumos, G. L. and Deeming, T. J.: 1978, *Ap&SS* **56**, 285

Montgomery, M. and O'Donoghue, D.: 1999, *Delta Scuti Newsletter* **13**, p28

Morel, P.: 1997, *A&AS* **124**, 597

Moya, A., Garrido, R., and Dupret, M. A.: 2004, *A&A* **414**, 1081

Pamyatnykh, A. A.: 1999, *Acta Astronomica* **49**, 119

Percy, J. R., Marinova, M. M., BožiĆ , H., and Harmanec, P.: 1999, *A&A* **348**, 553

Schwarzenberg-Czerny, A.: 1991, *MNRAS* **253**, 198

Unno, W., Osaki, Y., Ando, H., Saio, H., and Shibahashi, H.: 1989, *Non-radial oscillations of stars*, Nonradial oscillations of stars, Tokyo: University of Tokyo Press, 1989, 2nd ed.

Vaníček, P.: 1971, *Ap&SS* **12**, 10

Walker, G. A. H., Kuschnig, R., Matthews, J. M., Cameron, C., Saio, H., Lee, U., Kambe, E., Masuda, S., Guenther, D. B., Moffat, A. F. J., Rucinski, S. M., Sasselov, D., and Weiss, W. W.: 2005a, *ApJ Lett.* **635**, L77

Walker, G. A. H., Kuschnig, R., Matthews, J. M., Reegen, P., Kallinger, T., Kambe, E., Saio, H., Harmanec, P., Guenther, D. B., Moffat, A. F. J., Rucinski, S. M., Sasselov, D., Weiss, W. W., Bohlender, D. A., Božić, H., Hashimoto, O., Koubský, P., Mann, R., Ruždjak, D., Škoda, P., Šlechta, M., Sudar, D., Wolf, M., and Yang, S.: 2005b, *ApJ Lett.* **623**, L145

Watson, R. D.: 1988, *Ap&SS* **140**, 255

Chapter 4

Spectroscopic variability in NW Ser

4.1 Introduction

NW Ser (HD 168797, HR 6873, $V = 6.14$) is a short-period variable Be star preselected for the short runs of the COROT mission. In order to characterise its variability, different photometric studies have been performed during the last decade. Using Hipparcos data, Hubert and Floquet (1998) and Percy et al. (1999) found a period of 0.488 d and 0.46 d respectively. Later on, Aerts (2000) suggested the possibility of the presence of multi-periodicity in the Hipparcos light curve. Finally, we have detected four significant frequencies (1.197 c d^{-1}, 1.126 c d^{-1}, 3.304 c d^{-1}, 1.412 c d^{-1}) which produce a rapid variation in the observed amplitude of the light curve (see Chapt. 3). The frequencies have been modelled as non-radial low-degree modes. However, the preliminary model used in Chapt. 3 did not take into account the rotational velocity and spectroscopic data were required to make a clearer mode identification.

These considerations motivated us to undertake spectroscopic observations in 2004 and 2005 in order to analyse the pulsational properties of the star. In this chapter, we present the results of this campaign. In Sect. 4.2 we report on the spectroscopic observations and we determine improved stellar parameters taking into account rotational effects in Sect. 4.3. In Sect. 4.4 we study the long-term variations of lines affected by the circum-

stellar disk. We search for rapid variability in the photospheric lines in Sect. 4.5 and results are interpreted in the frame of the non-radial pulsations model in Sect. 4.6. Finally, conclusions are presented in Sect. 4.7.

4.2 Observations and data reduction

NW Ser has been observed in 2004 from June 29 to July 17 at the Observatoire de Haute Provence (OHP) with the Aurélie spectrograph attached to the 1.52m telescope. A total of 26 spectra centred on the He I 4387 line and 6 spectra centred on the Hα line have been obtained with an exposure time between 5 and 20 min and a signal to noise (S/N) ratio between 100 and 400. Two different dispersion gratings have been used, one of 600 lines/mm and another of 1200 lines/mm, resulting in a resolving power of 10 000 and 20 000 respectively.

We also obtained observations from June 19 to July 3, 2005 at the David Dunlap Observatory (DDO) in Toronto with the 1.88m telescope. 64 spectra have been gathered in the spectral range from 4300-4600 with a resolving power of 10 000, a mean exposure time of 30 min and a signal to noise ratio between 100 and 450.

Additional data collected by the amateur astronomer C. Buil since 2001 have also been investigated to follow variations in the Hα and He I 6678 lines. The instrument to obtain these data is a spectrograph with a resolution of 7 000 mounted on a 21.2 cm telescope (see Buil 2006).

An échelle spectrum obtained at the OHP with the 1.93m telescope equipped with the ELODIE spectrograph (R $\sim$ 40000 $-$ 50000) is also studied in the present chapter. This data is available in GAUDI (Ground-based Asteroseismology Uniform Database Interface) (Solano et al. 2005).

A log of all the observations is given in Table 4.1.

Bias, flats and wavelength calibration exposures (Th-Ar and Fe-Ar comparison lamps at the OHP and DDO respectively) have been obtained for each night. Both sets of observations have been reduced with IRAF[1] using standard techniques for CCD data. All spectra have been corrected

[1]IRAF is distributed by the National Optical Astronomy Observatories, which is operated by the Association of Universities for Research in Astronomy (AURA) Inc., under cooperative agreement with the National Science Foundation.

Table 4.1: Log of spectroscopic observations.

Date	HJD- 2 450 000	site	mean S/N	# sp	wavelength range
25/07/1999	1835.44	OHP1.93	200	1	4000-6800
14/06/2001	2075.49	Buil (2006)	125	1	6330-6870
02/06/2002	2427.72	Buil (2006)	150	1	6330-6870
29/05/2003	2788.64	Buil (2006)	120	1	6330-6870
17/06/2004	3174.50	Buil (2006)	110	1	6330-6870
29/06/2004	3186.37-3186.49	OHP1.52	250	3	4370-4590
30/06/2004	3187.37-3187.50	OHP1.52	275	3	4370-4590
01/07/2004	3188.37-3188.51	OHP1.52	325	3	4370-4590
02/07/2004	3189.37-3189.58	OHP1.52	275	4	4370-4590
03/07/2004	3190.37-3190.59	OHP1.52	270	4	4370-4590
04/07/2004	3191.37	OHP1.52	240	1	4255-4710
05/07/2004	3192.37-3192.48	OHP1.52	275	2	4255-4710
06/07/2004	3193.51	OHP1.52	370	1	4255-4710
07/07/2004	3194.52	OHP1.52	250	1	4255-4710
08/07/2004	3195.45-3195.60	OHP1.52	210	2	6340-6795
09/07/2004	3196.37-3196.58	OHP1.52	250	2	6340-6795
10/07/2004	3197.42-3197.51	OHP1.52	250	2	6340-6795
11/07/2004	3198.48-3198.60	OHP1.52	250	2	4255-4710
17/07/2004	3204.35-3204.36	OHP1.52	170	2	4255-4710
19/06/2005	3541.59-3541.86	DDO	270	13	4300-4600
29/06/2005	3551.61-3551.86	DDO	200	12	4300-4600
30/06/2005	3552.59-3552.81	DDO	180	10	4300-4600
01/07/2005	3553.64-3553-84	DDO	230	10	4300-4600
02/07/2005	3554.64-3554.85	DDO	320	10	4300-4600
03/07/2005	3555.65-3555.83	DDO	300	9	4300-4600

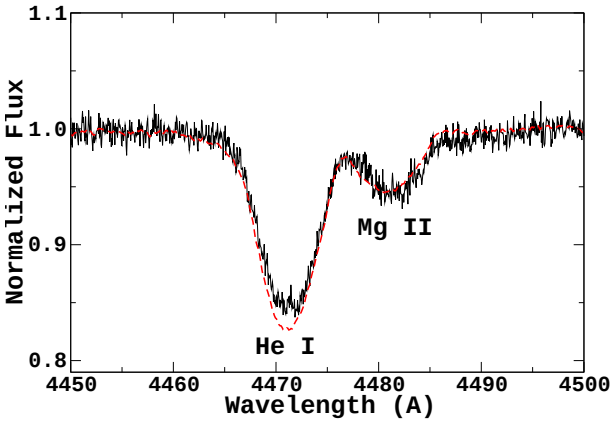

Figure 4.1: Comparison between the ELODIE spectrum obtained in 1999 (black full line), and the averaged spectrum of the 2005 observations (red broken line). The He I 4471 spectral line is weaker in the ELODIE spectrum, probably due to pulsation.

for heliocentric velocity. A cosmic rays removal program developed by Pych (2004) has been used for the DDO data reduction.

4.3 Stellar parameters determination

To account for stellar flattening and gravitational darkening induced by the fast rotation of NW Ser, we adopted an approach similar to the one described in Frémat et al. (2006) (which used the ELODIE spectrum) but, this time, it was applied on spectra obtained at higher signal-to-noise ratio and averaged over 15 days of observations (see Sect. 4.2 and Fig. 4.1). The procedure consists in fitting observed hydrogen and helium line-profiles with theoretical spectra obtained with the FASTROT computer code (Frémat et al. 2005) assuming different values of Ω/Ω_c. Local plane-parallel model atmospheres used in FASTROT are described in Sect. 4.3.1, while the procedure and its results are further detailed in Sect. 4.3.2.

Table 4.2: Atoms and ions for which NLTE level populations have been computed with TLUSTY.

Atom	Ion	Levels
Hydrogen	H I	8 levels + 1 superlevel
	H II	1 level
Helium	He I	24 levels
	He II	20 levels
	He III	1 level
Carbon	C II	53 levels (all individual levels)
	C III	12 levels
	C IV	9 levels + 4 superlevels
	C V	1 level
Nitrogen	N I	13 levels
	N II	35 levels + 14 superlevels
	N III	11 levels
	N IV	1 level
Oxygen	O I	14 levels + 8 superlevels
	O II	36 levels + 12 superlevels
	O III	9 levels
	O IV	1 level
Magnesium	Mg II	21 levels + 4 superlevels
	Mg III	1 level
Silicium	Si II	13 levels + 3 superlevels
	Si III	48 levels + 8 superlevels
	Si IV	20 levels + 3 superlevels
	Si V	1 level

4.3.1 Local plane-parallel model atmospheres

The model atmospheres we used for effective temperatures lower than 27 000 K are those computed by Kurucz (1993) and Castelli and Kurucz (2003) in LTE. However, for stars hotter than 15 000 K and cooler than 27 000 K, non-LTE level populations have been calculated for each

Table 4.3: Stellar parameters ($T_{\rm eff}^{\rm o}$, $\log g_{\rm o}$ and $V \sin i_{\rm\ true}$) of the non-flattened counterpart of NW Ser obtained with FASTROT for different values of $\Omega/\Omega_{\rm c}$. Apparent stellar parameters are $T_{\rm eff}$ = 17970 K, log g = 3.60 dex and $V \sin i$ = 245 km s^{-1}. Error bars on the parameters are of the same order as on the final adopted values (see Sect. 4.3.2).

$\Omega/\Omega_{\rm c}$	i (deg)	$T_{\rm eff}^{\rm o}$ (K)	$\log g_{\rm o}$ (cgs)	$V \sin i_{\rm\ true}$ (km s^{-1})
0.75	81	18970	3.85	245
0.80	59	18960	3.85	248
0.85	54	19300	3.87	258
0.90	48	19410	3.88	263
0.95	41	19560	3.88	260
0.99	41	19670	3.89	276

of the considered atoms using the TLUSTY code (Hubeny and Lanz 1995) and keeping fixed the temperature and density distributions. The surface chemical abundances we adopted are those published by Grevesse and Sauval (1998) for the Sun.

Table 4.2 lists the ions we introduced in the computations. Except for C II and Si III, the atomic models we used in this work have been downloaded from TLUSTY's homepage[2] maintained by I. Hubeny and T. Lanz. C II and Si III have been treated thanks to the MODION IDL package (Varosi et al. 1995) and by adopting the atomic data (oscillator strengths, energy levels and photoionization cross sections) selected from the TOPBASE database (Cunto et al. 1993)[3]. Model atmospheres with effective temperatures greater than 27000 K are taken from the OSTAR2002 NLTE grid (Lanz and Hubeny 2003). The grid of fluxes we use during the fitting procedure has finally been built with SYNSPEC and for effective temperatures and surface gravities ranging from 6000 to 50000 K and from 2.5 to 4.5 dex (cgs) respectively.

[2]http://tlusty.gsfc.nasa.gov

[3]The corresponding TLUSTY files can be downloaded from http://users.skynet.be/yves.fremat/soft-uk.html

4.3.2 Procedure and results

The Hγ line and the neutral helium line profiles at 4387 Å and 4471 Å are fitted with synthetic spectra computed with (i.e. stellar parameters of the non-flattened counterpart) and without (i.e. apparent stellar parameters) accounting for stellar flattening and gravitational darkening. The results are given in Table 4.3 and Fig. 4.2 for different values of $\Omega/\Omega_{\rm c}$. The surface gravity we derived in the present work is slightly higher than the one obtained in Frémat et al. (2006). This is due to the better quality of the data which now cover 15 days of observations (Fig. 4.1). The selection of the most appropriate set of parameters is based on the Si III triplet, from 4540 to 4580 Å. Since Si III is preferably formed at the stellar poles, larger $\Omega/\Omega_{\rm c}$ values lead to deeper and sharper line profiles. A better agreement between observations and computations is therefore obtained at the highest inclinations and for the following parameters:

$$
\begin{aligned}
T_{\rm eff}^{\rm o} &= 18600 \pm 1000 \text{ K} \\
\log g_{\rm o} &= 3.70 \pm 0.13 \text{ dex} \\
V \sin i_{\rm \ true} &= 250 \pm 10 \text{ km s}^{-1} \\
\Omega/\Omega_{\rm c} &= 0.79 \pm 0.05 \\
i &= 72 \pm 15 \text{ deg} \\
T_{\rm pol} &= 19490 \pm 1000 \text{ K} \\
\log g_{\rm pol} &= 3.74 \pm 0.13 \text{ dex} \\
T_{\rm eq} &= 16155 \pm 1000 \text{ K} \\
\log g_{\rm eq} &= 3.41 \pm 0.13 \text{ dex} \\
V_{\rm crit} &= 405 \pm 50 \text{ km s}^{-1}
\end{aligned}
$$

$T_{\rm eff}^{\rm o}$, $\log g_{\rm o}$ and $V \sin i_{\rm \ true}$ are the stellar parameters of the non-flattened counterpart. Adopting these parameters, we also computed the Hα line. We got a good match with our measurements (see Fig. 4.2) and we found no trace of emission in its core in the data of 2004.

Finally, we derived the following parameters using the evolutionary tracks taken from Schaller et al. (1992):

$$
\begin{aligned}
M &= 7.42 \pm 0.68 \, {\rm M}_{\odot} \\
R &= 6.44 \pm 1.08 \, R_{\odot} \\
\log L &= 3.63 \pm 0.19 \, L_{\odot} \\
f_{\rm rot} &= 0.82 \pm 0.12 \text{ c d}^{-1}.
\end{aligned}
$$

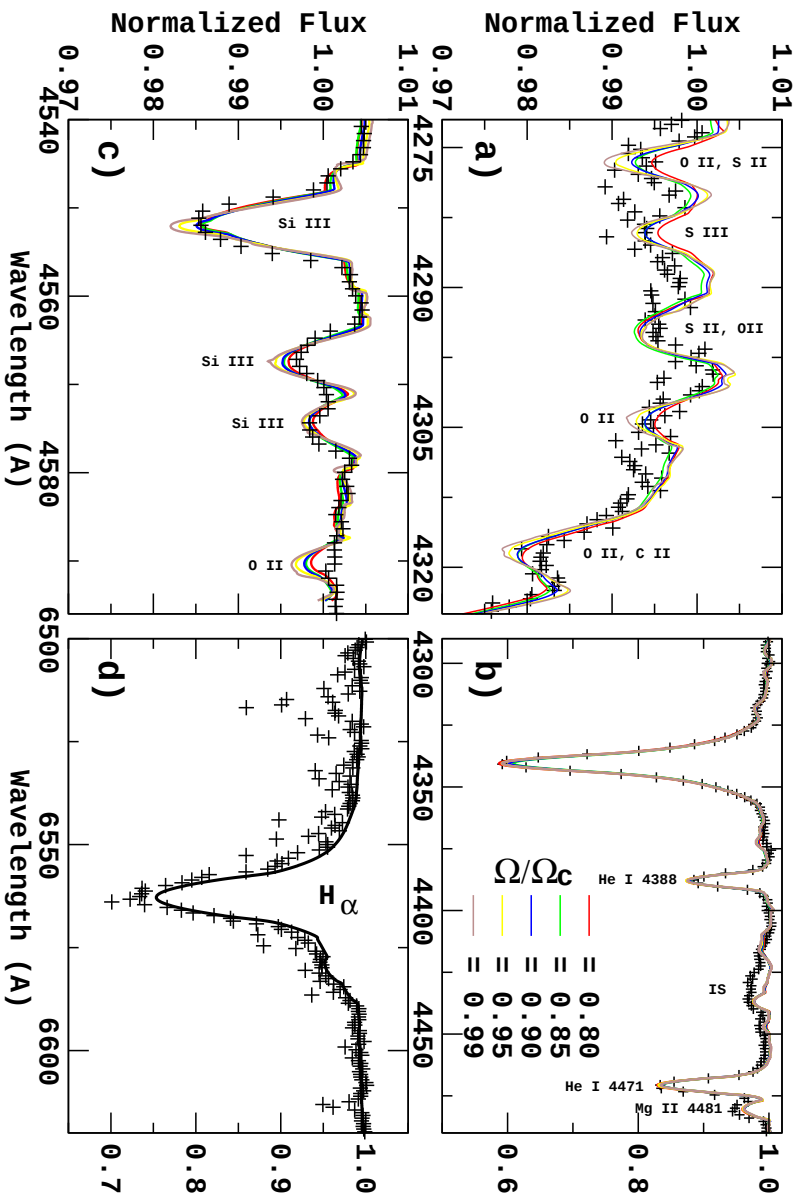

Figure 4.2: Comparison between observations (crosses) and synthetic spectra (lines) computed for different Ω/Ω_c values.

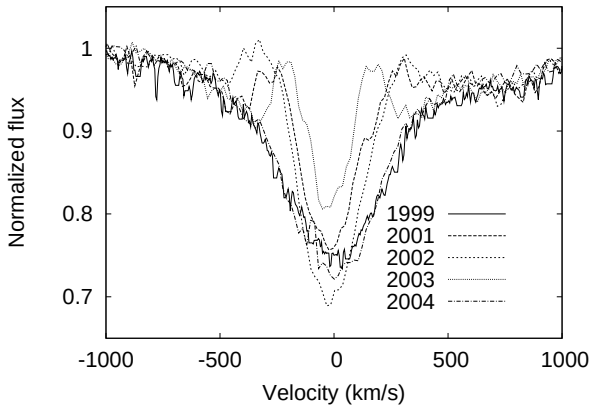

Figure 4.3: The H_α line profile is shown with a solid line for 1999, long-dashed line for 2001, middle long-dashed line for 2002, dot-dashed line for 2003 and long-and-dot-dashed line for 2004.

4.4 Long-term variation of the H_α and He I 6678 lines

NW Ser is included in the Atlas of Be stars published by Hubert-Delplace and Hubert (1979). This star exhibited successively a "B star", a "Be star", and then a "B star" phase again from 1953 to 1975. In more detail, from 1953 to 1961, Hα has been observed in absorption with a quite variable profile. In March 1961, a weak emission appeared and the line started to strengthen until the beginning of 1963. The Hα line showed a weak emission in 1964, a weak absorption in 1965 and again a weak emission in 1966-1967. Finally, the "B star" phase appeared in 1968 and lasted at least 7 years. No more observations have obtained afterwards by these authors. Slettebak (1982) observed NW Ser in 1979 and found a very weak flanking emission around a rather broad central absorption core at Hβ. From 1979 to 1999, there are no spectra of this star in the literature.

The H_α line profile observed in 1999, 2001, 2002, 2003 and 2004 is displayed in Fig. 4.3. We obtained only one spectrum per year, except for the year 2004 for which we show the average of 6 spectra.

In 1999, the ELODIE spectrum did not show emission in the Balmer lines. In 2001, emission clearly appeared in the wings of the Hα line with a broad absorption core, also observed in 2002 and 2003.

To compare emission in 2001, 2002 and 2003, Table 4.4 lists the value of several spectral parameters (equivalent width EW, full width at half maximum $FHWM$, radial velocity of the centroid RV, central depth of the core CD). These values have been measured on the absorption part of the line. We also show the peak separation of the emission components, calculated as the difference between the two closest emission peaks.

Assuming that the circumstellar disk is keplerian (Meilland et al. 2006), we derived the radius of the emission line forming region from the separation of the emission components, following the formula taken from Rivinius et al. (2001):

$$R_{\rm peak}/R_* = \left(\frac{2V_{\rm crit}{\rm sin}i}{\Delta\, v_{\rm peak}}\right)^2$$

The calculated values are reported in Table 4.4 for 2001, 2002 and 2003. The nearest region of the circumstellar disk was very close to the star for the 2002 data, suggesting that an outburst probably occurred just before our observations. Note that the V emission peak is higher than the R one. In addition, in 2002 the absorption was much deeper than in the other years of observations, even in years when there was no emission in the Hα line (1999 and 2004). This additional broad absorption was also observed in the He I 6678 line.

As shown in Table 4.4, the equivalent width of the Hα emission was weaker in 2003 than in 2001 and 2002, i.e. the star is probably loosing the disk. Moreover, the observed decrease in separation between the peaks of the emission components suggests that the ejected matter may have been detached from the star. Finally, no emission was detected in the 2004 observations.

No emission has been detected in the He I 6678 line from 1999 to 2004 (see Fig. 4.4). Note that, in 2002, the photospheric line profile of He I 6678 shows an additional broad absorption feature, as it is observed in the Hα line. Floquet et al. (2002) observed this feature in the Be star EW Lac and interpreted it as the result of the building of a pseudo-photosphere.

Unfortunately, the number of spectra at Hα and He I 6678 obtained

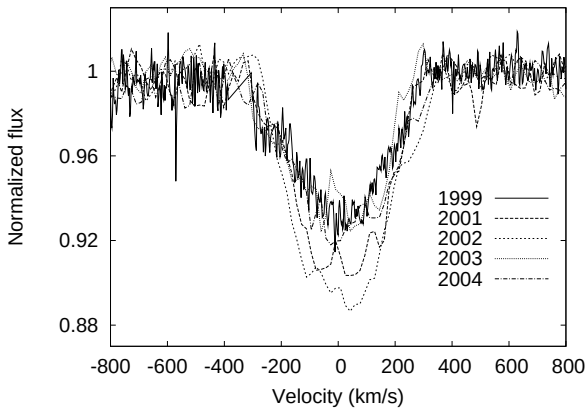

Figure 4.4: He I 6678 line profiles observed from 1999 to 2004.

before 2003 is not sufficient to reliably search for a long-term variability timescale.

Table 4.4: Hα line profile parameters in 2001, 2002 and 2003.

	2001	2002	2003
EW (Å)	1.3	2.2	0.8
FWHM ($\mathrm{km\,s^{-1}}$)	260	298	183
RV ($\mathrm{km\,s^{-1}}$)	-15	-14	-20
CD	-0.22	-0.31	-0.18
ΔPeak (Å)	500 ± 30	650 ± 30	350 ± 30
$R_{\mathrm{disk}}(R_*)$	2.4 ± 0.7	1.4 ± 0.4	5.1 ± 1.5

4.5 Time series analysis

A frequency analysis of line profiles and spectral parameters is performed separately for the 2004 and 2005 data. The He I 4387, He I 4471, Mg II 4481 and Si III 4553 lines have been obtained in both observing runs, whereas the $H\gamma$ line has only been observed in 2005. Data gathered in 2004 have

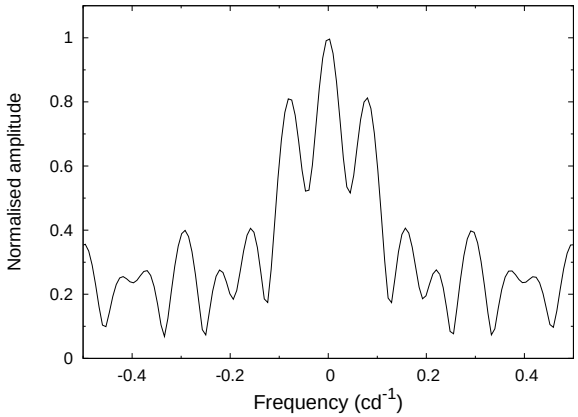

Figure 4.5: Example of spectral window for the DDO observations.

a longer time span but a data sampling between 1 and 4 spectra per day. On the contrary, data observed at the DDO in 2005 have a shorter time span but a data sampling of 10 spectra per day.

A time series analysis (TSA) is performed using Fourier Transform + CLEAN algorithm and least square fitting (LS) methods, as in Floquet et al. (2002) and Neiner et al. (2005). These methods are applied on each resolution bin of line-profile time series. Results obtained with the LS and FT + CLEAN methods are presented in Tables 4.5 and 4.6 for the dataset obtained in 2004 and 2005 respectively.

The radial velocity (RV) of the line centroid, the central depth (CD), the projected velocity ($V \sin i$), the full-width at half-maximum ($FWHM$) and the equivalent width (EW) are also studied in detail for each line profile with the standard Fourier techniques. Period04 (Lenz and Breger 2005) and a non-linear multi-parameter fitting code (Vaníček 1971) are used in order to search for frequencies in the spectral parameters.

The frequency resolution is $\sim$0.06 c d^{-1} for the OHP observations and $\sim$0.10 c d^{-1} for the DDO data. In Fig. 4.5 we show the aliases produced by the spectral window of the observations obtained at the DDO. In particular, note in this figure that a frequency $f*$ will produce peaks at frequencies $f = f* \pm 0.09$ c d^{-1} in the DDO data.

Table 4.5: Frequencies (in c d^{-1}) deduced from the time-series analysis of the dataset obtained in 2004 for He I, Si III, Mg II and Hγ line profiles obtained with the LS and FT + CLEAN methods. Frequencies are listed by decreasing power.

Line	*lpv*		RV	EW	CD	FWHM
	LS	CLEAN				
He I 4387	1.36	0.45	1.36	1.77	0.48	1.35
	0.76	1.36	2.67			0.16
	2.68	0.74	2.20			
He I 4471	1.35	1.34	1.36	1.16	1.43	1.34
	0.19	1.03	1.75	1.33	2.17	1.74
	2.69	0.19				
Mg II 4481	1.35	1.34	1.35	0.33	2.70	0.34
	0.19	1.03	1.42		3.34	0.47
	2.69	0.19				2.71
Si III 4553	0.44	0.11	1.22	2.28	0.40	
	1.35	2.34				

Table 4.6: Same as Table 4.5, but for the dataset obtained in 2005.

Line	*lpv*		RV	EW	CD	FWHM	$V \sin i$
	LS	CLEAN					
He I 4387	1.35	1.35	1.33	1.12	0.78	1.27	0.68
	1.12	0.04	1.29	3.33	2.71	1.21	1.34
	1.67	0.13					
He I 4471	1.26	1.35	1.34	1.27	1.35	1.27	
	1.13	1.26	0.30	2.20	1.42	1.21	
	2.70	0.04			2.20		
	1.39	0.12					
Mg II 4481	1.26	1.35	1.27	2.51	1.35	2.60	
	1.13	1.26	0.20		0.49	2.26	
	2.70	0.04					
	1.39	0.12					
Si III 4553	0.12	2.98		0.13	0.19		
	3.31	0.48		1.34			
Hγ	0.12	0.04	1.33	0.94	1.35	1.04	1.41
	1.35	1.29	0.13	1.28	0.11	0.32	
	1.82	1.35					
	3.68	1.12					

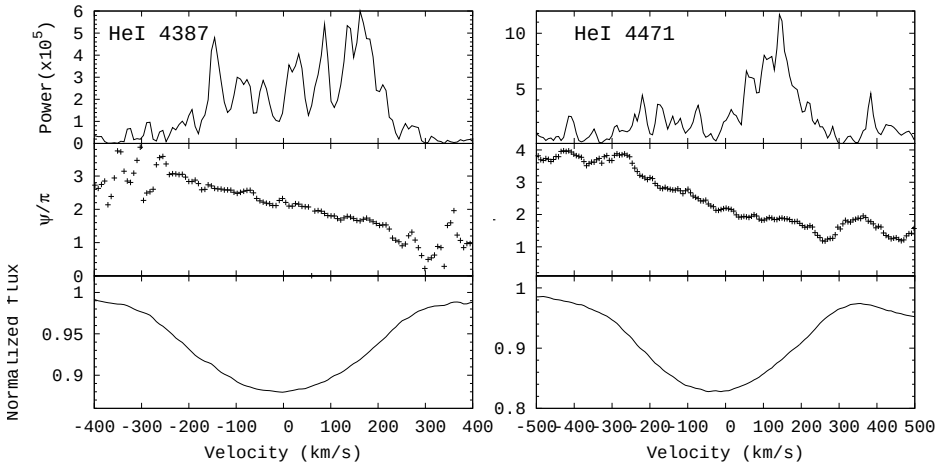

Figure 4.6: Power and phase distributions and averaged line profile of the frequency $f = 1.35$ c d^{-1} for the He I 4387 and 4471 lines observed in 2004.

4.5.1 Data obtained in 2004

In the line-profile variations (*lpv*), *RV* and *FWHM*, the main frequency obtained with the different search programs is $f_1 = 1.35$ c d^{-1}(see Table 4.5). The power and phase distributions of this frequency are displayed in Fig. 4.6 for the He I 4387 and 4471 lines. The power distribution is higher in the wings than in the centre. In addition, the first harmonic of f_1 (2.7 c d^{-1}) is also observed, although with much less power. Note that the *lpv* of the He I 4471 and Mg II 4481 lines have been analysed together because these lines are blended, and thus we present the same results for both lines.

The following frequencies have been detected in the *lpv* after prewhitening for f_1: 0.76, 0.19, 0.44 c d^{-1}. None of them have coherent phase distributions, although almost all these frequencies (or their 1-day aliases) have also been detected in the *lpv* of the observations obtained in 2005.

A main frequency at 1.42 c d^{-1} instead of $f_1 = 1.35$ c d^{-1} is found in the spectral analysis of the *CD* variations. The phase diagram is not very

convincing, probably due to the few datapoints of the light curve.

A frequency at 1.16 c d^{-1} is detected as the most powerful in the *EW* variations of the He I 4471 line instead of the main frequency f_1 = 1.35 c d^{-1}. A similar frequency (1.12 c d^{-1}) is also found in the *lpv* of the observations obtained in 2005, and is considered as f_2.

4.5.2 Data obtained in 2005

Line-profile variations

Frequencies detected in the line profiles are presented in Table 4.6. Note that the blended He I 4471 and Mg II 4481 lines have been analysed together, and thus we present the same results for both lines.

The main frequency at f_1 = 1.35 c d^{-1} is present in all the studied lines. This frequency appears powerfully with the least-square and FT + CLEAN methods. On the contrary, for the He I 4471 and Mg II 4481 lines, the most powerful frequency is 1.26 c d^{-1}. The difference between both frequencies is around 0.09 c d^{-1}, and thus, they are likely to be aliases produced by the spectral window (see Sect. 4.5). If we analyse the 5 consecutive days of observations (from 29/06 to 03/07), the intermediate frequency 1.30 c d^{-1} is detected.

The power and phase distributions of this frequency are displayed in Fig. 4.7. Note that the power is higher in the wings than in the centre of the lines. Moreover, the centre of the phase distribution of the He I 4471 line is blue-shifted in the observations of both years. The wing of the Mg II 4481 line is seen next to the He I 4471 line profile and vice-versa in Fig. 4.7 and further figures where the He I 4471 or Mg II 4481 lines are displayed.

The first harmonic of f_1 appears in the TSA of the He I 4471 and Mg II 4481 lines and as 1-day aliases in He I 4387 and Hγ lines (1.67c d^{-1} and 3.68 c d^{-1} respectively) with the LS method. The 1.67 c d^{-1} appears more powerfully in the power spectrum of the He I 4387 line, but the phase distribution is more convincing with the frequency 2.68 c d^{-1}. Fig. 4.8 represents the power and phase distributions of frequency $2f_1$ = 2.68 c d^{-1} across the He I 4387 and 4471, Mg II 4481 and Hγ line profiles. The power is high in the blue wing and in the centre of the lines.

Another frequency at f_2 = 1.12 c d^{-1} is also detected in the He I 4387 and 4471 lines in 2005, and as a one-day alias (f = 0.12 c d^{-1}) in the He I

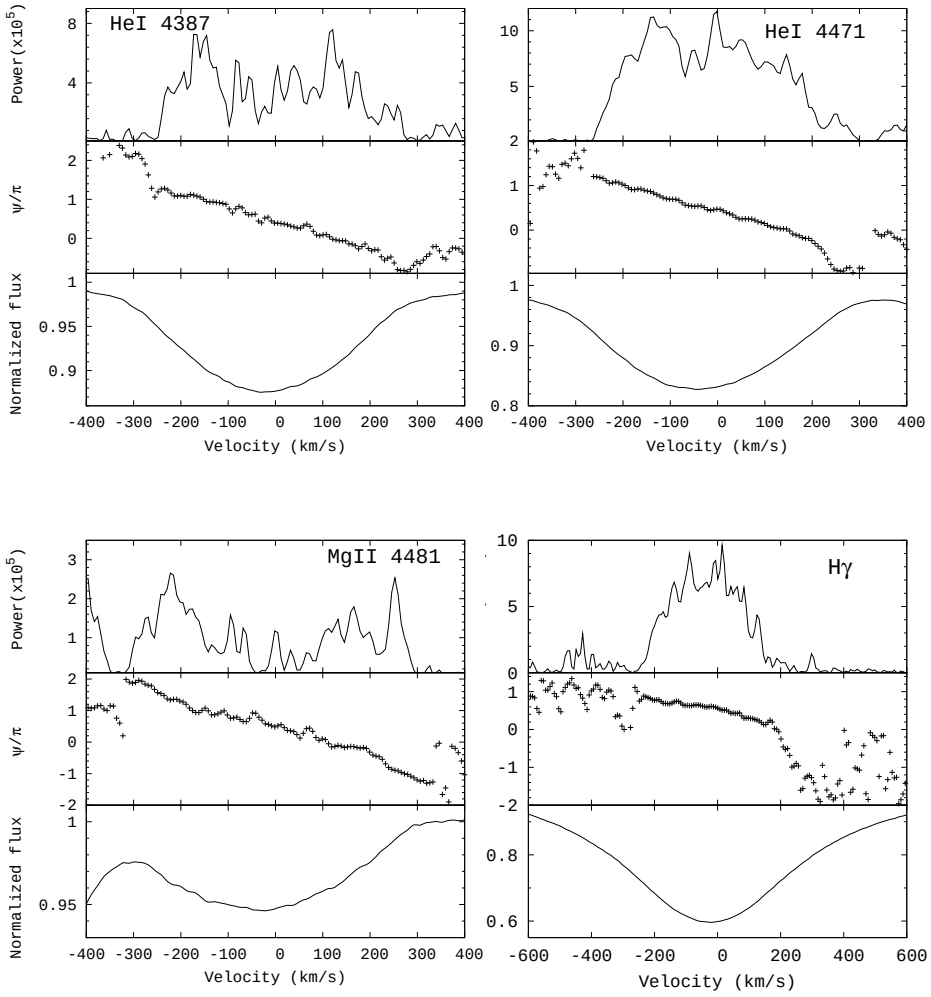

Figure 4.7: Power and phase distributions and averaged line profile of the frequency $f_1 = 1.35$ c d^{-1} for the He I 4387 and 4471, Mg II 4481 and Hγ lines observed in 2005.

4471, Mg II 4481 and Hγ lines. The upper panels of Fig. 4.9 represent the power and phase distributions of frequency f_2 across the line profiles, after prewhitening for frequency f_1 and its first harmonic. The phase velocity of this frequency is not very convincing in the red part of the line profiles. Frequencies 0.12 and 2.11 c d^{-1} are also detected in the frequency analysis, but gives less good phase distributions than f_2. Only in the case of the Hγ line and examining the 5 consecutive days (from 29/06 to 03/07) of the He I 4387 line profile variations does the 2.11 c d^{-1} show a coherent phase distribution (see lower panels of Fig. 4.9).

The frequency $f_2 = 1.12$ c d^{-1} could be a 1-day alias of a long-term period (0.12 or 0.04 c d^{-1}, also detected with the FT + CLEAN method), although the phase velocity is always better for f_2 than for its aliases. In order to check this possibility, we applied the same frequency analysis to the data of the 5 consecutive days (from 29/06 to 03/07). After prewhitening for f_1 and $2f_1$, the frequency $f = 1.12$ or $f = 1.18$ c d^{-1} is found, depending on the line. This shows that this frequency is not caused by the time sampling of the time series. In addition, this result suggests that the most probable frequency is $f = 1.12$ c d^{-1}, and not its long-term 1-day aliases. Moreover, the frequency 0.04 c d^{-1} is not detected anymore with the FT + CLEAN method in the analysis of the 5 consecutive days.

Other frequencies at 2.80, 0.86, 0.76, 1.75, 0.94 c d^{-1} are deduced from the time series, however they do not have coherent phase distributions.

Radial velocities

The radial velocity (RV) of all the studied lines shows a long-term variation (see for example the RV for the He I 4387 line in Fig. 4.10). Nevertheless, $f_1 = 1.35$ c d^{-1} is detected in the periodogram of the RV variations in the majority of the studied lines, as shown in Table 4.6. Phase plots of the radial velocity folded with f_1 are depicted in Fig. 4.11 for the Hγ and He I 4387 and 4471 lines. He I 4471 line is highly blended in the blue wing, so that the mean value is quite different from that of the other lines. Note the different mean RV value for each day for the three lines, probably caused by the long-term variation.

Two possible causes may produce this low trend: a long period (0.13, 0.20 or 0.30 c d^{-1} detected after prewhitening for f_1 in the Hγ, Mg II 4481 and He I 4471 lines respectively) or a frequency close to f_1 (1.29 c d^{-1}

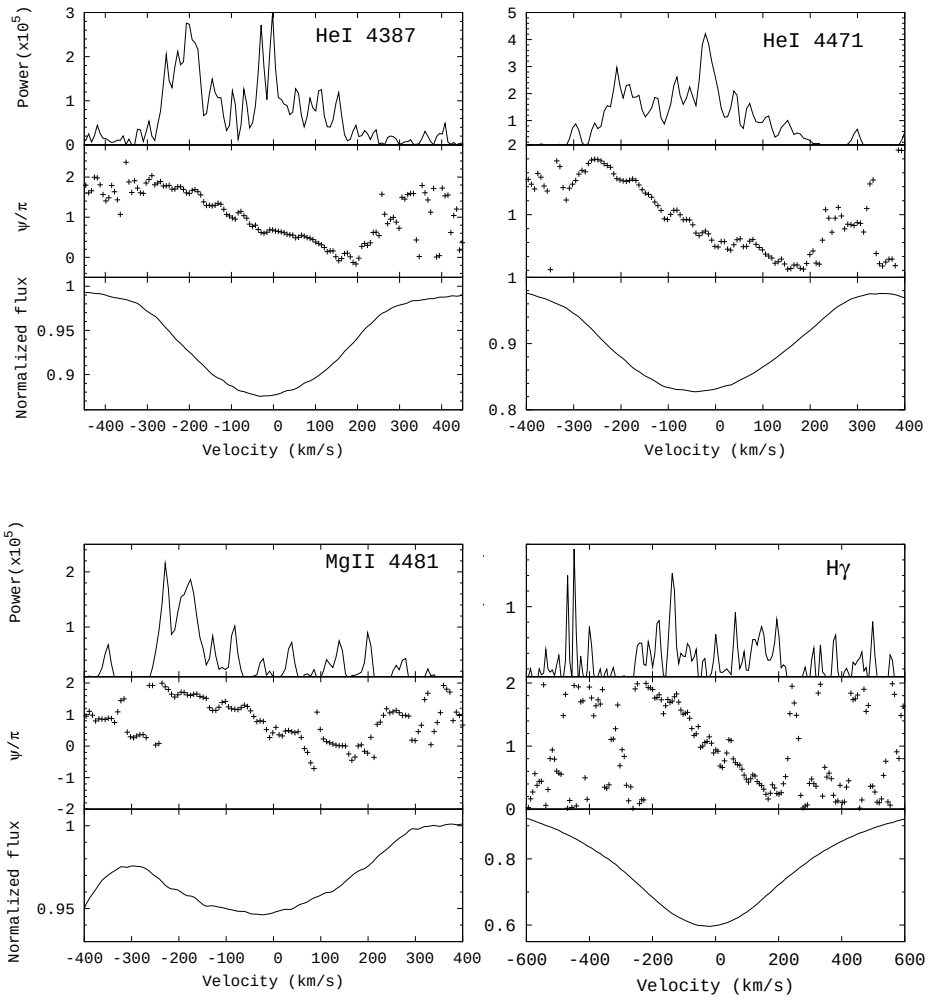

Figure 4.8: Power and phase distributions and averaged line profile of the frequency $f = 2.68$ c d^{-1} for the He I 4387 and 4471, Mg II 4481 and Hγ lines observed in 2005.

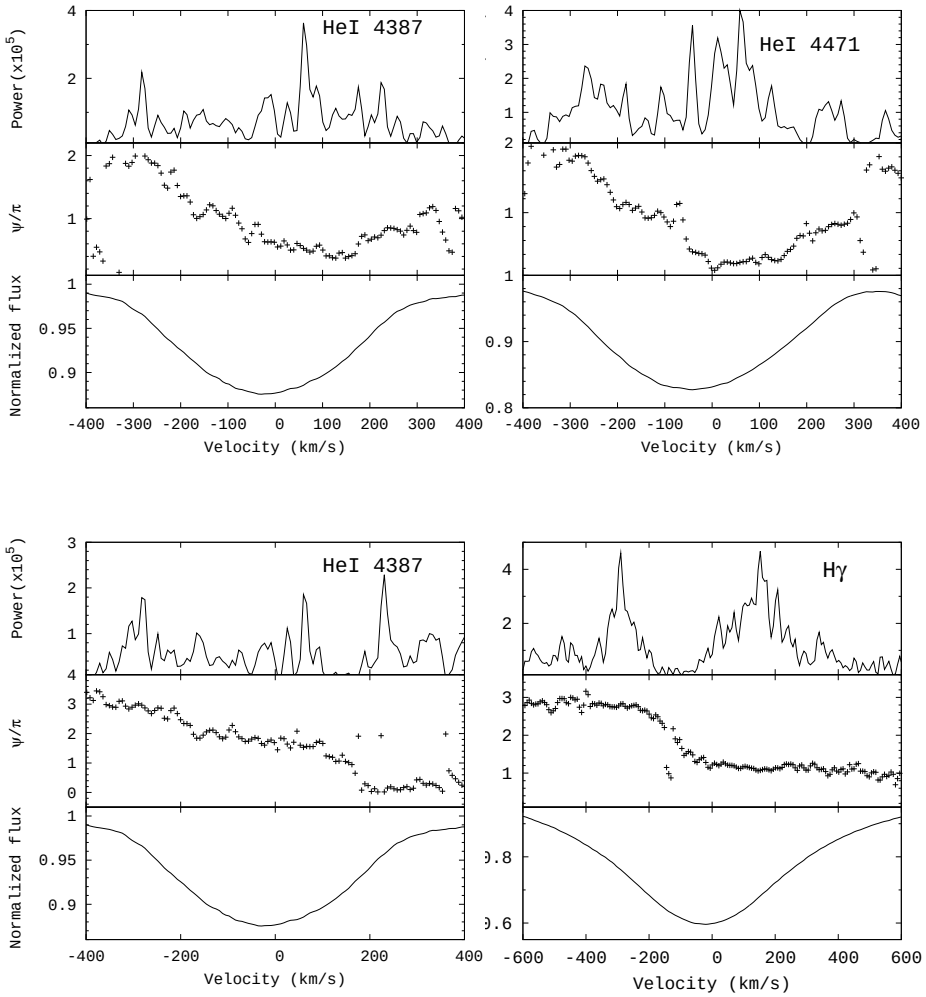

Figure 4.9: **Top left and right**: Power and phase distributions and averaged line profile of the frequency $f = 1.12$ c d^{-1} for the He I 4387 and 4471 lines observed in 2005, after prewhitening for f_1 and $2f_1$. **Bottom left and right**: Power and phase distributions and averaged line profile of the frequency $f = 2.11$ c d^{-1} for the He I 4387 (only the last five days) and Hγ lines observed in 2005 after prewhitening for f_1 and $2f_1$.

in the He I 4387 line and the 1-day aliases of the long-term frequencies). Since the observations have been obtained only on one site at a time, strong aliases are observed in the periodogram, in particular the 1-day alias. Thus, it is difficult to distinguish between the detected long periods and their 1-day aliases.

A spectral analysis of the data of the 5 consecutive days (from 29/06 to 03/07) yields to similar results, i.e. a main frequency around $f_1 = 1.35$ c d^{-1} and an additional long-term frequency (0.13, 0.30 c d^{-1} or their 1-day aliases). Therefore, an additional frequency seems to be present in the *RV* variations, although more observations are required to conclude on this issue.

Central depth

The central depth (*CD*) is derived using a Gaussian fit to each line profile with IRAF. In Fig. 4.10 we show an example of the *CD* variations for the He I 4387 line.

As for the *RV* parameter, the spectral analysis of the *CD* is dominated by the main frequency $f_1 = 1.35$ c d^{-1}, except for the He I 4387 line. An example of a phase diagram with this frequency is displayed in Fig.4.12 The long-term trend is also observed in the *CD*, but the amplitude of the variation is not as large as for the *RV*. Again, another frequency may be present, apart from f_1.

Unfortunately, the phase diagrams of the rest of the detected frequencies, after prewhitening for $f_1 = 1.35$ c d^{-1}, are not very convincing.

Equivalent widths

The main frequencies found in the variations of the equivalent width are 1.12, 1.34, 1.27, 0.94, 2.51 c d^{-1} and their one-day aliases, as found in the analysis of the other spectral parameters. The 1.34 and 1.12 c d^{-1} frequencies can be identified with f_1 and f_2.

Full width at half maximum

A pair of frequencies at 1.27, 1.21 c d^{-1} appears in the periodogram of the *FWMH* variations of the He I 4387 and 4471 line profiles. These

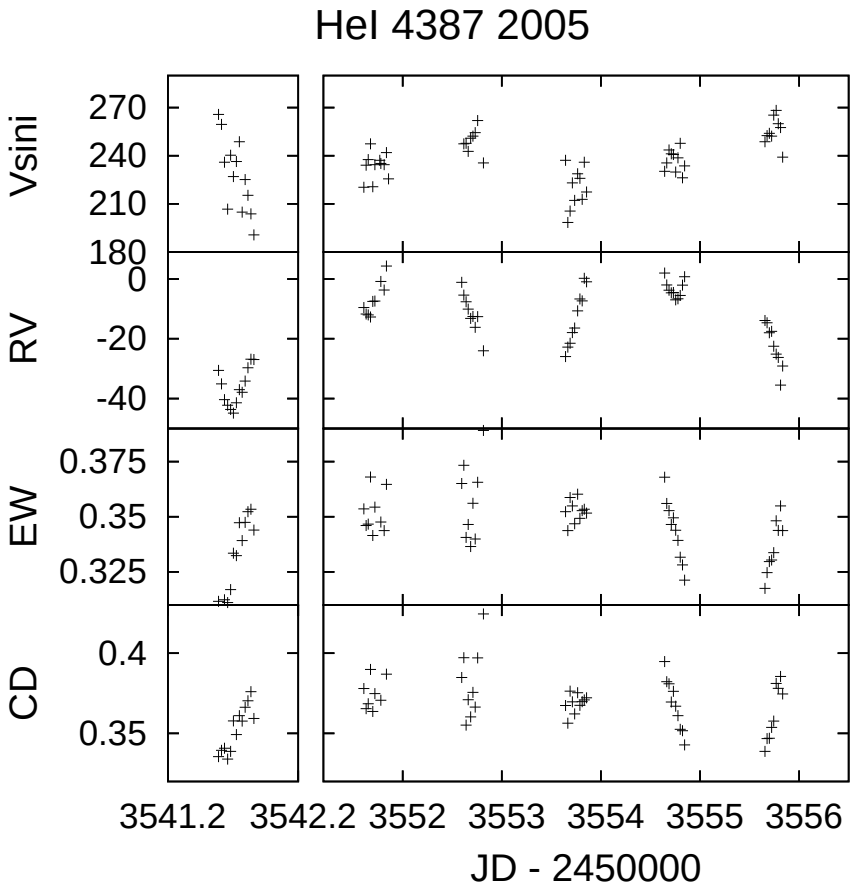

Figure 4.10: Variations in time of $V \sin i$, RV (in km s^{-1}), EW and CD (in normalised intensity) for the He I 4387 line in 2005.

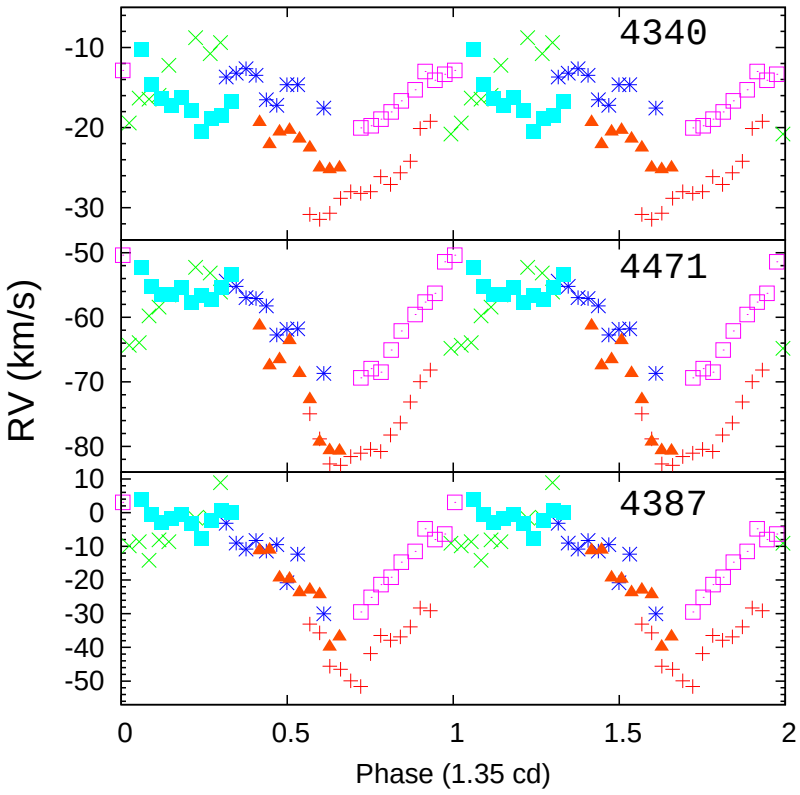

Figure 4.11: Radial velocities of the Hγ, He I 4387 and 4471 lines folded in phase with frequency $f_1 = 1.35$ c d^{-1}. Symbols mark datapoints obtained in different nights.

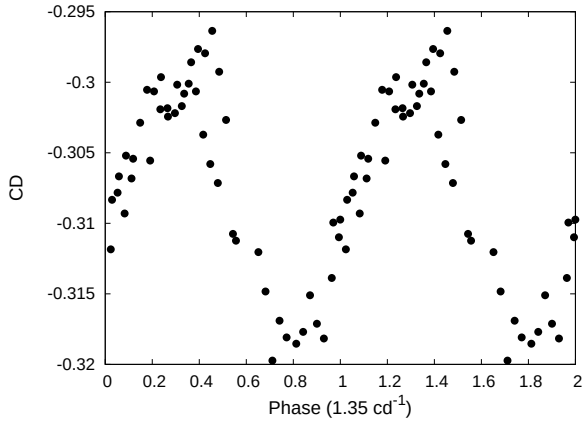

Figure 4.12: Phase diagram of the *CD* variations with frequency $f_1 = 1.35$ c d^{-1} for the Hγ line. Only the 5 consecutive days of observations (from 29/06 to 03/07) are plotted.

frequencies are 0.09 c d^{-1} away from the main frequencies detected in the other spectral parameters, which suggests that they can be aliases of f_1 and f_2 respectively.

Vsini

In order to estimate variations in $V \sin i$, we determined the first minimum of the Fourier transform of each individual spectrum (Gray 1976). We calculated the variation in time of $V \sin i$ only for the Hγ and He I 4387 lines. In addition, we calculated the mean $V \sin i$ over the run, which gives 250 km s^{-1} for the He I 4387 line. It appeared that the Hγ line is not appropriate for the $V \sin i$ determination, since it is formed in zones of extensive depth and it is blended on the wings with O II and C II lines. Inspecting individual spectra, two significant peaks appear in the periodogram for the He I line at frequencies $f = 0.68$ c d^{-1} and f_1. Note that $f = 0.68$ c d^{-1} is the 1-day alias of $2f_1$. A frequency at $f = 1.41$ c d^{-1} is also present in the $V \sin i$ variations for the Hγ line, but its phase diagram is not very convincing.

Phase diagrams

The mean profile has been subtracted from the line profiles in order to produce greyscale dynamical plots of the residual spectra. Greyscale dynamical spectra of the He I 4387 line folded in phase with f_1 and $2f_1$ are shown in Fig. 4.13. The $\pm V \sin i$ domain is depicted in the diagram with a dashed white line. Clear patterns appear in these figures.

In Fig. 4.14 we display the greyscale dynamical spectra of the same line folded in phase with $f_2 = 1.12$ c d^{-1} and 2.11 c d^{-1}. Note that the same patterns are seen in both diagrams, although the amplitude is higher in the 2.11 c d^{-1} one. This might be due to the fact that we cannot distinguish between the frequencies 2.11 c d^{-1} and $2f_2 = 2.24$ c d^{-1}, since they differ by less than our frequency resolution. Signal from f_1 and $2f_1$ have been removed in generating these plots.

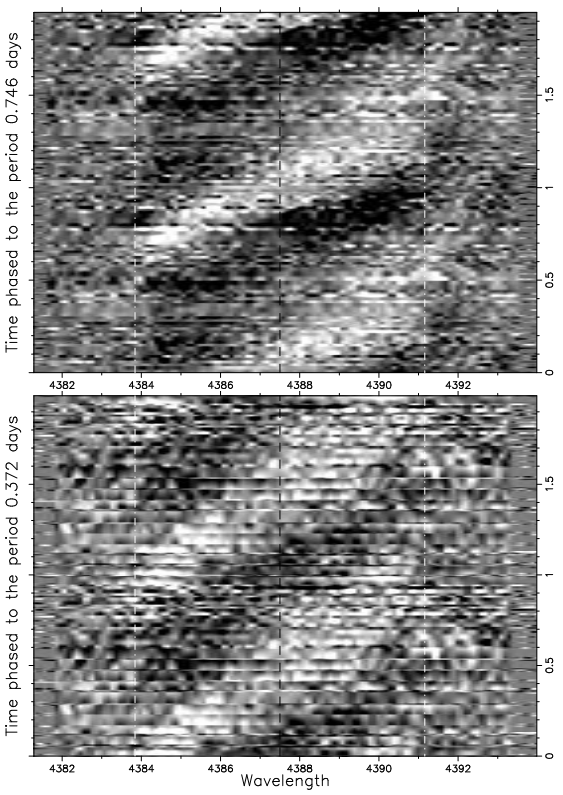

Figure 4.13: Greyscale dynamical spectra of the residual spectra folded in phase with frequencies $f_1 = 1.35$ c d^{-1} and $2f_1 = 2.68$ c d^{-1} for the He I 4387 line observed in 2005. The centre of the line is shown with a dashed black line, while the $\pm V \sin i$ domain is shown with a dashed white line.

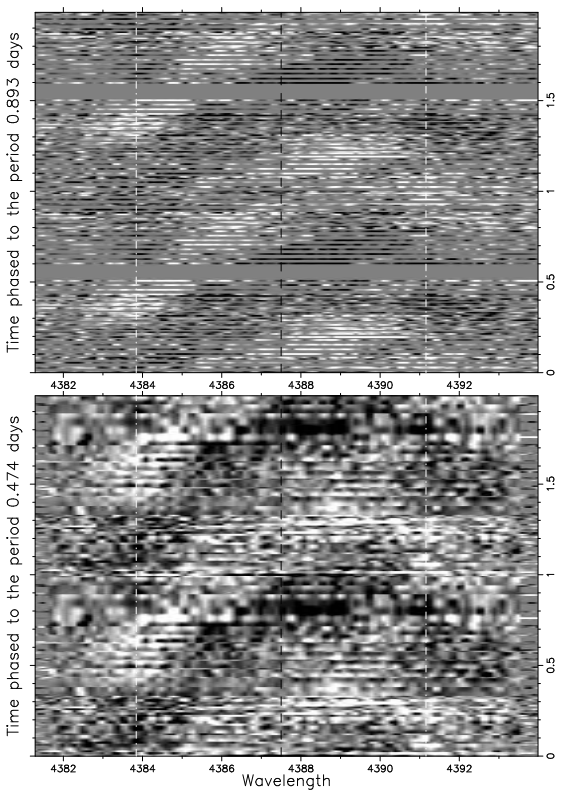

Figure 4.14: Greyscale dynamical spectra of the residual spectra folded in phase with frequencies $f_2 = 1.12$ c d^{-1} and 2.11 c d^{-1} for the He I 4387 line observed in 2005. The centre of the line is shown with a dashed black line, while the $\pm V \sin i$ domain is shown with a dashed white line.

4.6 Mode determination of the NRPs

4.6.1 Velocity phase

In terms of non-radial pulsations, estimates of ℓ and $|m|$ can be obtained from the slope of the velocity phase of the frequency and its first harmonic respectively. Telting and Schrijvers (1997) derived the following relations for $\ell - |m| < 2$:

$$\ell = 0.076 + 1.110 \times \frac{|\Delta\Psi_0|}{\pi}$$

$$|m| = -1.028 + 0.613 \times \frac{|\Delta\Psi_1|}{\pi}$$

where $|\Delta\Psi_0|$ and $|\Delta\Psi_1|$ are the slope of the phase diagram over the whole profile for the studied frequency and its first harmonic. The obtained values have uncertainties of ± 1 for ℓ and ± 2 for $|m|$. Estimates of the pulsating modes for the detected frequencies are reported in Table 4.7.

The slope of the phase velocity of the majority of the studied lines indicates a pulsating mode $\ell \sim 2$ for frequency $f_1 = 1.35$ c d^{-1}. Only in the case of Hγ, the value is much lower. However, the results found with this line are less reliable. In addition, the first harmonic is detected with a $|\Delta\Psi|$ indicative of $|m| \sim 1$.

The case of the $f_2 = 1.12$ c d^{-1} is more puzzling. The slope of the phase diagram over the whole profile is not easily determined from the figures (see upper panels of Fig. 4.9), since it changes from negative to positive within the $\pm V \sin i$ domain. In the case of the one-day alias of f_2, the slope does not change sign but two different values are obtained for the He I 4387 and Hγ lines (see lower panels of Fig. 4.9).

4.6.2 Fourier Doppler Imaging

The mode parameters of the pulsations have also been determined by Fourier Doppler Imaging (FDI, see Kennelly et al. 1992; Jankov et al. 2006). In a rapidly rotating star, the pulsation velocity field and the temperature perturbations are mapped onto a wavelength positions corresponding to the rotationally induced Doppler shift. When the oscillations

Table 4.7: ℓ and $|m|$ values deduced from the phase difference $\Delta\Psi/\pi$ measured from the phase distribution of different frequencies in the *lpv* of several lines.

Line	Year	Freq (c d^{-1})	$\Delta\Psi/\pi$	ℓ	$\|m\|$
He I 4387	2004	1.35	2	2	
		2.68	2.6		1
	2005	1.35	2	2	
		2.68	2.2		1
He I 4471	2004	1.35	2.1	2	
	2005	1.35	2.2	2	
		2.68	1.6		1
Mg II 4481	2005	1.34	2.6	2	
		2.68	2.2		1
Si III 4553	2005	1.34	2.5?		
		2.68			
Hγ	2005	1.34	1	1	
		2.68	2		1

are confined to the equatorial region, which is particularly true for sectoral $\ell = |m|$ oscillations, the obtained normalised wavelength frequency corresponds to $|m|$. In the general case, when tesseral modes are present, the normalised wavelength frequency represents the non-radial degree ℓ more closely than the azimuthal order $|m|$.

The Fourier-Doppler diagram is plotted in Fig. 4.15 for the He I 4387 line obtained in 2005 for $f_1 = 1.35$ c d^{-1} and $2f_1 = 2.68$ c d^{-1}, assuming a $V \sin i = 250\,\mathrm{km\,s^{-1}}$. The analysis of FDI diagrams implies $\ell = 2 - 3$ for the main frequency $f_1 = 1.35$ c d^{-1}.

The FDI method also allows us to estimate the value of $|m|$. The dynamic spectrum of residuals folded with $f_1 = 1.35$ c d^{-1} is presented in Fig. 4.16 (top-left) where the "bump" paths correspond to a $|m| = 3$ mode confined to the equator. In the bottom-left panel the measured NRP phases (in 2π radians) are plotted as circles, while the solid line represents the sinusoidal fit. The right panels of Fig. 4.16 show the "bump" and phase paths corresponding to mode $|m| = 2$ with latitude of 45 deg (full line).

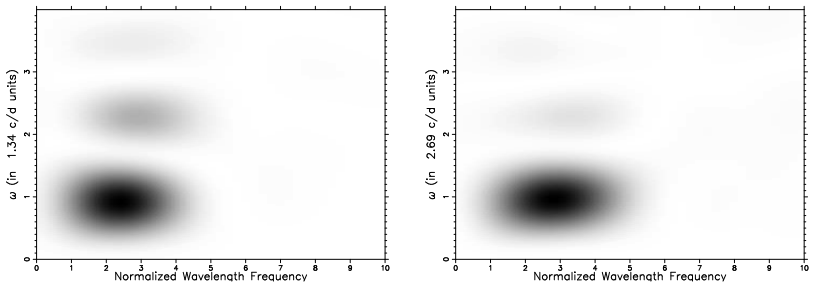

Figure 4.15: Two dimensional Fourier spectrum of the variations for $f_1 = 1.35$ c d^{-1} and $2f_1 = 2.68$ c d^{-1}.

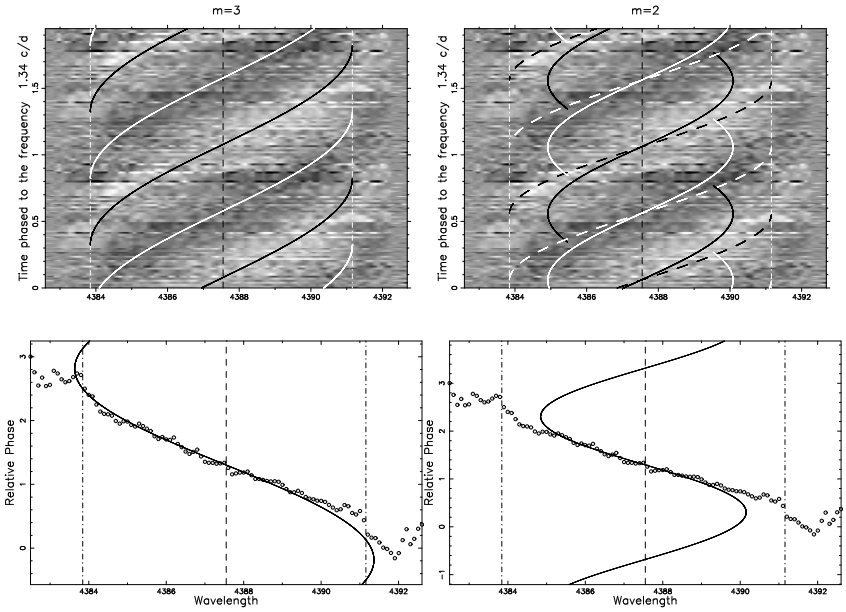

Figure 4.16: **Top-left**: dynamic spectrum of residuals folded with frequency $f_1 = 1.35$ c d^{-1}. Solid line represents the $|m| = 3$ mode confined to the equator. **Bottom-left**: phase distribution and sinusoidal fit for this mode. **Top-right and bottom-right**: Same as left panels, but for the mode $|m| = 2$ with latitude of 45 deg (solid line).

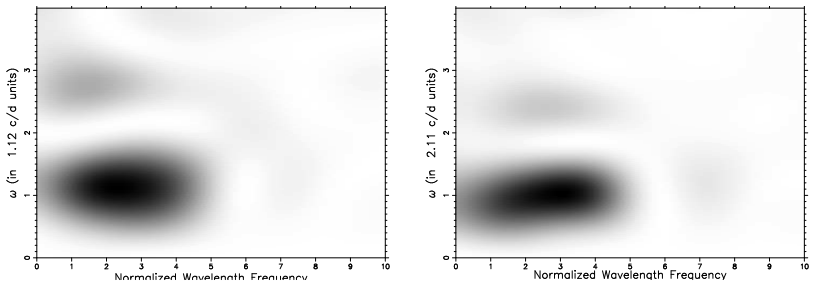

Figure 4.17: Two dimensional Fourier spectrum of the variations for $f_2 = 1.12$ c d^{-1} and 2.11 c d^{-1}.

This $|m| = 3$ mode fits much better than the $|m| = 2$, since the latter requires a latitude of 45 deg and for such a high latitude the pulsation cannot extend to the equator ($\pm V \sin i$), as it is our case.

In the case of frequencies $f_2 = 1.12$ c d^{-1} and 2.11 c d^{-1}, the Fourier-Doppler analysis implies a ℓ-value of 1-4 (Fig. 4.17).

4.6.3 Models

To test the results presented above, we performed a serie of models with a procedure similar to Neiner et al. (2005). The computer code we used is based on a grid of NLTE stellar models calculated with TLUSTY (Hubeny and Lanz 1995) with steps of 1000 K in temperature, 0.2 dex in log g and 0.05 in projection angle. We use solar chemical composition. Perturbations due to non-radial pulsations and fast rotation are calculated with a modified version of the Bruce/Kylie codes (Townsend 1997), which provides the corrected stellar parameters at each point on the visible stellar hemisphere. We used a surface grid of $\sim 50\,000$ points. Integration over the stellar disk is then performed. The final result is a series of time-resolved synthetic spectra of the rotating pulsating star.

We computed 101 spectra per model with frequency $f_1 = 1.35$ c d^{-1}. From the modelled line profiles, we produce greyscale plots of the variation of the line profiles over the pulsation phase. The wavelength resolution is 0.1 Å, the same as the one of the observations presented in this chapter. Models of line profiles and their variations are produced using the

parameters determined in Sect. 4.3.

Fig. 4.18 shows the results obtained for $f_1 = 1.35$ c d^{-1} with $1 \leq \ell \leq 3$ and $-3 \leq m \leq 2$.

Visual comparison of these figures with the corresponding observations (Fig. 4.13) shows that the pattern is correctly reproduced by modes with negative values of m, since these non-radial modes give rise to bumps that move from blue to red through the line profile. We conclude that the waves are prograde in the observer's frame. In addition, the pattern observed for $f_1 = 1.35$ c d^{-1} seems to be best reproduced by a mode with $\ell = 2$, 3 and $m = -2$, -3.

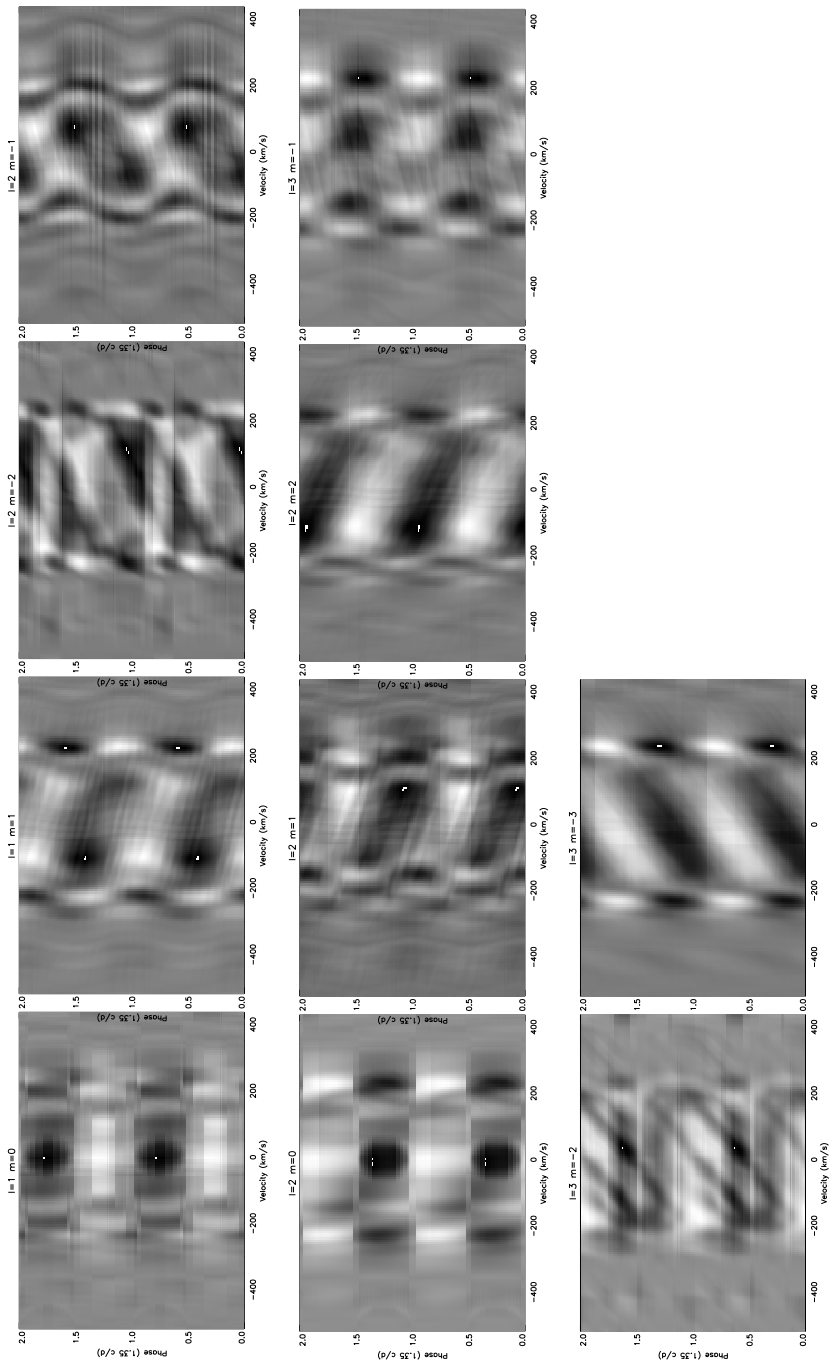

Figure 4.18: Series of pulsation models of the He I 4713 line for $1 \leq \ell \leq 3$ and $-3 \leq m \leq 2$.

4.7 Conclusions

Frequency $f_1 = 1.35$ c d^{-1} and its first harmonic are clearly detected in the line profiles and in the spectral parameters variations of the Be star NW Ser. In addition, this frequency has been found during two consecutive years (2004 and 2005).

Its power distribution concentrated in the line wings indicates dominating horizontal velocities and favours a g-mode identification. Values of ℓ and m have been obtained for this frequency. From the slope of the velocity phase we derive a $\ell = 2 \pm 1$ and $|m| = 1 \pm 2$, whereas the best fit is found for $|m| = 3$ with the FDI method. In order to test these results we have performed a serie of synthetic models, taking into account the high rotational velocity of the star. The pattern is correctly reproduced by modes with negative m, and in particular with $\ell = 2$, 3 and $m = -2$, -3.

An additional frequency is probably present. While the *lpv* analysis yields a frequency at $f_2 = 1.12$ c d^{-1}, a long-term frequency (in the range of 0.12 to 0.30 c d^{-1}) is detected in the analysis of the spectral parameters. In addition, the phase velocity of frequency f_2 is not very convincing. Its 1-day alias 2.11 c d^{-1} shows a better phase distribution and dynamic spectra. Moreover, it was found by Aerts (2000) using Hipparcos data. Thus it could be the actual frequency. More observational work is needed to confirm this frequency.

Finally, note that the frequencies $f_1 = 1.35$ c d^{-1} and $f_2 = 1.12$ c d^{-1} have also been detected photometrically in Chapt. 3 and modelled as non-radial modes. The frequency $f_1 = 1.35$ c d^{-1} is similar within errors to the frequency $F_4 = 1.412$ c d^{-1} detected in photometry, which was modelled as a g-mode with $\ell \sim 3$.

A new campaign has been performed in the summer 2006, which will allow us to refine the parameters of the pulsating mode corresponding to the dominant frequency $f_1 = 1.35$ c d^{-1}, and to confirm the presence of the second frequency $f_2 = 1.12$ c d^{-1}.

Bibliography

Aerts, C.: 2000, in *ASP Conf. Ser. 214: IAU Colloq. 175: The Be Phenomenon in Early-Type Stars*, p. 192

Buil, C.: 2006, *Be stars Atlas on the web, http://www.astrosurf.com/buil/us/bestar.htm*

Castelli, F. and Kurucz, R. L.: 2003, in N. Piskunov, W. W. Weiss, and D. F. Gray (eds.), *IAU Symposium*, p. 20

Cunto, W., Mendoza, C., Ochsenbein, F., and Zeippen, C. J.: 1993, *A&A* **275**, L5

Floquet, M., Neiner, C., Janot-Pacheco, E., Hubert, A. M., Jankov, S., Zorec, J., Briot, D., Chauville, J., Leister, N. V., Percy, J. R., Ballereau, D., and Bakos, A. G.: 2002, *A&A* **394**, 137

Frémat, Y., Neiner, C., Hubert, A.-M., Floquet, M., Zorec, J., Janot-Pacheco, E., and Renan de Medeiros, J.: 2006, *A&A* **451**, 1053

Frémat, Y., Zorec, J., Hubert, A.-M., and Floquet, M.: 2005, *A&A* **440**, 305

Gray, D. F.: 1976, *The observation and analysis of stellar photospheres*, New York, Wiley-Interscience, 1976. 484

Grevesse, N. and Sauval, A. J.: 1998, *Space Science Reviews* **85**, 161

Hubeny, I. and Lanz, T.: 1995, *ApJ* **439**, 875

Hubert, A. M. and Floquet, M.: 1998, *A&A* **335**, 565

Hubert-Delplace, A.-M. and Hubert, H.: 1979, *An atlas of Be stars*, Paris-Meudon: Observatory, 1979

Jankov, S., Mathias, P., Chapellier, E., Le Contel, J.-M., and Sareyan, J.-P.: 2006, *A&A* **453**, 1041

Kennelly, E. J., Walker, G. A. H., and Merryfield, W. J.: 1992, *ApJ Lett.* **400**, L71

Kurucz, R. L.: 1993, *CD-ROM No.13. Cambridge, Mass.: Smithsonian Astrophysical Observatory.*

Lanz, T. and Hubeny, I.: 2003, *ApJS* **146**, 417

Lenz, P. and Breger, M.: 2005, *Communications in Asteroseismology* **146**, 53

Meilland, A., Stee, P., Vannier, M., Millour, F., Domiciano De Souza, A., Malbet, F., Martayan, C., Paresce, F., Petrov, R., Richichi, A., Spang, A., and the AMBER Consortium Collaboration: 2006, *A&A in press*

Neiner, C., Floquet, M., Hubert, A. M., Frémat, Y., Hirata, R., Masuda, S., Gies, D., Buil, C., and Martayan, C.: 2005, *A&A* **437**, 257

Percy, J. R., Marinova, M. M., BožiĆ , H., and Harmanec, P.: 1999, *A&A* **348**, 553

Pych, W.: 2004, *PASP* **116**, 148

Rivinius, T., Baade, D., Štefl, S., Townsend, R. H. D., Stahl, O., Wolf, B., and Kaufer, A.: 2001, *A&A* **369**, 1058

Schaller, G., Schaerer, D., Meynet, G., and Maeder, A.: 1992, *A&AS* **96**, 269

Slettebak, A.: 1982, *ApJS* **50**, 55

Solano, E., Catala, C., Garrido, R., Poretti, E., Janot-Pacheco, E., Gutiérrez, R., González, R., Mantegazza, L., Neiner, C., Fremat, Y., Charpinet, S., Weiss, W., Amado, P. J., Rainer, M., Tsymbal, V., Lyashko, D., Ballereau, D., Bouret, J. C., Hua, T., Katz, D., Lignières, F., Lüftinger, T., Mittermayer, P., Nesvacil, N., Soubiran, C., van't Veer-Menneret, C., Goupil, M. J., Costa, V., Rolland, A., Antonello, E., Bossi, M., Buzzoni, A., Rodrigo, C., Aerts, C., Butler, C. J., Guenther, E., and Hatzes, A.: 2005, *AJ* **129**, 547

Telting, J. H. and Schrijvers, C.: 1997, *A&A* **317**, 723

Townsend, R. H. D.: 1997, *MNRAS* **284**, 839

Vaníček, P.: 1971, *Ap&SS* **12**, 10

Varosi, C., Lanz, T., Dekoter, A., and Hubeny, I.: 1995, *http://idlastro.gsfc.nasa.gov/ftp/pub/contrib/varosi/modion/*

Chapter 5

The search for Be stars in the exoplanet fields of COROT

5.1 Introduction

In addition to the bright Be stars to be observed in the COROT seismology fields as described in the previous chapters, we will also observe faint Be stars in the COROT exoplanet fields. Our goal is to obtain photometric time series for seismologic studies. Although the photometric accuracy in the exoplanet fields will be lower than in the seismology fields, in the former we can have colour information that will be useful to identify modes in large amplitude pulsators, as shown in Garrido (2000) and in Chapt. 3. This project is part of the COROT Additional Science Programme. The corresponding proposal has been sent to answer the first Announcement of Opportunity for COROT Additional Science, and has been approved by the COROT scientific committee. This proposal has been sent in the framework of an international collaboration, and one of our responsibilities is to select the list of Be targets to be observed.

In general, very few Be stars are known in the COROT cones within the appropriate range of magnitudes for the exoplanet CCDs. So, our first task is to detect Be stars included in the exoplanet fields of the first COROT pointings. Up to now, we explored the exoplanet fields of the

two first COROT long runs.

In this chapter, I explain the photometric technique we employed to detect faint Be stars, describe the observations performed until now and the corresponding data reduction, and present the lists of faint Be stars already found in the COROT exoplanet fields.

5.2 Photometric techniques to detect Be stars

Photometric detection of emission-line stars can be performed by observing through a narrow filter centred on the Hα line and a wider filter also containing the Hα line. By comparing the photometric colour obtained with the difference between the light detected through both filters with another photometric colour measured in the slope of the Paschen continuum, emission-line stars can easily be identified. This has been demonstrated by several authors (Grebel et al. 1992; Pigulski et al. 2001; McSwain and Gies 2005) and is shown later on in Fig. 5.6 for our data.

Line emission occurs at different places in the HR diagram. Moreover, M-type stars mimic the behaviour of emission-line stars in the colour-colour diagram described above, because the TiO absorption bands depress the continuum around the Hα line. As we are interested only in early-type stars, additional photometric information is needed to select the B-type stars among all emission-line stars detected with the Hα photometry. Wide-band photometric systems are not well-suited for this purpose, because with these systems is very difficult to distinguish between reddened early-type stars and intrinsically red ones. We expect most of the Be stars in the exoplanet fields to be significantly reddened, as they are placed in the galactic plane.

For the photometric spectral classification of the emission-line stars, we have thus used additional observations in the Strömgren photometric system. This system was developed by Strömgren (1966) in order to determine high precision observables with a direct link to the astrophysical parameters. It is defined by four narrow filters *uvby* and a list of standard stars, which was published by Crawford and Barnes (1970b).

Three indices are then defined, the colour index $(b-y)$ and

$m1 = (v-b)-(b-y)$ and
$c1 = (u-v)-(v-b)$,

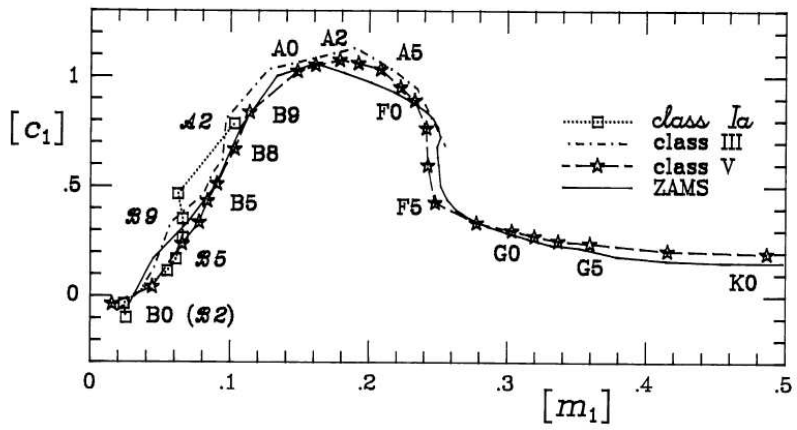

Figure 5.1: The [m1]-[c1] diagram taken from Moon (1986).

which are the metal-line and Balmer discontinuity indices respectively. These indices are affected by interstellar reddening. However, the indices:

$[m1] = m1 - 0.2(b-y)$ and
$[c1] = c1 + 0.32(b-y)$

are reddening free, since

$E(m1) = 0.2E(b-y)$ and
$E(c1) = -0.32E(b-y)$.

Therefore, we can consider a classification diagram free of reddening effects in which [m1] is the abscissa and [c1] the ordinate. The location of stars of various spectral types in the [m1]-[c1] diagram is shown in Fig. 5.1.

Spectral classification from the photometric indices can be applied to faint stars where previous MK classification is not available and for which extensive programs of spectroscopic determination of MK types would be very time consuming.

Table 5.1: The six filters and exposure times (in s) for each filter used for the observations.

Filter	Central λ (Å)	Equivalent Width (Å)	Exposure time Short	Large
u	3500	340	80	800
v	4110	200	40	400
b	4670	160	20	200
y	5470	240	20	200
Sloan r	6240	1347	5	50
Hα	6568	95	60	600

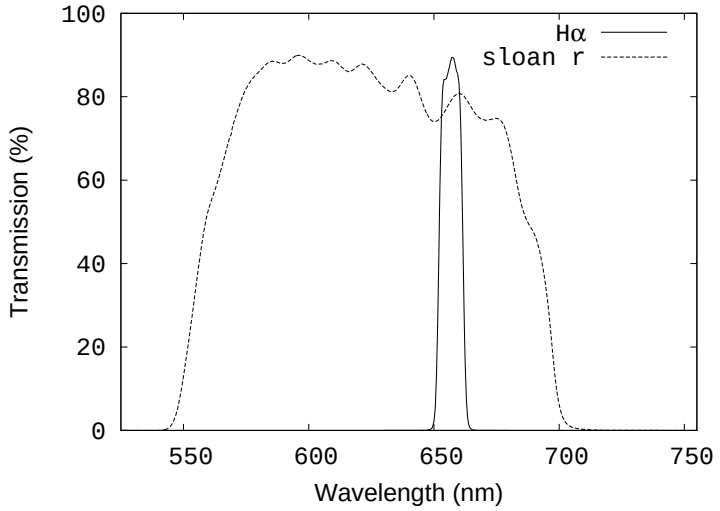

Figure 5.2: Transmission curve of the Hα and Sloan r filters.

5.3 Observations

CCD photometry has been obtained at the 2.5 m Isaac Newton Telescope (INT) in La Palma (Spain). A total of 6 nights, three in August and three in December, have been granted in 2005, observing in the directions of the two first COROT long runs.

The Wide Field Camera (WFC), with four thinned EEV 4128×2148 CCDs, has been used as detector. The field of view of the WFC at the INT is $33'.8 \times 33'.8$, with an angular scale of 0.33 arcsec pixel^{-1}. Observations have been done through the four Strömgren *uvby* filters, a narrow filter centred on the Hα line and the Sloan r filter (Table 5.1 and Fig.5.2). Each field has been sequentially measured through the six filters. Two different exposure times have been used for each filter, in order to ensure a wide range of stellar magnitudes. Exposure times in each filter, presented in Table 5.1, have been selected such that a B type star produces approximately equal count rates through all filters. With this configuration, the exposure times provide the optimum S/N for stars of magnitudes between 10 and 18 and thus, the range of magnitudes from 12 to 16 used in the COROT exoplanet fields is well covered.

The observations have been performed towards the Galactic Centre and Anticentre directions, around the first two long runs already selected by the COROT scientific committee. In Table 5.2 we show the coordinates of the first two long runs of the COROT mission followed by the coordinates of the centre of CCD4 for each pointing. As shown in Fig 5.3, the centre of CCD4 is a few arcminutes away from the rotator centre (the centre of the ig rectangle formed by the 4 CCDs).

An example of mosaic of 8 frames obtained with the INT data is displayed in Fig. 5.4. Each pointing consist of two exposures of 1200 s in the Hα filter. This image, showing the cluster Dolidze25 in its centre, has been kindly provided by Elena Puga.

5.4 Data reduction

This section describes in detail all the required steps for the successful cleaning and reduction of CCD frames. Two steps are involved: a pre-reduction procedure in which the frames are calibrated (cleaned); the

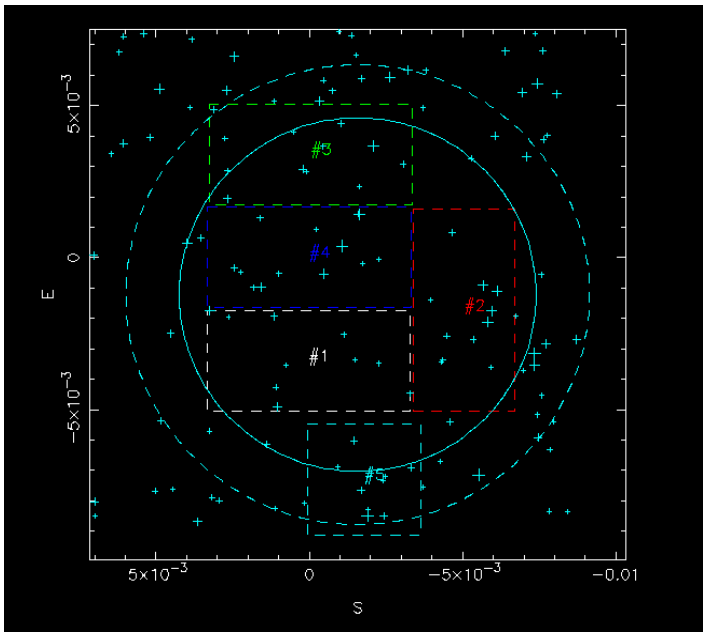

Figure 5.3: The layout of the WFC, showing the relative CCD positions (#1, #2, #3 and #4). Image courtesy of the CASU INT Wide Field Survey.

Table 5.2: Coordinates of the observations performed at the INT, meant to map the exoplanet fields of the first two long runs to be observed by COROT.

Long run INT pointing	RA	DEC
LRC1	$19^h23^m28^s$	$+00:28:48$
INT 1	$19^h27^m30^s$	$+00:14:00$
INT 2	$19^h26^m02^s$	$+00:14:00$
INT 3	$19^h28^m58^s$	$+00:14:00$
INT 4	$19^h27^m29^s$	$+00:46:00$
INT 5	$19^h25^m22^s$	$+01:29:30$
LRA1	$6^h46^m48^s$	$-00:05:24$
INT 1	$6^h45^m06^s$	$+00:47:38$
INT 2	$6^h42^m36^s$	$+00:46:34$
INT 3	$6^h45^m11^s$	$+00:08:38$
INT 4	$6^h42^m40^s$	$+00:07:26$
INT 5	$6^h45^m16^s$	$-00:33:00$
INT 6	$6^h42^m46^s$	$-00:34:40$
INT 7	$6^h45^m22^s$	$-01:13:26$
INT 8	$6^h42^m52^s$	$-01:14:38$

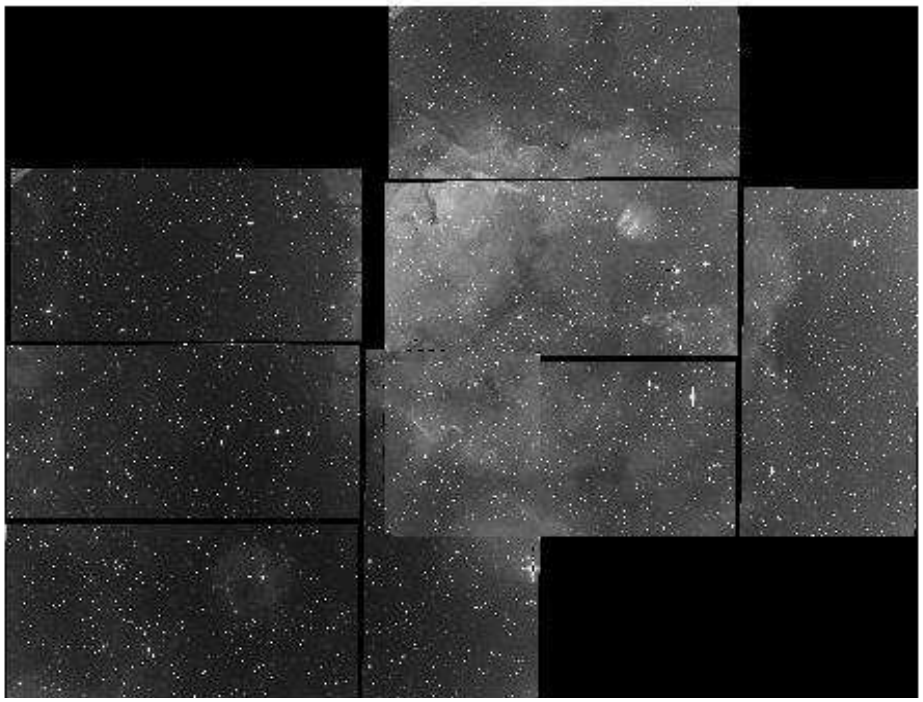

Figure 5.4: A mosaic obtained with the INT observations. Image courtesy of Elena Puga.

cleaned frames are then submitted to further reduction using DoPHOT (Schechter et al. 1993) in which PSF-fitting and aperture photometry are calculated. A fairly good astrometric solution is then calculated for each frame.

5.4.1 Removal of instrumental signatures

Images have been processed using IRAF[1]. Since each WFC image is a mosaic of four frames, we have used the *mscred* package, which operates on mosaic data files as single files. Only bias and flat-fields of the same observing run have been used to reduce the given science images.

The average value in the overscan region of each image has been subtracted. Then, the overscan region has been trimmed off the image.

A master-bias has been built for each observing season and CCD frame. Each pixel of the master bias is the median value of the same pixel in all the bias frames.

A master-flat-field image has been produced for each observing season, CCD frame and filter. The bias have been subtracted from each flat-field frame. The resulting frames have been corrected for non-linearity effects[2] and averaged to produce the master-flat-field image.

The science images have been processed by subtracting the bias frame, correcting for non-linearity and flat fielding. In this step, each resulting image is separated into four images, one per CCD.

Once these corrections have been performed, the images are fully calibrated and are ready to be processed.

5.4.2 Instrumental magnitudes extraction

Due to the large number of images to be processed, I have developed an automatic procedure to extract the photometric and astrometric data from each bias- and flat-subtracted image with minimal user interaction. This

[1]IRAF is distributed by the National Optical Astronomy Observatories, which is operated by the Association of Universities for Research in Astronomy (AURA) Inc., under cooperative agreement with the National Science Foundation.

[2]Coefficients have been obtained from the web page: http://www.ast.cam.ac.uk/∼wfcsur/technical/foibles

procedure consist in a set of programs written in C-Shell, which call different well-known astronomical packages, as IRAF, SExtractor (Bertin and Arnouts 1996), DoPHOT and wcstools (Mink 1999, 2002). These packages have been selected depending on the following requirements: 1.- little human intervention ; 2.- PSF photometry to deal with crowded images; 3.- astrometry; 4.- high speed algorithms.

Photometry has been performed using the DoPHOT program (Schechter et al. 1993). A C-version of this program developed by Mike Reid[3] has been used. DoPHOT has been used in the reduction of the most important photometric surveys, as for example OGLE-I and OGLE-II (Udalski et al. 1997) and MACHO (Alcock et al. 1999). The latter uses a code called SoDoPHOT, which is DoPHOT optimised to the MACHO image data.

DoPHOT is a computer program design to search for objects on a digital image of the sky and to produce positions, magnitudes and crude classification for those objects. A major advantage of the program is to operate with minimal user interaction. The user supplies only rough estimates of the seeing and background sky for each digital frame. The parameters for a given instrument (e.g., gain and readnoise) need to be provided only once for a set of images.

DoPHOT uses an initial guess of the FWHM of the stellar images to identify stars brighter than some fairly high initial detection threshold. The analytic function used to represent a star is then fitted to a number of subrasters centred on different objects in order to determine a better estimate of the shape of a typical star. The appropriate fitted model is subtracted from the image, producing a "working" image. In this object-subtracted working image, the program then searches for fainter stars by progressively lowering the detection threshold.

When the footprint of an object (i.e. the half intensity contour, which is modelled as an ellipse) is bigger than that of the "typical" star, it is declared to be "extended" and DoPHOT classifies the object as a galaxy or a double star.

In our case, we have benefited from the empirical PSF-fitting, added to the version 3.0 of the program. The empirical fitting proceeds in parallel with the analytic fitting and is used to create the star-subtracted image.

[3]http://www2.vuw.ac.nz/staff/michael_reid/software.html

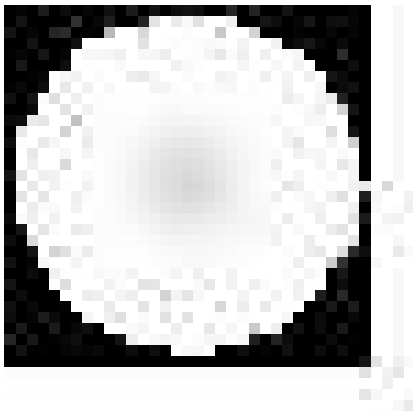

Figure 5.5: An empirical template of the PSF.

An empirical template is written out as a subraster for examination. In Fig. 5.5 we show an example of an empirical template. A single star, cleaned of its neighbours, is used as template. It is chosen automatically, starting from the brightest star and working downwards in magnitude. A priori, empirical PSF-fitting produce better photometry and clearer star subtracted images. It allows to deal with images that are slightly moved, due to bad tracking at the time of observations.

Preliminary attempts to apply DoPHOT to our images showed that the ability of the program to identify stars and to manage arbitrary FWHM guesses is not satisfactory. To overcome this problem, we took advantage of DoPHOT allowing for a "warmstart" in which it reads a list of objects with their positions in the image, subtract them from the working image, and then searches for new objects. This permits to obtain improved photometry in cases where the positions of the objects are previously known. In our case, to produce the initial list of stars, we benefit from the SExtractor program (Bertin and Arnouts 1996), which proves to be much more suitable than DoPHOT in the identification of stars and the automatic computation of a first guess of the FWHM. In addition, cosmic rays are removed from the list of objects, in order to ensure that none of the cosmic rays encountered are accidentally classified as stars.

An exposure-time correction has been applied to each image in order to convert the total number of counts in flux.

For each individual frame, we obtained the mean difference between the aperture photometry and the PSF-fitting based instrumental magnitudes only for bright stars with a photometric error below 0.05 mag. PSF instrumental magnitudes for all stars in the frame are then transformed to the instrumental system defined by the aperture photometry by adding the mean difference value. To calculate this mean difference we have applied the 3σ-clipping algorithm to reject outliers.

Before applying the photometric programs, we need to perform some preparatory treatment in the images. First of all, DoPHOT can only handle image data that are 2 byte integers, and thus the pixel values of the images are divided by two, to get numbers below 32 000. Moreover, all the images are converted from real to integer, since DoPHOT only works with short-type (integer) pixels, Secondly, the images are rotated in order to have the north up, since it is required for the astrometric package. A rotation of 270 degrees is applied to the CCDs 1,3 and 4, whereas CCD 2 requires a 180-degrees rotation. Thirdly, the alignment of the different filters has been performed with the *imalign* task of IRAF, which measures in batch mode the X and Y shifts between a list of images, and produces a new list of images aligned and trimmed to include only the overlapping region.

Although precise astrometry is beyond the scope of this work, we have transformed the instrumental pixel coordinates into equatorial coordinates in order to facilitate the identification of all the observed stars and their cross-correlation with other photometric lists. Standard coordinates have been determined with the wcstools package (Mink 1999, 2002). Typically, the program automatically finds about $50-100$ stars from the USNO-A2.0 catalogue (Monet 1998) in each image to perform the cross-correlation. The rms errors in the fitting give total uncertainties of less arcsec for equatorial coordinates.

5.4.3 Standard photometry

To compute the atmospheric extinction coefficients, several of the standard fields used for the photometric transformation (see below) have been observed from two to five times at different airmasses ranging from one to

two.

The atmospheric extinction has been determined by the multi-night multi-star method described by Manfroid (1993). Computations have been performed by using the RANBO2 package, written by J. Manfroid. The implementation of this reduction procedure allows the construction of a consistent natural system, which contains the extra-atmospheric instrumental magnitudes of all constant stars included in the computation procedure. Stars from all observed fields are included in the building of the natural system.

In order to obtain accurate standard photometry, an adequate set of *uvby* standard stars for CCD photometry has to be chosen. Our standard list is composed of stars in young open clusters with *uvby* photometry published by Crawford et al. (1970) for NGC 869 and 884, Canterna et al. (1979) for NGC 1039, Crawford et al. (1977) for NGC 6910 and NGC 6913, Nissen et al. (1987) for M67, Crawford and Barnes (1970a) for NGC 752 and Perry et al. (1978) for NGC 2169. As the V values for NGC 752, 869 and 884 are not included in the corresponding *uvby* photometric lists, we have used the values given by Johnson (1953) for the former and by Johnson and Morgan (1955) for the latter two. The suitability of this standard list to obtain magnitudes and indices well tied to the standard photometric system and free from systematic errors has been discussed by Capilla and Fabregat (2002).

Transformations have been computed from the natural system to the standard *uvby* system defined by the standard star list described above. The obtained transformation equations are the following:

$$V = 12.249 + 0.010(b-y)_n + y_n$$
$$(b-y) = 0.392 + 0.911(b-y)_n$$
$$m_1 = 0.142 + 0.826m_{1,n} - 0.030(b-y)$$
$$c_1 = 0.192 + 1.092c_{1,n} + 0.148(b-y)$$

where the subscript "n" refers to the natural system. All scaling coefficients in the *uvby* transformation are close to unity, while the colour terms are small, indicating a good conformity between the instrumental and standard photometric systems.

Table 5.3: Photometric accuracy of the transformation.

V	(b-y)	m1	c1
0.020	0.020	0.024	0.028

A measure of the photometric accuracy is the standard deviation of the mean catalogue minus the transformed values for the standard stars. These values are presented in Table 5.3.

In the case of the Sloan r and Hα filters, we corrected the values from atmospheric extinction with the same procedure as explained above for the other filters, but no transformation has been calculated and thus we have worked with the instrumental colour (Sloan r)-Hα.

5.5 Discussion

In Fig. 5.6 we illustrate with an example the procedure to find Be stars. In the top panel we show the (Sloan r -Hα) vs (b-y) photometric diagram for all stars in a frame. Stars without emission occupy a narrow sequence in the diagram. Three emission-line stars clearly show up above this sequence. The following step consists in obtaining a spectral classification of these stars. To do so, we use the reddening-free [m1]-[c1] photometric diagram (bottom panel of Fig. 5.6). Placing the emission-line stars in this diagram, we can estimate the spectral type as a function of their position. Two of the three stars are OB-type stars and the third one is a M star. In the top panel of Fig. 5.6 we marked all early-type stars with blue crosses.

We have applied this procedure to all our photometric images. For the detected Be stars, we have obtained an estimate of the spectral subtypes from their [m1] and [c1] values, using the calibration by Moon (1986).

The list of Be stars located in the exoplanet CCDs close to the primary targets HD 49933 + HD 49434 and HD 180642 + HD 181555 that we found with the method presented in this chapter is presented in Table 5.4. The ID of the star (USNO-A2.0 number when it exists, otherwise 2MASS number), the V standard magnitude, an estimate of the spectral type, the associated COROT-ID number and other identifiers are reported in these

tables for each star.

Note that in the Galactic Centre direction we have found very few Be stars. The main reason is the high interstellar extinction towards this direction which does not allow us to observed far in distance and so, only a small volume of space is observed. The OB-type stars, and in particular Be stars, have a low space density and in a space-limited sample, their number is much lower than the number of other types of stars.

5.5.1 Other detections of Be stars in the exoplanet fields

We performed a preliminary campaign in 2003 in order to test the method to search for faint Be stars with CCD photometry. Observations have been made at Observatorio Astronómico Nacional (OAN) at Calar Alto through the Strömgren *uvby* and Hα and Hβ filters. Since the field of view of the camera was only 11 square arcminutes, we observed a list of emission-line stars found by Kohoutek and Wehmeyer (1999) and Robertson and Jordan (1989), whose spectral types were not yet known. Three Be stars located close to the primary stars HD 49333 + HD 49434 were detected. These stars are included in Table 5.4.

In addition, we have cross-correlated the emission-line stars located in the exoplanet fields close to the primary stars HD 49333 + HD 49434 found by Kohoutek and Wehmeyer (1999) and Robertson and Jordan (1989) with the Johnson photometry gathered by the exoplanet community to the EXODAT database. Three emission-line stars are considered as A-type stars, so they are probably reddened Be stars. These probable Be stars are also included in Table 5.4.

Other members of the COROT Be stars team have contributed to the search for Be stars in the exoplanet fields. Martayan et al. (priv. comm.) performed spectroscopic observations with VLT-Giraffe multifiber spectrograph in order to search for Be stars in the exoplanet fields next to HD 49933 + 49434 stars. Two faint Be stars, included in Table 5.4, have been detected.

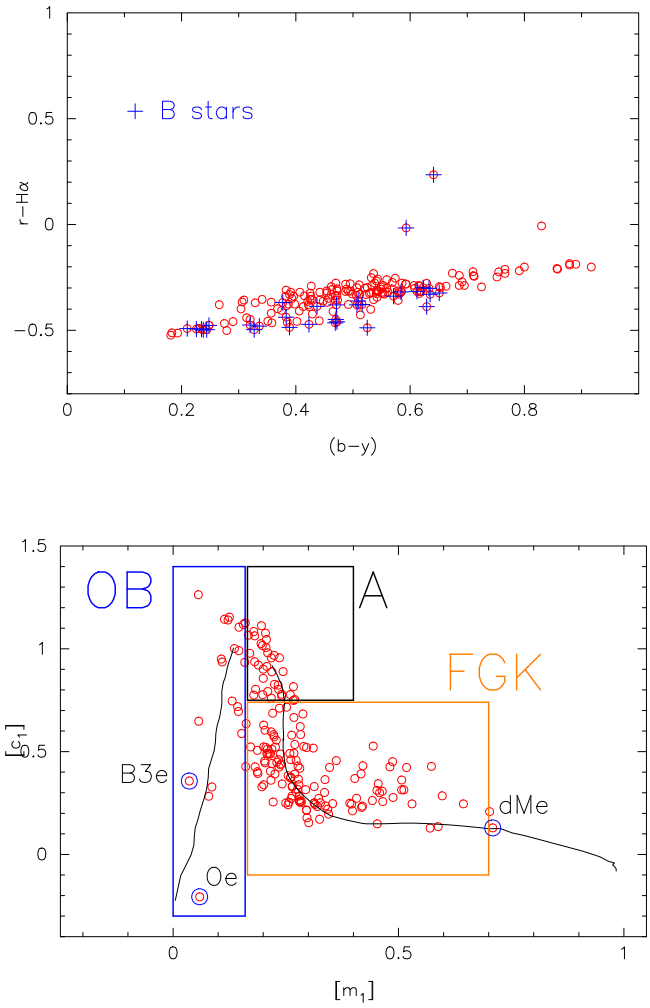

Figure 5.6: **Top**: (Sloan r-Hα) vs (b-y) diagram for a pointing. The blue crosses mark the OB stars. Note that three emission-line stars show up above the narrow sequence. **Bottom**: [m1]-[c1] diagram for the same pointing. The three boxes represent three regions which divide the diagram in stars with spectral types OB, A and FGK. The emission-line stars found in the top panel and their spectral type are indicated.

Table 5.4: Be stars located in the exoplanet fields close to the primary targets HD 49933 + HD 49434 and HD 180642 + HD 181555. The ID number (USNO-A2.0 when it exists, otherwise 2MASS number), the standard V magnitude, the spectral type, the associated COROT-ID number and other identifiers are shown for each star. Notes: 1.- found with VLT-Giraffe; 2.- type A0 with strong emission, probably a Herbig/AeBe star; 3.- marginal detection; 4.- detected at the OAN; 5.- probable Be stars, which have been cross-correlated with the emission-line star catalogues and EXODAT.

USNO-A2.0 2MASS	V	Sp. T.	COROT-ID	Other ID	Notes
HD 49933 + HD 49434					
0825-02964178	12.68		102617376	EM* RJHA 39	4
0825-02946092	17.01	B3			3
0825-02956066	17.09	B2			
0900-03332328	14.86	B3	102638133		
0825-02986310	15.39	B9	102640224		
0900-03337088	13.18	B0	102645018	EM* RJHA 40	
0825-02992046	13.81	A2	102646349		2
06423521+0043212	13.99	A0	102649238		
0825-03001155	14.02	B3	102656190		1
0825-03029064	13.47		102686433		1
0825-03011674	13.24	B5	102667801		
0825-03016556	14.43	A0	102673096		3
0900-03358811	14.87	B3	102675453		
0825-03033218	14.02	B5	102690931		
0900-03375309	12.84		102696078	EM* RJHA 44	5
0900-03387134	14.61	B8	102710394		
0900-03390126	13.45	B4	102713600	EM* RJHA 46	4
0825-03060502	14.25	B9	102719279		
0825-03066991	15.31	B6	102725623		
0900-03403786	12.10		102728404	EM* RJHA 47	5
0900-03410680	12.99	B2	102736797		
0900-03411580	12.50		102737893	EM* RJHA 48	5
0900-03420934	14.18	B3	102749390		
0900-03427546	16.00	B8	102757172		
0825-03100827	14.12	B0	102762536		
0825-03104592	13.22	B2	102766835	EM* RJHA 51	4
0900-03449051	12.69	B3	102781703		
0900-03452139	12.08	B0	102785204	EM* RJHA 53	

Continued...

Table 5.4: Continued.

USNO-A2.0 2MASS	V	Sp. T.	COROT-ID	Other ID	Notes
0900-03452381	12.98	B2	102785480	EM* RJHA 52	
		HD 180642 + HD 181555			
0900-15067137	17.72	B2			
0900-15155630	18.24	B0			
0900-14955653	17.07	B5			3
0900-14992185	14.54	B5	100915020		
0900-14975609	13.32	B5	100870830		3
0900-14965129	18.26	B9			
0900-15006064	17.32	B4			3
0900-15210634	15.97	A2	101370131		3
0900-15081007	16.61	B1	101110409		3
0900-15150414	11.18	B3			
0900-15145462	17.72	B0			
0900-15212504	15.03	B3	101372042		3
0900-15143314	16.44	B6	101242425		
0900-15174166	17.80	B2			

5.6 Conclusions

We have found 43 Be stars located in the first two exoplanet fields to be observed by COROT. 29 Be stars are close to the primary targets HD 49933 + HD 49434 and 14 vlose to HD 180642 + HD 181555. These stars have been proposed as targets for COROT.

We developed an automatic procedure to reduce the photometry obtained with the WFC at the INT. We have demonstrated that this process produces photometric results with the adequate accuracy. This tool will allow us to perform a precise and fast reduction of future CCD photometric data.

We plan to continue to this observing program to detect the Be-star content of the successive COROT long and short runs, once their position has been decided.

Bibliography

Alcock, C., Allsman, R. A., Alves, D. R., Axelrod, T. S., Becker, A. C., Bennett, D. P., Cook, K. H., Drake, A. J., Freeman, K. C., Geha, M., Griest, K., Lehner, M. J., Marshall, S. L., Minniti, D., Peterson, B. A., Popowski, P., Pratt, M. R., Nelson, C. A., Quinn, P. J., Stubbs, C. W., Sutherland, W., Tomaney, A. B., Vandehei, T., Welch, D. L., and The MACHO Collaboration: 1999, *PASP* **111**, 1539

Bertin, E. and Arnouts, S.: 1996, *A&AS* **117**, 393

Canterna, R., Crawford, D. L., and Perry, C. L.: 1979, *PASP* **91**, 263

Capilla, G. and Fabregat, J.: 2002, *A&A* **394**, 479

Crawford, D. L. and Barnes, J. V.: 1970a, *AJ* **75**, 946

Crawford, D. L. and Barnes, J. V.: 1970b, *AJ* **75**, 978

Crawford, D. L., Barnes, J. V., and Hill, G.: 1977, *AJ* **82**, 606

Crawford, D. L., Glaspey, J. W., and Perry, C. L.: 1970, *AJ* **75**, 822

Garrido, R.: 2000, in *ASP Conf. Ser. 210: Delta Scuti and Related Stars*, p. 67

Grebel, E. K., Richtler, T., and de Boer, K. S.: 1992, *A&A* **254**, L5+

Johnson, H. L.: 1953, *ApJ* **117**, 356

Johnson, H. L. and Morgan, W. W.: 1955, *ApJ* **122**, 429

Kohoutek, L. and Wehmeyer, R.: 1999, *A&AS* **134**, 255

Manfroid, J.: 1993, *A&A* **271**, 714

McSwain, M. V. and Gies, D. R.: 2005, *ApJ* **622**, 1052

Mink, D. J.: 1999, in D. M. Mehringer, R. L. Plante, and D. A. Roberts (eds.), *ASP Conf. Ser. 172: Astronomical Data Analysis Software and Systems VIII*, p. 498

Mink, D. J.: 2002, in D. A. Bohlender, D. Durand, and T. H. Handley (eds.), *ASP Conf. Ser. 281: Astronomical Data Analysis Software and Systems XI*, p. 169

Monet, D. G.: 1998, *Bulletin of the American Astronomical Society* **30**, 1427

Moon, T.: 1986, *Ap&SS* **122**, 173

Nissen, P. E., Twarog, B. A., and Crawford, D. L.: 1987, *AJ* **93**, 634

Perry, C. L., Lee, P. D., and Barnes, J. V.: 1978, *PASP* **90**, 73

Pigulski, A., Kopacki, G., and Kołaczkowski, Z.: 2001, *A&A* **376**, 144

Robertson, T. H. and Jordan, T. M.: 1989, *AJ* **98**, 1354

Schechter, P. L., Mateo, M., and Saha, A.: 1993, *PASP* **105**, 1342

Strömgren, B.: 1966, *ARA&A* **4**, 433

Udalski, A., Kubiak, M., and Szymanski, M.: 1997, *Acta Astronomica* **47**, 319

Chapter 6

Multiperiodic Be stars in the Small Magellanic Cloud

6.1 Introduction

The aim of this chapter is to test our period-determination techniques in data as similar as possible to the COROT data. For this purpose we use photometric time series of Be stars of the Small Magellanic Cloud (SMC) provided by the MACHO survey (Alcock et al. 1999). Although the photometric accuracy is much lower than the one expected for COROT, the time span of the MACHO observations is large enough to provide a very good frequency resolution in the spectral analysis and hence allow us to distinguish between very close frequencies, which may produce a beating phenomenon. This kind of analysis is much more difficult with the other datasets we have used, such as ASAS-3, Hipparcos or ground-based observations (see Chapt. 2). The disadvantage of the MACHO data in comparison with the COROT data are, e.g., the presence of 1-day aliases, the much lower precision and less coverage of the duty cycle.

The analysis of stars in the SMC has the interesting advantage of extending our pulsational study to Be stars with low metallicity. The pulsational study of massive stars in a low-metallicity environment is a very important issue. Theoretically, the pulsational instability of β Cephei, SPB and Be stars has a great dependence on the metallicity, since the bump driving pulsations in these stars originates from a large number of

transitions in the iron-group ions. Pamyatnykh (1999) showed that the β Cephei and SPB instability strips practically vanish at $Z < 0.01$ and $Z < 0.006$ respectively. As the metallicity of the LMC and SMC are 0.008 and 0.004 respectively, the Magellanic Clouds are among the best objects to test this prediction.

A large sample of B and Be stars in the Magellanic Clouds have been observed by Martayan (2005) with the multi-object spectrograph GIRAFFE at ESO/VLT. Martayan et al. (2006, hereafter M06) presented a preliminary analysis of the MACHO light-curves of 13 Be stars in the SMC. They used PDM and FT+CLEAN methods to search for frequencies. Here we apply our period-determination techniques to the same time series in an attempt to compare our methods with those employed by M06, and possibly refine their analysis and detect additional frequencies.

6.2 Data analysis

The data have been retrieved from the MACHO database[1]. Magnitudes in the b and r bands are provided here for each star. In the majority of the studied stars we have analysed both datasets in order to confirm or reject the detected frequencies. For the sake of simplicity, for most of the stars we only provide the detailed analysis of the data in one filter.

Period analysis was performed by means of standard Fourier analysis and least-square fitting (see Chapts. 2 and 3). The data have not been detrended with polynomial functions.

In order to know whether the frequencies are significant, we follow the *signal to noise amplitude ratio* requirement (see Chapts. 2 and 3).

The time span of the observations is ~ 2690 d in the majority of stars, and thus, the resolution in frequency is ~ 0.000372 c d^{-1}. The determination of the error in frequency was obtained with Period04 (Lenz and Breger 2005), which follows equations derived by Montgomery and O'Donoghue (1999). In our case, the estimate of the error in frequency, accounting for the correlation in the residuals (Schwarzenberg-Czerny 1991), is of the order of $1 - 5 \times 10^{-5}$ c d^{-1}.

[1] http://wwwmacho.mcmaster.ca/

Table 6.1: Results of the frequency analysis for Be stars in the SMC. Frequencies are in c d^{-1}. $f_{\rm Balona}$ stands for frequencies previously obtained by Balona (1992).

Be star	MACHO	$f1$	$f2$	$f_{\rm Balona}$
SMC5_3296	207.16373.5496	2.0032		
SMC5_13978	207.16373.58	1.37946	0.59335	1.361
SMC5_14727	207.16373.63	1.12291		1.120
SMC5_16523	207.16316.30	1.29297	1.29344	
SMC5_16544	207.16373.129	1.70774	1.64993	
SMC5_21152	207.16147.14	0.98514	1.00443	
SMC5_37162	207.16259.57	0.88531	0.90612	
SMC5_43413	207.16315.41	2.0071		
SMC5_82042	207.16375.41	2.48834	1.16625	
SMC5_82941	207.16203.47	0.62483	0.15324	
MHF[S9]35238	207.16372.22	1.32661	1.32616	
MHF[S9]37842	207.16315.26	1.18153	1.21709	
MHF[S9]39981	207.16259.29	1.27691		

6.3 Results on individual stars

We present here the detailed analysis of each of the 13 studied Be stars. In Table 6.1, we show the ID number of the stars from the EIS survey (Nonino et al. 1999), followed by the MACHO number, the detected frequencies and frequencies previously obtained by Balona (1992).

6.3.1 SMC5_3296, MACHO207.16373.5496

M06 found a frequency at 2.0032 c d^{-1}, i.e. a period of 0.4992 d. We have only analysed the data in the b filter of this star. The highest peak in the periodogram corresponds to a frequency at 0.00048 c d^{-1}, which is a very long period of 2083.33 d and is probably a result of a long-term trend in the light curve. After prewhitening for this frequency, we found a frequency at 1.00289 c d^{-1}. Note that the frequency obtained by M06 is similar to a 1-day alias or twice this frequency. The frequency obtained

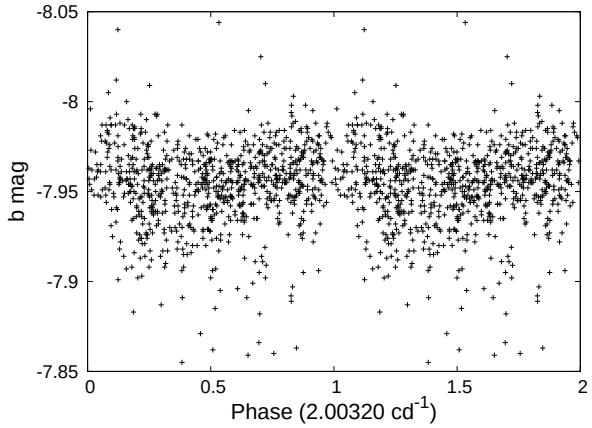

Figure 6.1: Phase curve of SMC5_3296 folded with the frequency 2.00320 c d^{-1}.

by M06 (2.0032 c d^{-1}) has a less scattered phase diagram (Fig. 6.1) and therefore it is more likely to be the actual one.

6.3.2 SMC5_13978, MACHO207.16373.58

This star was observed by Robertson (1974) and has been included in his list with number NGC 330-B5. Balona (1992) also observed this star (#964 in his list) and found it variable with a period of 0.735 d (i.e. $f = 1.361$ c d^{-1})

M06 found a period of 1.685 d, i.e. a frequency at 0.59347 c d^{-1}. A 3σ-clipping has been applied to the r filter dataset, in order to determine more accurately the fitting parameters. The periodogram of the b light curve shows significant peaks at frequencies F1 = 1.37946 c d^{-1} and F2 = 0.59335 c d^{-1} and their daily aliases (see top panel of Fig. 6.2). It is important to highlight that F1 = 1.37946 c d^{-1} is similar to the frequency obtained by Balona (1992). The amplitudes and phases for each frequency, obtained with the least-square fitting code, are reported in Table 6.2. The phase plots with frequencies F1 and F2 are presented in the middle and bottom panels of Fig. 6.2.

Note that the amplitude of F1 is higher than the amplitude of F2 in the b filter, but it is in the other way around in the red filter (Table 6.2).

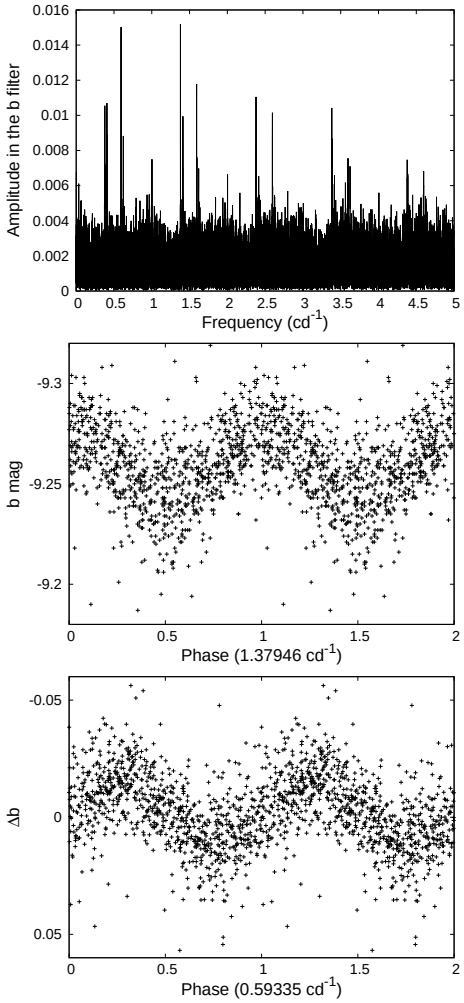

Figure 6.2: **Top**: periodogram of SMC5_13978 in the b filter. **Middle**: phase diagram of SMC5_13978 folded with the frequency F1 = 1.37946 c d^{-1}. **Bottom**: phase diagram folded with the frequency F2 = 0.59335 c d^{-1}, after prewhitening for F1 = 1.37946 c d^{-1}.

Table 6.2: Results of the frequency analysis for SMC5_13978. T stands for the elapsed time length, N the number of datapoints and σ_{res} the standard deviation of the residuals.

No.	Freq. c d^{-1}	Amp. mmag	Phase rad	S/N	σ_{res} mmag
	b filter	T = 2690.85 d	N=860	σ_{init} = 29.6 mmag	
F1	1.37946	15.5	2.91	11	26.3
F2	0.59335	14.4	0.52	10	24.2
	r filter	T = 2690.85 d	N=869	σ_{init} = 26.1 mmag	
F1	1.37947	12.7	2.73	11	22.5
F2	0.59338	13.2	0.45	12	20.5

After prewhitening for this frequencies, two frequencies $\sim$ 1.00261 and $\sim$ 0.00039 c d^{-1} appeared in the periodogram. These frequencies are not real and are probably due to the data sampling or to systematic errors in the observations.

6.3.3 SMC5_14727, MACHO207.16373.63

This star has been observed by Robertson (1974) and has been included in his list with number NGC 330-B14. It was also observed by Balona (1992) (#585 in his list) who found the star variable with a period of 0.893 d. M06 found a period of 0.8905 d, i.e. a frequency at 1.1230 c d^{-1}. Moreover, they detected an additional frequency at 2.00241 c d^{-1}. We have only analysed the data in the b filter for this star. A peak at frequency 1.12291 c d^{-1} clearly appears in the periodogram, as shown in the upper panel of Fig. 6.3. A phase plot for this frequency is displayed in the lower panel of Fig. 6.3. After prewhitening for the main frequency, we found the second frequency detected by M06. In our analysis, this frequency is not significant enough (SNR $\sim$ 3.3) and this suggests that this frequency is probably an artifact.

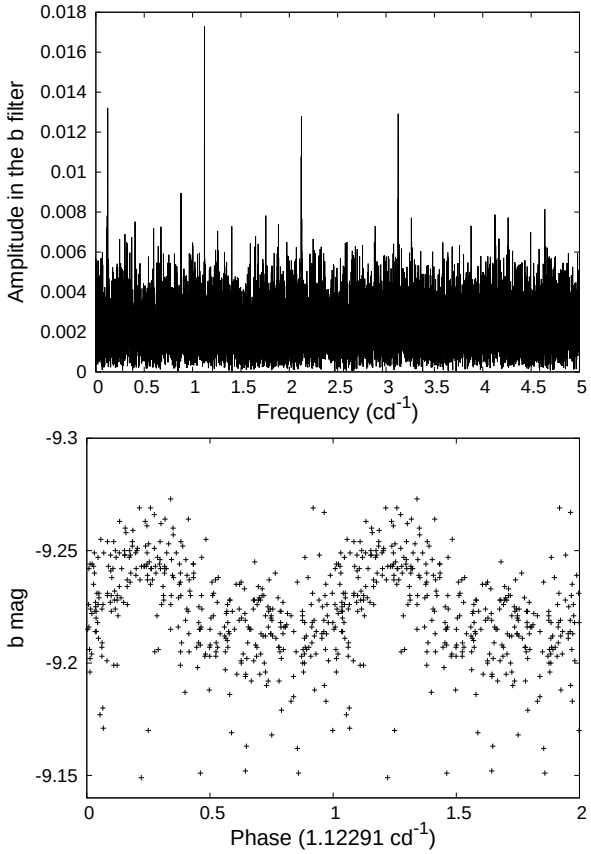

Figure 6.3: **Top**: periodogram of SMC5_14727 in the b filter. **Bottom**: phase diagram of SMC5_14727 folded with the frequency 1.12291 c d^{-1}.

Table 6.3: Results of the frequency analysis for SMC5_16523.

No.	Freq. c d^{-1}	Amp. mmag	Phase rad	S/N	σ_{res} mmag
	b filter	T = 2690.85 d	N=967	σ_{init} = 45.8 mmag	
F1	1.29297	40.0	0.94	23	34.8
F2	1.29344	23.7	3.82	14	31.1
	r filter	T = 2690.85 d	N=1019	σ_{init} = 38.7 mmag	
F1	1.29297	33.9	0.90	24	30.7
F2	1.29343	20.7	3.78	15	27.0

6.3.4 SMC5_16523, MACHO207.16316.30

M06 found a period of 1.547 d, i.e. a frequency at 0.6464 c d^{-1}. From the spectral analysis, we found a frequency at 1.29297 c d^{-1}, i.e. twice the one obtained by M06. The phase diagram with the frequency F1 = 1.29297 c d^{-1} is displayed in the upper panel of Fig. 6.4 for the b filter. Prewhitening for this frequency, we obtained a significant (SNR $\sim$ 14) frequency at F2 = 1.29344 c d^{-1}(bottom panel of Fig. 6.4). Frequencies, amplitudes and phases are listed in Table 6.3.

The difference between F1 and F2 is $\sim$ 0.00043, which is larger than our frequency resolution (1/T $\sim$ 0.000371) and thus this frequency is likely to be real.

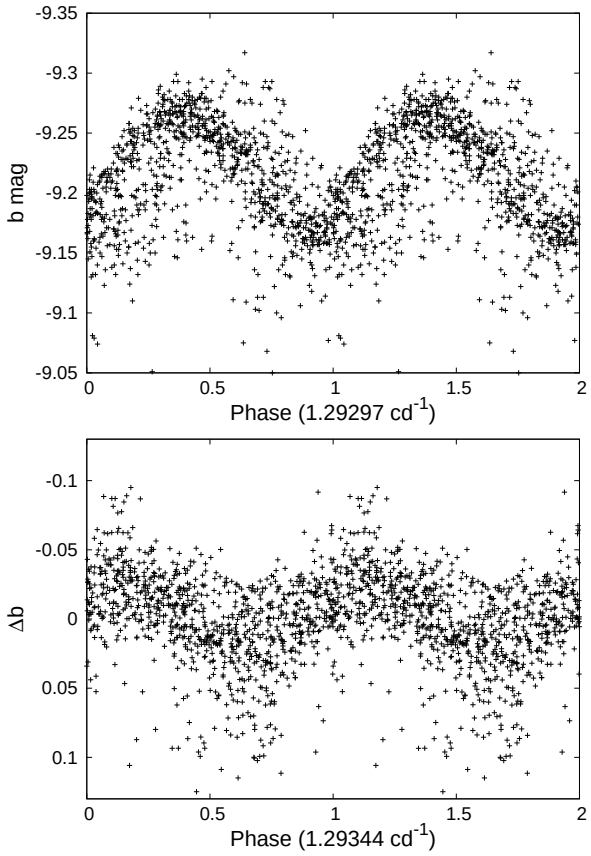

Figure 6.4: **Top**: phase diagram of SMC5_16523 folded with the frequency F1 = 1.29297 c d^{-1}. **Bottom**: phase diagram of SMC5_16523 folded with the frequency F2 = 1.29344 c d^{-1} after prewhitening for frequency F1.

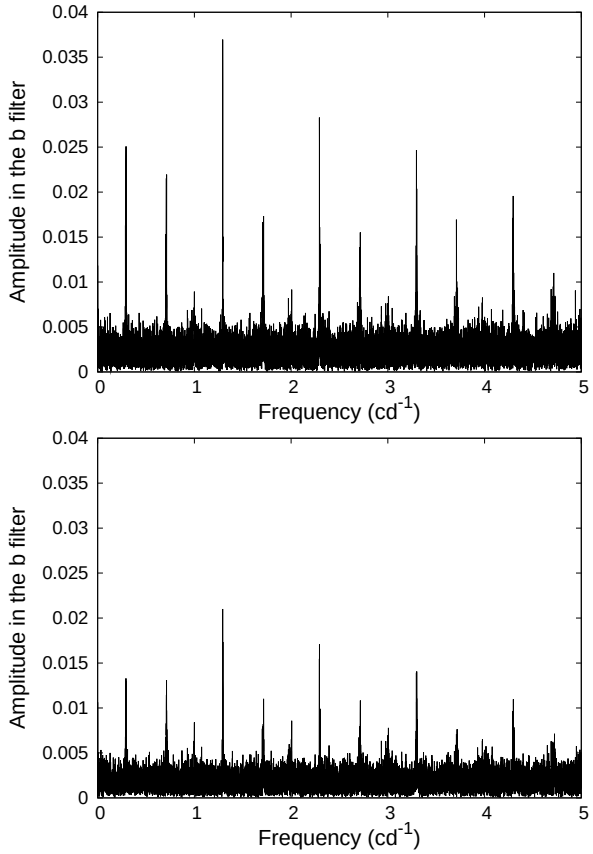

Figure 6.5: **Top**: periodogram of SMC5_16523 in the b filter. **Bottom**: periodogram of SMC5_16523, after prewhitening for F1 = 1.29297 c d^{-1}.

Table 6.4: Results of the frequency analysis for SMC5_16544.

No.	Freq. c d^{-1}	Amp. mmag	Phase rad	S/N	σ_{res} mmag
	b filter	T = 2690.85 d	N=923	σ_{init} = 35.3 mmag	
F1	1.70774	29.8	2.66	23	30.9
F2	1.64993	25.3	2.76	19	24.9
	r filter	T = 2690.85	N=952	σ_{init} = 40.6 mmag	
F1	1.70774	31.5	2.61	20	35.9
F2	1.64992	25.9	2.74	17	30.9

6.3.5 SMC5_16544, MACHO207.16373.129

M06 found a period of 0.586 d, i.e. a frequency at 1.7064 c d^{-1}.

We did not find a long-term variation in the light curve of this star. Applying a Fourier analysis we found two significant frequencies at F1 = 1.70774 c d^{-1} and F2 = 1.64993 c d^{-1}, as shown in Fig. 6.6. Frequencies, amplitudes and phases are reported in Table 6.4. The phase plots with these frequencies are depicted in Fig. 6.7. After prewhitening for the first two frequencies we found another significant frequency (SNR $\sim$ 8) at 1.65030 c d^{-1}. This frequency differs from F2 by only 0.00037 c d^{-1}, which is similar to our frequency resolution, and thus we cannot confirm this frequency. This third detected frequency may be produced by the variation in time of frequency F2, as it occurs in Be/X systems (Schmidtke and Cowley 2005).

In order to confirm the presence of frequencies F1 = 1.70774 c d^{-1} and F2 = 1.64993 c d^{-1}, we folded the light curve of this star with the frequency $F_{beating} = 1.70774 - 1.64993 = 0.05781$ c d^{-1} produced by the beating of the two detected frequencies (see left panel of Fig. 6.8). In the right panel we show the sum of the two sinusoidal functions with parameters obtained with the least-square fitting (given in Table 6.4).

In order to better understand the beating phenomenon observed in this star, we explain below its mathematical description.

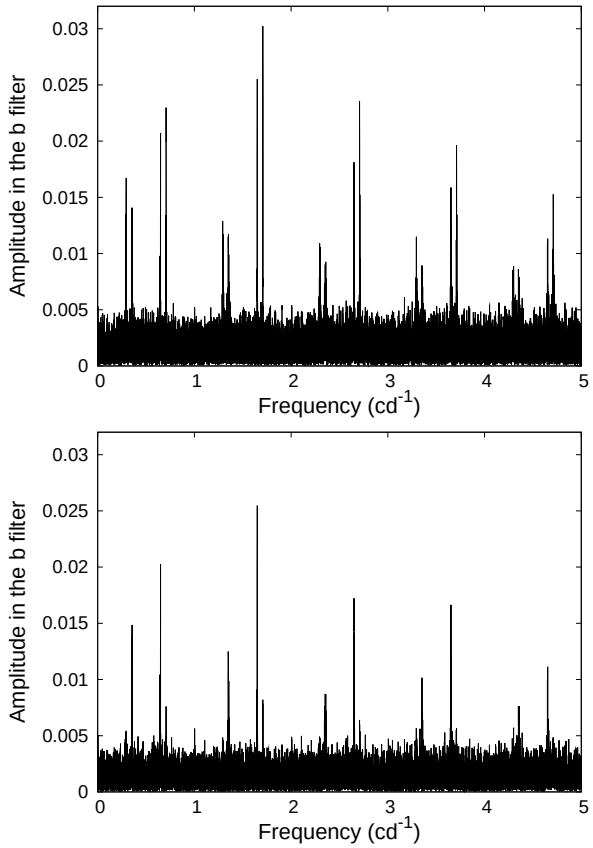

Figure 6.6: **Top** : periodogram of SMC5_16544. **Bottom**: periodogram after prewhitening for the first frequency.

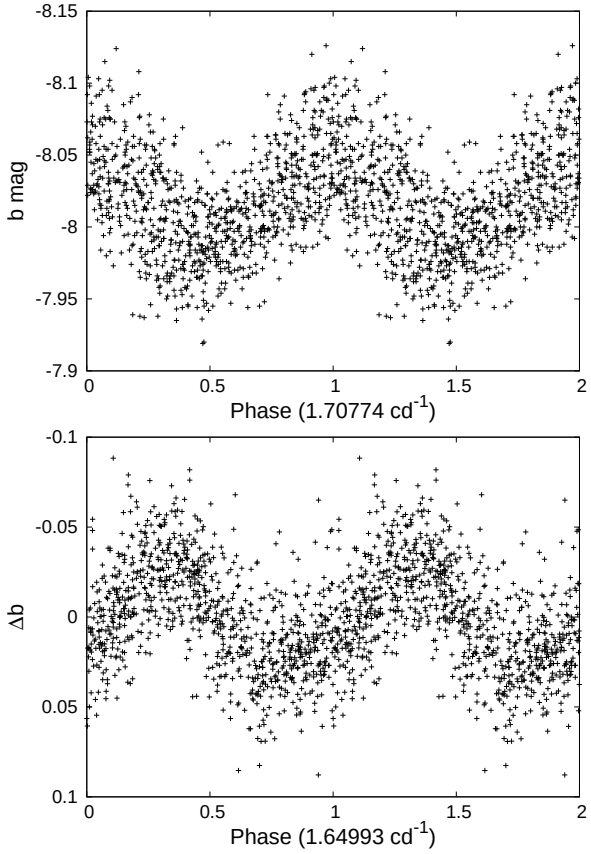

Figure 6.7: **Top**: phase diagram of SMC5_16544 folded with the frequency F1 = 1.70774 c d^{-1}. **Bottom**: phase diagram in phase with the frequency F2 = 1.64993 c d^{-1}, after prewhitening for F1 = 1.70774 c d^{-1}.

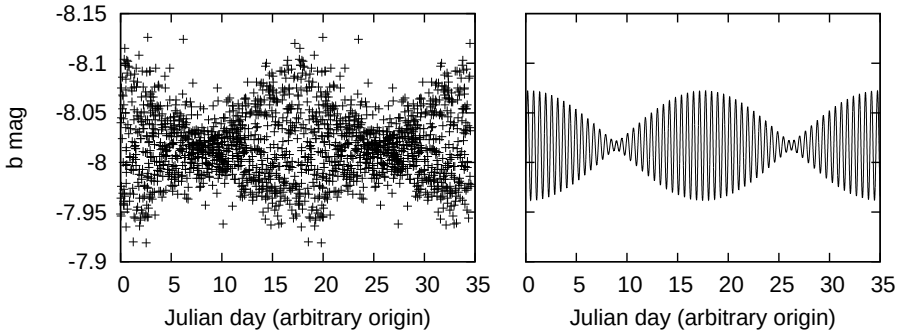

Figure 6.8: **Left**: Composite light curve of SMC5_16544 folded with the beating frequency 0.05781 c d^{-1} produced by the frequencies F1 = 1.70774 c d^{-1} and F2 = 1.64993 c d^{-1}. **Right**: Sum of the two sinusoidal functions with parameters given in Table 6.4.

The sum of two waves is given by the following equation:

$$\begin{aligned} &A_1 \sin(\mathrm{F1}\, t + \varphi_1) + A_2 \sin(\mathrm{F2}\, t + \varphi_2) = \\ &(A_1 + A_2)\, \sin \frac{1}{2}\left((\mathrm{F1} + \mathrm{F2})t + \varphi_1 + \varphi_2\right)\, \cos \frac{1}{2}\left((\mathrm{F1} - \mathrm{F2})t + \varphi_1 - \varphi_2\right) + \\ &(A_1 - A_2)\, \cos \frac{1}{2}\left((\mathrm{F1} + \mathrm{F2})t + \varphi_1 + \varphi_2\right)\, \sin \frac{1}{2}\left((\mathrm{F1} - \mathrm{F2})t + \varphi_1 - \varphi_2\right), \end{aligned} \tag{6.1}$$

where F1 and F2 represent the frequencies, A_1 and A_2 the associated amplitudes and φ_1 and φ_2 the corresponding phases. Now let us suppose that the two frequencies are nearly the same, so that $\frac{1}{2}(\mathrm{F1} + \mathrm{F2})$ is the average frequency, and is about the same as either one. However, $\mathrm{F1} - \mathrm{F2}$ is much smaller than F1 or F2. That means that we can represent the solution with a high-frequency sine wave similar to the one we started with, but its "size" (i.e. amplitude) is slowly changing with a frequency which appears to be $\frac{1}{2}(\mathrm{F1} - \mathrm{F2})$. Although Eq. 6.1 means that the amplitude goes as $\frac{1}{2}(\mathrm{F1} - \mathrm{F2})$, what it is really telling us is that the high-frequency oscillations are contained between two opposed cosine curves (shown in

Table 6.5: Results of the frequency analysis for SMC5_21152.

No.	Freq. c d^{-1}	Amp. mmag	Phase rad	S/N	σ_{res} mmag
	b filter	T = 2690.85 d	N=1034	σ_{init} = 24.5 mmag	
F1	0.98514	18.9	2.53	24	20.5
F2	1.00443	19.0	4.33	24	15.4
	r filter	T = 2690.85	N=897	σ_{init} = 24.9 mmag	
F1	0.98514	17.1	2.58	17	22.3
F2	1.00437	16.9	4.80	17	18.7

right panel of Fig. 6.8). The modulation of the amplitude is at frequency F1 − F2.

Therefore, we conclude that if we add two waves of frequencies F1 and F2, we will get a net resulting wave of average frequency $\frac{1}{2}$(F1+F2) which oscillates in strength with a frequency F1 − F2.

6.3.6 SMC5_21152, MACHO207.16147.14

M06 found a frequency at 0.9852 c d^{-1}. Significant peaks appear in the periodogram at frequencies F1 = 0.98514 c d^{-1} and F2 = 1.00443 c d^{-1}, and their daily aliases (Fig. 6.9). The phase plots for these frequencies are plotted in Fig. 6.10. Sinusoidal parameters are reported for both filters in Table 6.5. A third frequency at 1.00272 c d^{-1}, which is very close to F2, is also detected. The difference between these two frequencies is greater than our frequency resolution and, moreover, this frequency fulfils the signal to noise ratio criterion. However, from the phase diagram we cannot conclude that the third frequency is real.

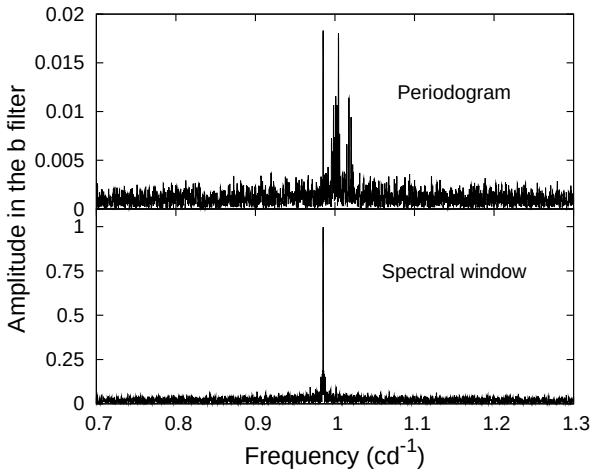

Figure 6.9: **Top**: periodogram of SMC5_21152. **Bottom**: spectral window shifted at frequency F1 = 0.98514 c d^{-1}.

6.3.7 SMC5_37162, MACHO207.16259.57

M06 found a period of 1.130 d, i.e. a frequency at 0.885 c d^{-1}. We only provide detailed analysis for the b filter, since results with the r filter are similar within errors. A 3σ-clipping has been applied to the data in the r filter. Significant peaks clearly appeared in the periodogram at frequencies F1 = 0.88531 c d^{-1} and F2 = 0.90612 c d^{-1} and their daily aliases (see Fig. 6.11, upper panel). This figure shows that the frequency F2 is not produced by the spectral windows. Note that F2 has a much lower amplitude, but it is significant enough to fulfil the SNR criterion (see Table 6.6). Light curve folded in phase with frequencies F1 and F2 are plotted in Fig. 6.12.

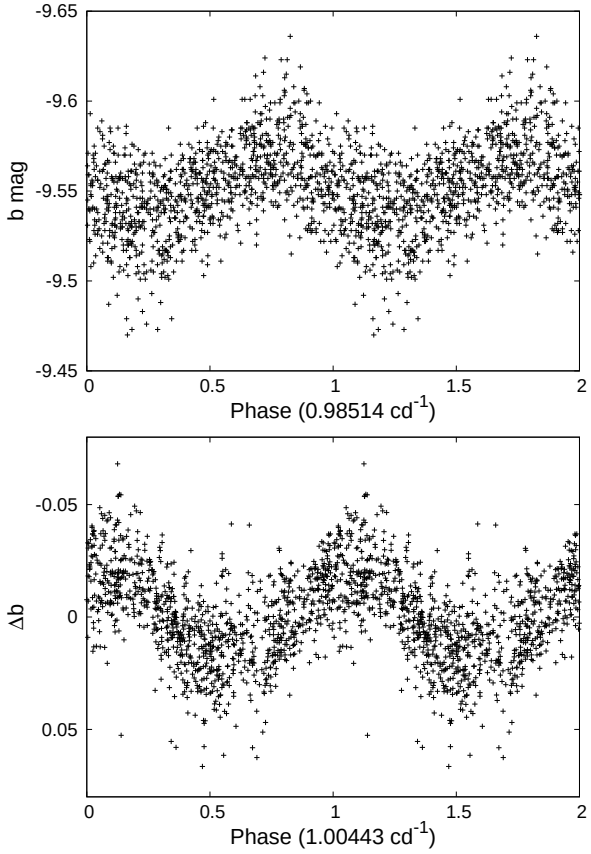

Figure 6.10: **Top**: phase diagram of SMC_21152 folded with the frequency F1 = 0.98514 c d^{-1}. **Bottom**: phase diagram in phase with the frequency F2 = 1.00443 c d^{-1}, after prewhitening for F1 = 0.98514 c d^{-1}.

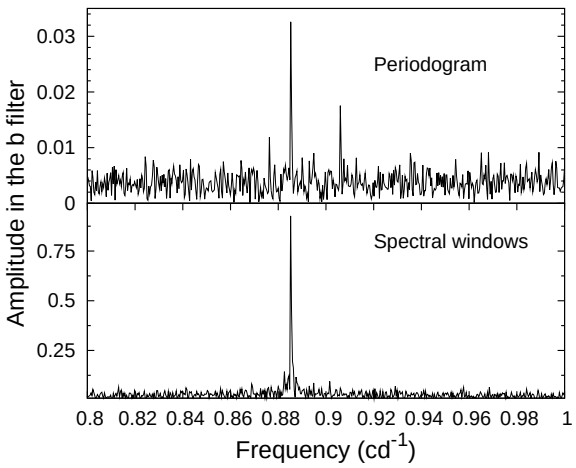

Figure 6.11: **Top**: periodogram of SMC5_37162. **Bottom**: spectral window shifted at frequency F1 = 0.88531 c d^{-1}.

Table 6.6: Results of the frequency analysis for SMC5_37162.

No.	Freq. c d^{-1}	Amp. mmag	Phase rad	S/N	σ_{res} mmag
	b filter	T = 2690.85 d	N=1029	σ_{init} = 67.4 mmag	
F1	0.88531	37.3	4.93	17	63.0
F2	0.90612	19.2	5.67	6	61.5
	r filter	T = 2690.85	N=1013	σ_{init} = 56.5 mmag	
F1	0.88532	40.2	4.72	13	49.3
F2	0.90622	13.7	4.62	5	48.4

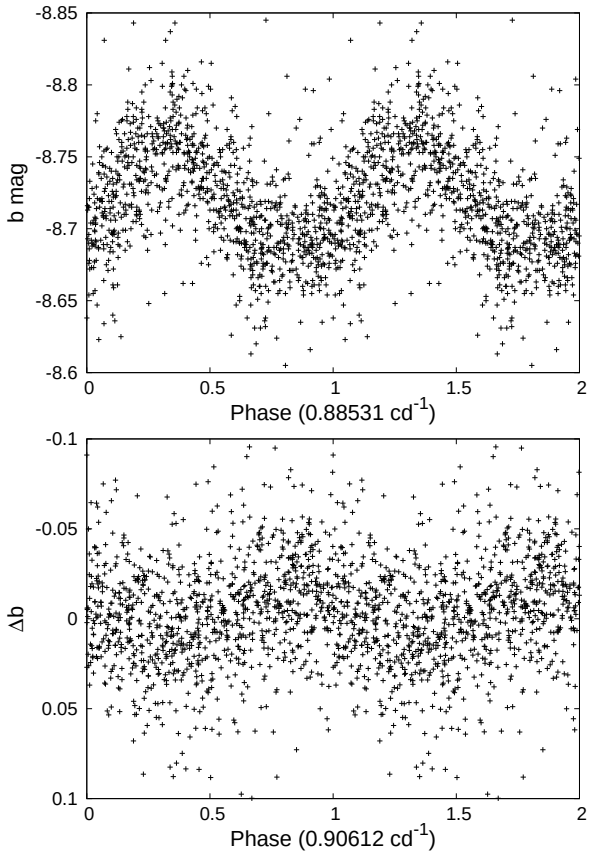

Figure 6.12: **Top**: phase diagram of SMC5_37162 in phase with the frequency F1 = 0.88531 c d^{-1}. **Bottom**: phase diagram of SMC5_37162 folded with the frequency F2 = 0.90612 c d^{-1}, after prewhitening for F1 = 0.88531 c d^{-1}.

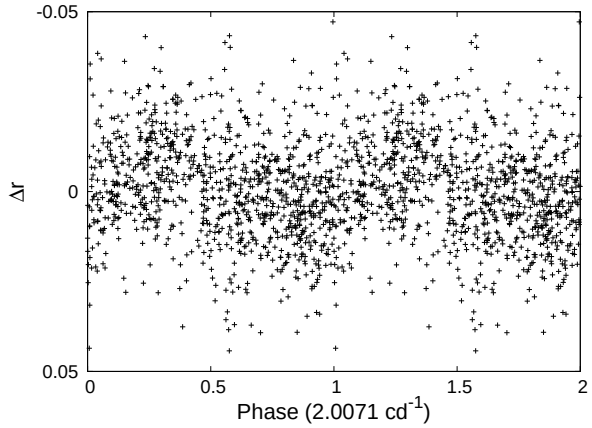

Figure 6.13: Phase diagram of SMC5_43413 in phase with the frequency 2.0071 c d^{-1}, after prewhitening for the long-term period.

6.3.8 SMC5_43413, MACHO207.16315.41

M06 found a period of 1.0004 d, i.e. a frequency at 0.9996 c d^{-1}.

The light curve in the r filter shows a long- and medium-term trend, which is probably produced by a frequency very close to 1 or a very short-term frequency. The spectral analysis shows the presence of a very short-term frequency at 0.00034 which is similar to a 1-day alias of the first frequency detected by M06. After prewhitening for this frequency, a frequency at 2.0071 c $d^{-1}$is found, with a very low amplitude. The SNR of this frequency is 7, and thus, following Breger et al. (1993), it fulfils the signal to noise requirement. The phase diagram of SMC5_43413 with the frequency 2.0071 c d^{-1}, after prewhitening for the short-term frequency is displayed in Fig. 6.13, The phase plot is very scattered, probably due to the low amplitude of the variation.

Table 6.7: Results of the frequency analysis for SMC5_82042.

No.	Freq. c d^{-1}	Amp. mmag	Phase rad	S/N	σ_{res} mmag
	b filter	T = 2690.85 d	N=1037	σ_{init} = 31.0 mmag	
F1	2.48834	19.3	5.22	15	27.1
F2	1.16625	16.8	2.57	13	24.3
	r filter	T = 2690.85	N=977	σ_{init} = 32.2 mmag	
F1	2.48834	13.1	5.10	8	31.2
F2	1.16628	13.8	2.41	9	29.6

6.3.9 SMC5_82042, MACHO207.16375.41

M06 found two frequencies at F1 = 2.48834 c d^{-1} and F2 = 1.16625 c d^{-1}. Detailed analysis for the b filter is provided here, since results with the r filter are similar within errors. 3σ-clipping has been applied to the r dataset, in order to better determine the sinusoidal parameters. Significant peaks clearly appear in the periodogram at frequencies obtained by M06 and their aliases, as can be seen in Fig. 6.14. The best fit given by the least-square method is presented in Table 6.7 for both filters.

The phase plots folded with the detected frequencies are depicted in Fig. 6.15.

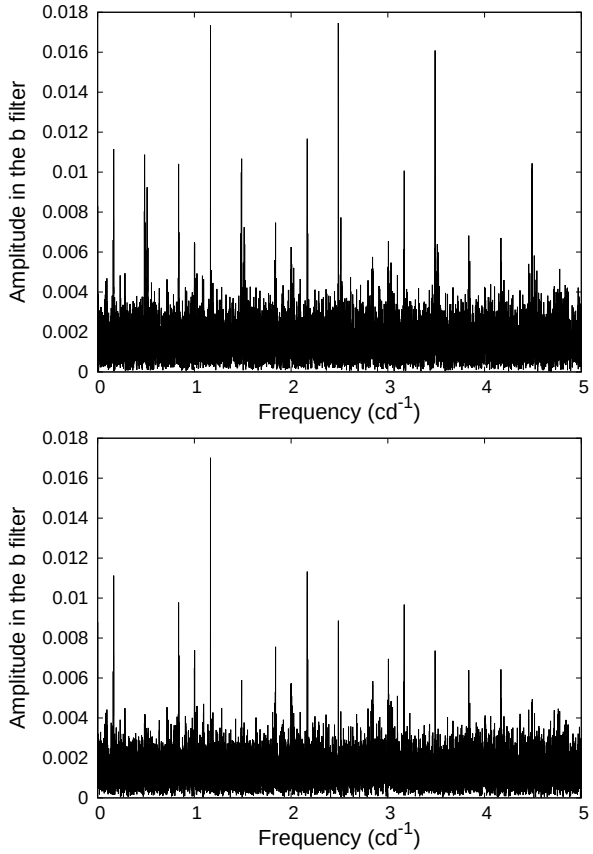

Figure 6.14: **Top**: periodogram of SMC5_82042 with the b filter. **Bottom**: periodogram of SMC5_82042, after prewhitening for the first frequency.

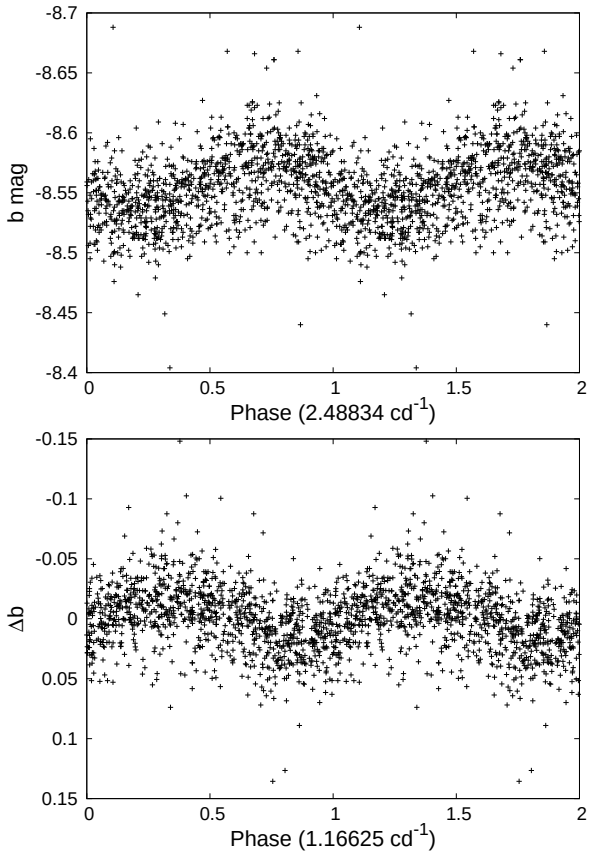

Figure 6.15: **Top**: phase diagram of SMC5_82042 folded with the frequency F1 = 2.48834 c d^{-1}. **Bottom**: phase diagram of SMC5_82042 in phase with the frequency F2 = 1.16625 c d^{-1}, after prewhitening for F1 = 2.48834 c d^{-1}.

Table 6.8: Results of the frequency analysis for SMC5_82941.

No.	Freq. c d^{-1}	Amp. mmag	Phase rad	S/N	σ_{res} mmag
	b filter	T = 2690.85 d	N=1023	σ_{init} = 43.3 mmag	
F1	0.62483	51.7	1.75	41	24.9
F2	0.15324	11.5	5.94	9	23.5
	r filter	T = 2690.85	N=970	σ_{init} = 39.8 mmag	
F1	0.62485	45.6	1.57	38	22.1
F2	0.15324	8.1	5.93	7	21.4

6.3.10 SMC5_82941, MACHO207.16203.47

M06 found a frequency at 0.625 c d^{-1}.

We have studied the b- and r-filter datasets, although we only provide a detailed analysis of the light curve in the b filter. A frequency at F1 = 0.62483 c d^{-1} is detected in the periodogram, as shown in Fig. 6.16. After prewhitening for the first frequency, we have found a significant frequency at F2 = 0.15324 c d^{-1}, i.e. a period of 6.526 d. This period is too long to be due to pulsations and is probably resulting from the fact that this star is a member of a binary system. The phase diagrams for frequencies F1 and F2 are shown in Fig. 6.17. Amplitudes, phases corresponding to the detected frequencies are reported in Table 6.8. After prewhitening for the first two frequencies, a third frequency at 0.62525 c d^{-1} is detected in the spectral analysis. The SNR is 7, and thus it is likely to be real. In addition, the difference between F1 and this frequency is greater than our frequency resolution. Another possibility is that this frequency is caused by the variation in time of frequency F1 = 0.62483 c d^{-1}. A deeper investigation is required to conclude on this issue.

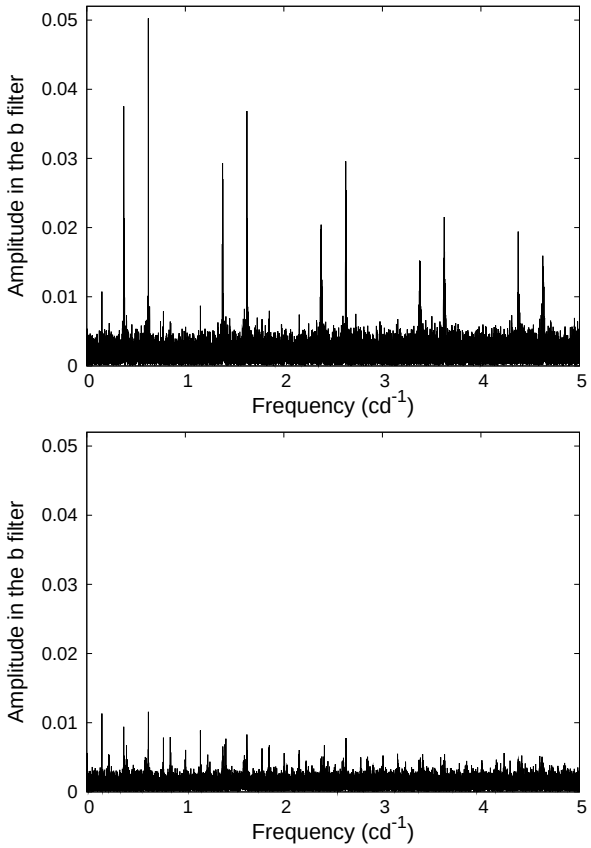

Figure 6.16: **Top**: periodogram of SMC5_82941. **Bottom**: periodogram after prewhitening for the first frequency.

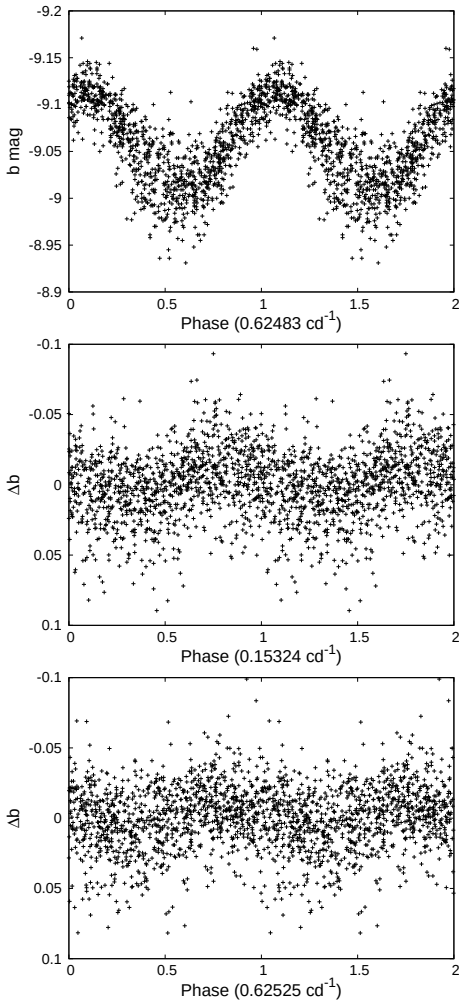

Figure 6.17: **Top**: phase diagram of SMC5_82941 folded with the frequency F1 = 0.62483 c d^{-1}. **Middle**: phase diagram in phase with the frequency F2 = 0.15324 c d^{-1} after prewhitening for F1 = 0.62483 c d^{-1}. Bottom: Phase diagram folded with the frequency 0.62525 c d^{-1}, after prewhitening for the two previously detected frequencies.

Table 6.9: Results of the frequency analysis for MHF[S9]35238.

No.	Freq. c d^{-1}	Amp. mmag	Phase rad	S/N	σ_{res} mmag
	b filter	T = 2690.85 d	N=1035	σ_{init} = 39.7 mmag	
F1	1.32655	24.2	0.05	15	31.1
F2	1.32625	15.2	0.90	9	29.5
	r filter	T = 2690.85	N=1029	σ_{init} = 38.2 mmag	
F1	1.32661	33.0	1.89	26	27.2
F2	1.32616	17.5	5.59	14	24.2

6.3.11 MHF[S9]35238, MACHO207.16372.22

M06 found a frequency of 1.3263 c/d.

We only provide the analysis of the r filter, since results with the b filter are similar within errors. A significant peak is found in the periodogram (Fig. 6.18) at frequency F1 = 1.32661 c d^{-1}. After prewhitening for the first frequency, we obtained a very high frequency at 0.00027 c d^{-1}, i.e. a period of 3703.70 d, which is larger than the time span of the observations. Therefore, this frequency can be an artifact or a long-term trend. Prewhitening for F1 and 0.00027 c d^{-1}, we found an additional frequency at F2 = 1.32616 c d^{-1}. The phase diagram folded with this frequency after prewhitening for F1 is displayed in Fig. 6.19. Note that the difference between F1 and F2 is similar to our resolution in frequencies. In spite of this fact, the phase diagram folded with F2 = 1.32616 c d^{-1}(after prewhitening for only F1 = 1.32661 c d^{-1}) is very convincing and thus F2 is likely to be real.

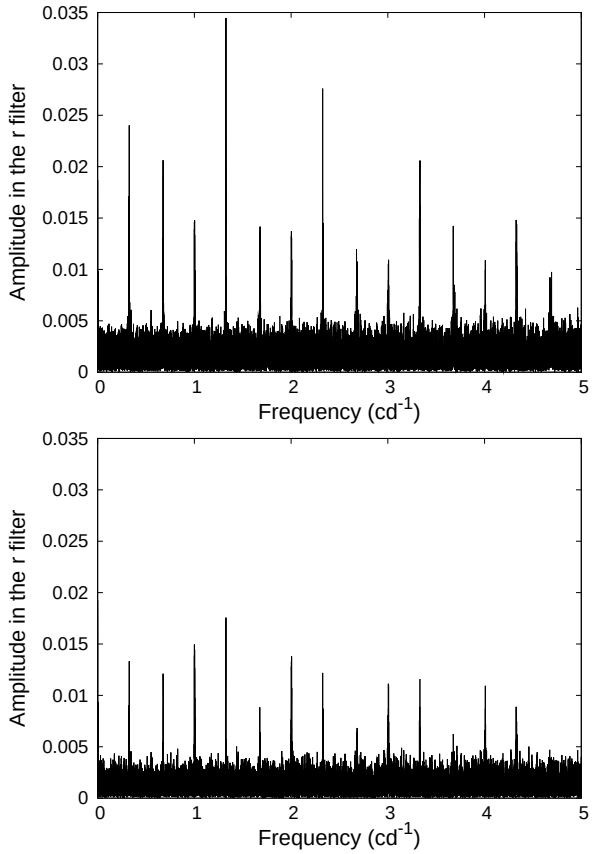

Figure 6.18: Successive periodograms of MHF[S9]35238.

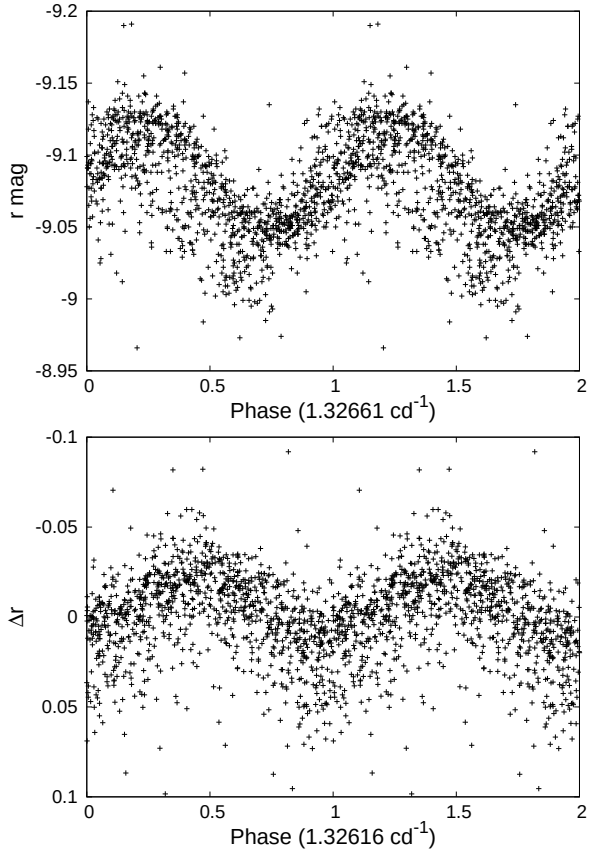

Figure 6.19: **Top**: phase diagram of MHF[S9]35238 folded with the frequency F1 = 1.32661 c d^{-1}. **Bottom**: phase diagram in phase with the frequency F2 = 1.32616 c d^{-1}, after prewhitening for F1 = 1.32661 c d^{-1}.

Table 6.10: Results of the frequency analysis for MHF[S9]37842.

No.	Freq. c d^{-1}	Amp. mmag	Phase rad	S/N	σ_{res} mmag
	b filter	T = 2401.72 d	N=942	σ_{init} = 22.8 mmag	
F1	1.18153	15.2	1.86	15	21.9
F2	1.21709	8.9	0.34	9	20.9
	r filter	T = 2401.72	N=1018	σ_{init} = 25.5 mmag	
F1	1.18153	19.7	1.85	15	21.2
F2	1.21709	9.3	0.08	8	20.9

6.3.12 MHF[S9]37842, MACHO207.16315.26

M06 found two significant frequencies at F1 = 1.18525 c d^{-1} and F2 = 1.217093 c d^{-1}.

The r filter is only provided here, since results with the b filter are similar within errors. The periodogram shows significant peaks at frequencies obtained by M06 and their daily aliases (see Fig. 6.20). Frequencies obtained with the least-square fitting code are displayed in Table 6.10 for both filters.

Fig. 6.21 represents the phase diagrams folded with frequencies F1 and F2. After prewhitening for F1 and F2, a frequency at F3 = 1.18113 c d^{-1} is present in the periodogram, with a SNR of 6, i.e. the frequency fulfils the signal-to-noise requirement. However, the difference between F1 and F3 is lower than our resolution in frequency, and thus we cannot confirm this frequency.

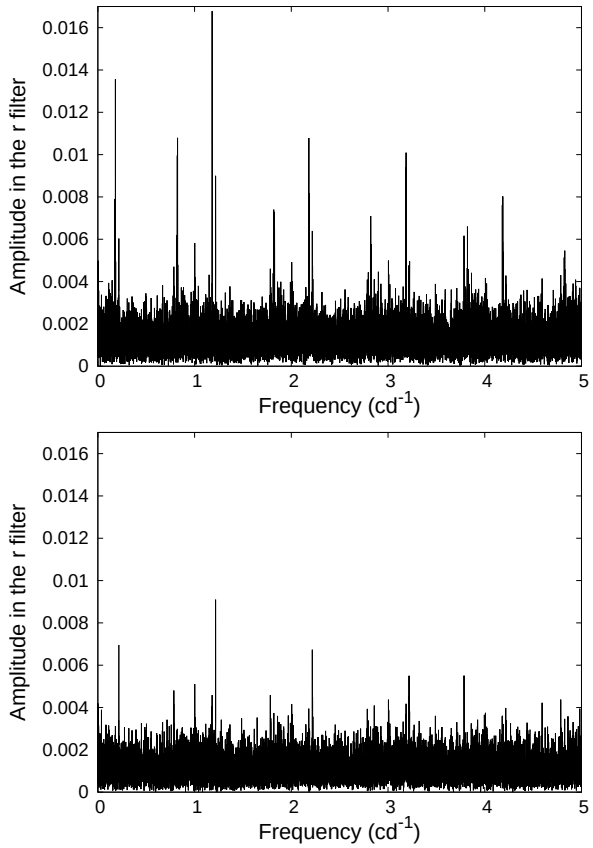

Figure 6.20: Successive periodograms of MHF[S9]37842.

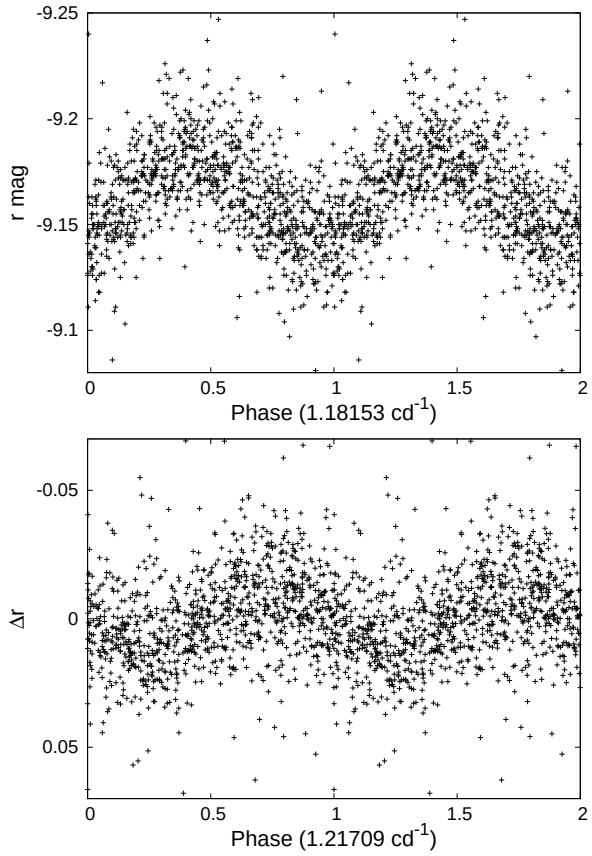

Figure 6.21: **Top**: phase diagram of MHF[S9]37842 folded with the frequency F1 = 1.18525 c d^{-1}. **Bottom**: phase diagram of MHF[S9]37842 in phase with the frequency F2 = 1.217093 c d^{-1}, after prewhitening for F1 = 1.18525 c d^{-1}.

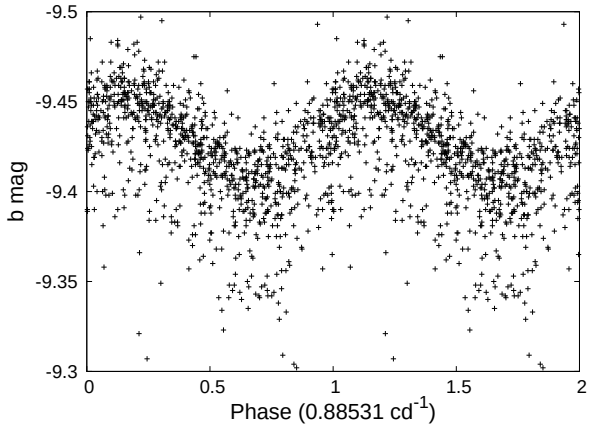

Figure 6.22: Phase diagram of MHF[S9]39981 folded with the frequency 1.27691 c d^{-1}.

6.3.13 MHF[S9]39981, MACHO207.16259.29

M06 found a frequency at 1.2771 c d^{-1}.

The spectral analysis of the light curve yields a main frequency at 1.27691 c d^{-1}. The phase plot for the detected frequencies is depicted in Fig. 6.22. A long-term trend is present in the light curve, which produces a variation of the average magnitude in time, as can be seen in the phase diagram. Note that the frequency does not change significantly during the observations, although the amplitude changes by 10 mmag.

6.4 Discussion

Several authors have previously investigated the pulsational behaviour of Be stars in the SMC, by means of photometric and spectroscopic techniques, with negative results. Balona (1992) conducted a photometric variability study of Be stars in the region of the young open cluster NGC 330 in the SMC. He found many of them to be short-period variables, but he was able to found only one period in each star. He concluded that the short-term variability was produced by rotational modulation of the light curve caused by inhomogeneities in the stellar photospheres. Baade et al. (2002) obtained time-resolved high-resolution spectroscopy of two bright Be stars close to NGC 330. They failed to found line-profile variability, and their analysis casts doubts on the presence of pulsations in these two stars.

Our finding of photometric multiperiodicity in nine SMC Be stars clearly shows that they are indeed pulsating stars. The current theoretical models do not predict the presence of pulsational instabilities in massive stars at metallicities much lower than the galactic one (Pamyatnykh 1999). However, these models have recently been challenged by several observational results:

Kołaczkowski et al. (2004) detected some β Cephei and SPB stars in the Large Magellanic Cloud. The LMC metallicity of $Z = 0.008$ is slightly lower than the limit of 0.01 set by Pamyatnykh (1999) for the presence of β Cep-type pulsations.

Very recently, with the help of the lensing photometric surveys (OGLE and MACHO), Fabrycky (2005) and Schmidtke et al. (2004) detected multiple periods in high mass X-ray binaries with a Be primary component (Be/X systems) in the SMC. However, Be/X binaries are post-mass transfer systems in which the current primary may have had its chemical abundances enhanced by the processed material transferred from its companion as a result of the early binary evolution. Unless the chemical abundances of these systems are accurately determined and proved to be similar to the mean SMC metallicity, these results do not constitute a proof against the current theoretical models of stellar pulsations.

Our results provide a much more robust indication against the predictions of the current models. The SMC metallicity ($Z = 0.004$) is significantly below the lower limit of 0.01 for which the models predict

pulsations for β Cep stars and not only marginally below as is the case of the LMC. Moreover, the stars we have studied do not show any indication of binarity and there is thus no reason to suspect that their metallicity is significantly different from the mean SMC one.

These results point towards the necessity of new modelling or improved determination of the opacities used in the current models. On the other hand, the discovery of multiperiodic Be stars in the SMC should encourage the community to regularly observe these stars in order to perform a study similar to the one performed by Rivinius et al. (1998) for the Be star μ Cen in the galaxy, which explained the occurrence of mass-loss events as a consequence of constructive interference between modes.

Bibliography

Alcock, C., Allsman, R. A., Alves, D. R., Axelrod, T. S., Becker, A. C., Bennett, D. P., Cook, K. H., Drake, A. J., Freeman, K. C., Geha, M., Griest, K., Lehner, M. J., Marshall, S. L., Minniti, D., Peterson, B. A., Popowski, P., Pratt, M. R., Nelson, C. A., Quinn, P. J., Stubbs, C. W., Sutherland, W., Tomaney, A. B., Vandehei, T., Welch, D. L., and The MACHO Collaboration: 1999, *PASP* **111**, 1539

Baade, D., Rivinius, T., Štefl, S., and Kaufer, A.: 2002, *A&A* **383**, L31

Balona, L. A.: 1992, *MNRAS* **256**, 425

Breger, M., Stich, J., Garrido, R., Martin, B., Jiang, S. Y., Li, Z. P., Hube, D. P., Ostermann, W., Paparo, M., and Scheck, M.: 1993, *A&A* **271**, 482

Fabrycky, D.: 2005, *MNRAS* **359**, 117

Kołaczkowski, Z., Pigulski, A., Soszyński, I., Udalski, A., Szymański, M., Kubiak, M., Żebruń, K., Pietrzyński, G., Woźniak, P. R., Szewczyk, O., Wyrzykowski, L., and The Ogle Team: 2004, in D. W. Kurtz and K. R. Pollard (eds.), *ASP Conf. Ser. 310: IAU Colloq. 193: Variable Stars in the Local Group*, pp 225–+

Lenz, P. and Breger, M.: 2005, *Communications in Asteroseismology* **146**, 53

Martayan, C.: 2005, *Ph.D. Thesis*

Martayan, C., Floquet, M., Hubert, A.-M., and Mekkas, M.: 2006, *ArXiv Astrophysics e-prints, astro-ph/0602148*

Montgomery, M. and O'Donoghue, D.: 1999, *Delta Scuti Newsletter* **13**, p28

Nonino, M., Bertin, E., da Costa, L., Deul, E., Erben, T., Olsen, L., Prandoni, I., Scodeggio, M., Wicenec, A., Wichmann, R., Benoist, C., Freudling, W., Guarnieri, M. D., Hook, I., Hook, R., Mendez, R., Savaglio, S., Silva, D., and Slijkhuis, R.: 1999, *A&AS* **137**, 51

Pamyatnykh, A. A.: 1999, *Acta Astronomica* **49**, 119

Rivinius, T., Baade, D., Stefl, S., Stahl, O., Wolf, B., and Kaufer, A.: 1998, *A&A* **336**, 177

Robertson, J. W.: 1974, *A&AS* **15**, 261

Schmidtke, P. C. and Cowley, A. P.: 2005, *AJ* **130**, 2220

Schmidtke, P. C., Cowley, A. P., Levenson, L., and Sweet, K.: 2004, *AJ* **127**, 3388

Schwarzenberg-Czerny, A.: 1991, *MNRAS* **253**, 198

Chapter 7

Conclusions

The main objective of our project is to study the pulsational characteristics of Be stars using data from the space mission COROT, to be launched in December 2006. COROT will provide high precision photometric data for long continuous observing runs, which will allow us to better understand the Be phenomenon.

The work presented here includes the selection and the study of the Be stars samples, which have been proposed to the COROT scientific committee. The two samples we have elaborated have been accepted and will be observed. Bright Be stars will be observed in the seismology fields as part of the COROT seismology Core Programme. A total of 5 stars have already been selected in the two first long runs. Faint Be stars will be observed in the exoplanet fields as a part of the Additional Programme. Therefore, the first objective has satisfactorily been reached.

The study of the Be star samples mentioned above allowed us to obtain several results of scientific interest:

- We have studied the pulsational characteristics of an homogeneous and unbiased set of bright Be stars by means of photometric data. 77% of the early-type Be stars and 26% of the late-to-mid Be stars have been detected to be short-period variables. This result agrees with other studies based on different samples and instrumentation. Most of the Be stars with short-period variability are found in or near the β Cephei and SPB instability strips, suggesting that Be

stars are the high-rotational velocity counterparts of these two types of variables.

- In the sample of Be stars studied with photometry, two Be stars have shown multiperiodic behaviour. The presence of multiperiodicity proves that the short-period variability is due to the presence of stellar pulsations. Four frequencies have been found for each star and have been attributed to non-radial pulsations with a preliminary theoretical model. NW Ser is a candidate hybrid pulsator of β Cep and SPB type.

- A spectroscopic study has been performed in order to better characterise the pulsational properties of the multiperiodic Be star NW Ser. Two frequencies have been clearly detected and one of them has been modelled with a pulsating mode with $\ell = 2{,}3$ and $m = -2, -3$.

- We developed a photometric technique to find faint Be stars. This technique is based on imaging fields of stars through a narrow band filter centred on the Hα line to detect emission-line stars, and on Strömgren photometry to obtain a spectral classification unaffected by interstellar reddening. By applying this technique, we found 43 Be stars in the COROT exoplanet fields, which will be observed during the two first long runs. We developed an automatic pipeline to reduce the CCD data, which will allow us to easily search for faint Be stars in exoplanet fields corresponding to successive COROT pointings.

- We analysed the pulsational properties of a sample of Be stars in the SMC. We presented the first detection of multiperiodic non-binary Be stars outside the galaxy. These results prove that Be stars in the SMC are non-radial pulsators. Pulsations of B-type stars at low metallicity, such as in the SMC, are not predicted by the current stellar models based on the commonly accepted opacities. Our result points towards the necessity of new modelling or improved determination of opacities.

7.1 Future work

The work presented here is the first part of a large project aimed at studying the physics of Be stars using data from the COROT satellite. The launch is scheduled for December 2006 and the first Be star will be observed at the beginning of 2007. The natural follow-up of our work is to start the analysis of the data relative to Be stars produced by COROT. These new data will allow us to perform in-depth analysis of Be stars pulsational properties and to address most of the problems raised in this thesis in much deeper detail.

In addition, immediate follow-up studies of several particular topics presented in this work are the following:

- New spectroscopic observations of NW Ser have been obtained in the summer 2006. We are now reducing them and we will analyse them together with the data presented in Chapt. 4 to study in more detail the spectroscopic variability of this star and to refine our determination of the pulsational modes.

- We will continue our photometric programme for the identification of new Be stars in the exoplanet fields for the successive COROT pointings. Due to the fact that we have developed an automatic procedure for the data reduction (Chapt. 5) we can proceed with this task in a very fast and efficient way.

- Our group is involved in a related project aimed at studying B and Be stars with the KEPLER satellite. Much as the COROT exoplanet programme, the KEPLER mission is devoted to find Earth-size extrasolar planets with the transits technique and will also host an additional science programme to obtain photometric time series with different scientific purposes. The KEPLER mission consists in a single pointing lasting four years without interruption and with a field of view of 105 square degrees, i.e. much larger than the COROT exoplanet fields. We are planning to start photometric observations of the KEPLER field of view to identify B and Be stars using the techniques described in Chapt. 5.

- Due to the interesting results obtained in our study of the pulsational properties of a few Be stars in the Small Magellanic Cloud (see

Chapt. 6), we plan to extend our research to a significantly larger sample of stars in both Small and Large Magellanic Clouds.

Appendix A

Resumen

Este apéndice constituye un resumen en castellano de los contenidos de esta tesis doctoral. Se trata de una breve descripción de los resultados y discusiones más interesantes de la tesis. No se incluyen figuras ni tablas, refiriéndonos siempre a las ya incluidas en el cuerpo del trabajo.

A.1 Introducción

El objetivo general de la tesis es el estudio pulsacional de las estrellas Be. La observación de estas estrellas con el satélite COROT aportará importantes claves en la comprensión del fenómeno Be.

La misión espacial COROT, prevista para el lanzamiento en Diciembre del 2006, obtendrá fotometría de muy alta precisión (hasta 1 ppm) y de muy larga duración (hasta 150 días). Las datos observados por COROT tendrán una calidad sin precedentes, cuyo análisis nos permitirá una mejora cualitativa en la comprensión de las características pulsacionales de las estrellas Be. En consecuencia hemos comenzado un proyecto de investigación con la finalidad de observar estrellas Be en los campos de asterosismología y exoplanetas de COROT.

En esta tesis presentamos la primera parte de este proyecto, que es la preparación y estudio de una muestra de estrellas Be para ser observada por COROT. Con este fin, hemos realizado un análisis fotométrico

de todas las estrellas Be que se encuentran en los campos de asterosismología de COROT basándonos en observaciones extraídas de grandes proyectos fotométricos (Hipparcos y ASAS-3) y realizadas por nosotros mismos en el Observatorio de Sierra Nevada en Granada (cap. 2). Dos estrellas (NW Ser y V1446 Aql) incluidas en esta muestra han sido estudiadas con más profundidad al detectar multiperiodicidad en sus curvas de luz (cap. 3). Las frecuencias detectadas han sido modelizadas en términos de pulsaciones no radiales. En el caso de la estrella NW Ser, además hemos realizado un estudio complementario basándonos en observaciones espectroscópicas con el fin de caracterizar los modos de pulsación teniendo en cuenta la alta rotación de la estrella (cap. 4). Con el propósito de encontrar estrellas Be débiles en los campos de exoplanetas de COROT, hemos desarrollado una técnica basada en fotometría CCD (cap. 5). En el mismo capítulo presentamos una lista de estrellas Be en los campos de exoplanetas que proponemos para su observación por el satélite COROT. Por último, hemos probado que nuestras técnicas de determinación de períodos son adecuadas al aplicarlas a curvas de luz de larga duración, al detectar hasta 2 ó 3 periodos en 9 estrellas Be en la Nube Pequeña de Magallanes con datos de MACHO (cap. 6).

A.1.1 Estrellas Be

Las estrellas Be son objetos de secuencia principal, con alta velocidad de rotación, que presentan un exceso infrarrojo y emisión en las líneas de Balmer, debido a la presencia de una envoltura circunestelar concentrada en el ecuador y generada por eyecciones discretas de materia originado por mecanismos que todavía no son bien conocidos.

El caso de las estrellas Be es especialmente complejo. Un estudio publicado por Hubert & Floquet en 1998 basado en fotometría de Hipparcos mostró que la mayoría de las estrellas Be tempranas presentan variabilidad fotométrica de corto período (86%), mientras que el porcentaje disminuye en los tipos más tardíos (18% en el rango B6-B9). Estas variaciones de corto período son atribuidas a la presencia de pulsaciones no radiales en estas estrellas.

Teóricamente, a lo largo de todo el rango del tipo espectral B podemos

encontrar estrellas pulsantes. En los tipos más masivos, la oscilación está causada por ondas de presión o "modos p" mientras que en los más tardíos se trata de ondas de gravedad o "modos g". Ambos tipos de estrellas pulsantes se denominan β Cephei y SPB (en inglés, Slowly Pulsating B stars) respectivamente. La detección de los diferentes modos de pulsación de este último tipo de estrellas, necesaria para el estudio asterosismológico, es extremadamente difícil debido a los largos períodos que presentan y a su baja amplitud asociada.

Los mecanismos propuestos para explicar la eyección de materia y por tanto, la formación del disco circunestelar que caracteriza a las estrellas Be, son hasta ahora las pulsaciones no radiales (NRP) y los campos magnéticos, combinados con la alta velocidad de rotación característica de este tipo de estrellas. En un trabajo reciente, Rivinius et al. (2001) ha mostrado que la interferencia constructiva de los diferentes modos de pulsación detectados determina los episodios de pérdida de masa en la estrella Be μ Centaurus. La cuestión es: es esto válido para todas las estrellas?

A.1.2 La misión espacial COROT

La misión COROT (COnvección, ROtación y Tránsitos planetarios) obtendrá fotometría de muy alta precisión de una muy larga duración. Los dos grandes objetivos científicos son la asterosismología de estrellas brillantes y la detección de planetas extrasolares por el método de los tránsitos. El campo de visión de COROT está dividido en dos sectores, con diferente configuración óptica y sensibilidad para cada uno de los objetivos. En el campo de asterosismología se observará, en cada uno de los apuntados previstos, una o dos estrellas brillantes seleccionadas como objetos principales y ocho o nueve estrellas más como objetivos secundarios. En los campos de búsqueda de exoplanetas se observará unas 12 000 estrellas por apuntado, de las cuales unos cuantos centenares formará parte de un programa adicional con diferentes objetivos científicos que será seleccionado a partir de propuestas de la comunidad científica en respuesta a un anuncio de oportunidad.

Los campos de visión de COROT son dos conos centrados en las di-

recciones del Centro ($\alpha = 18^{\rm h}50$, $\delta = 0°$) y Anticentro ($\alpha = 6^{\rm h}50$, $\delta = 0°$) Galáctico y radio de 10°. Las observaciones tendrán una duración de 150 días para los apuntados largos y entre 20 y 30 para los cortos. Cada año será dividido en dos apuntados largos y alrededor de cuatro cortos (mirar la Fig. 1.2 en la Pág. 6).

La asterosismología estudia la estructura interna de las estrellas a través de la interpretación de las oscilaciones. El interior de las estrellas es opaco a las observaciones directas y por tanto necesitamos de otras herramientas. Así como la sismología nos ha permitido conocer el interior de la tierra, el estudio de las oscilaciones estelares a partir de las variaciones en la luminosidad de la estrella o en las líneas espectrales nos permite conocer el interior de las estrellas. Dos objetivos diferentes se pretenden conseguir en el campo de asterosismología: el estudio de las capas internas y la física de los núcleos estelares (*Programa central*) y la determinación de los parámetros estelares en los cuales se puedan detectar oscilaciones (*Programa exploratorio*).

A partir de la detección del primer planeta fuera del sistema solar por Mayor y Queloz en 1995, el conocimiento de la formación de planetas extrasolares ha aumentado considerablemente. El desafío de COROT es la observación por primera vez de planetas tipo telúrico con el método de los tránsitos. El método de los tránsitos se basa en la detección de la pequeña disminución de la luminosidad de la estrella cuando es ocultada por uno de los planetas (mirar la Fig. 1.8 en la Pág. 12). Para ello se necesita mucha precisión fotométrica y observaciones de muy larga duración.

El lanzamiento está previsto para Diciembre del 2006. Alrededor de tres meses serán necesarios para la evaluación del satélite y calibraciones a principios del 2007 se empezarán las primeras observaciones de COROT, en forma de apuntados iniciales (IR). En Abril se empezarán los apuntados largos (LRC1, LRA1, ...) y los cortos (SR1, SR2 ,...) alternativamente en las direcciones del Centro y Anticentro Galáctico.

Durante los últimos años se han seleccionado las estrellas principales que serán observadas dependiendo de su interés científico. Las posiciones de los dos primeros apuntados iniciales y de los apuntados largos ya están fijas y se ha propuesto una lista de estrellas como objetos secundarios. Entre esos objetos se encuentran 5 estrellas Be (mirar la Tablas 1.3 y 1.4

en las Págs. 15 y 16).

La gran cantidad de datos que producirá COROT pueden servir para otros propósitos que los objetivos principales. El Programa Adicional engloba todas las propuestas que no forman parte del programa central. Así pues, proyectos como el estudio de oscilaciones en los campos de exoplanetas o de búsqueda de exoplanetas en los campos de asterosismología están comprendidos en el Programa Adicional. En Abril del 2005 un Anuncio de Oportunidad (AO) fue enviado a la comunidad científica solicitando las propuestas para los dos primeros apuntados largos. Los autores de las propuestas aceptadas tendrán derechos exclusivos sobre sus datos por el tiempo de un año.

A.1.3 El estudio de las estrellas Be con COROT

Dado el interés de la observación de estrellas Be por COROT, ilustrado en las secciones previas, una colaboración internacional (el COROT Be stars team en inglés) se ha establecido para proponer tales observaciones y estudiar y analizar los datos sobre las estrellas Be producidos por COROT.

El grupo ha propuesto la observación de estrellas Be por COROT en dos sentidos:

- Observaciones de estrellas brillantes como objetos secundarios en los campos de asterosismología. Esta propuesta ha sido aceptada y varias estrellas han sido incluidas en la lista de objetos de los dos primeros apuntados largos. Otras han sido consideradas para los siguientes apuntados largos todavía por fijar.

- Observaciones de estrellas débiles en los campos de exoplanetas. Estas observaciones serán comprendidas dentro del Programa Adicional. Hemos propuesto estas observaciones como respuesta del primer Anuncio de Oportunidad enviado en 2005. Nuestra propuesta ha sido aceptada y por tanto, las estrellas Be que estamos proponiendo serán realmente observadas y su tratamiento y explotación será parte de nuestra responsabilidad.

El grupo de la Universidad de Valencia es el responsable del estudio fotométrico de las estrellas Be brillantes que han sido propuestas como objetos secundarios en los campos de asterosismología y la detección de estrellas Be débiles en los campos de exoplanetas. El trabajo realizado hasta ahora es el presentado en esta tesis.

A.2 Estudio fotométrico de las estrellas Be en los campos de asterosismología de COROT

El objetivo de esta sección es la caracterización de la variación de corto período de las estrellas brillantes en los campos de asterosismología de COROT. Un total de 84 estrellas Be se encuentran en los campos de COROT con magnitudes entre 5.5 y 9.4. Dos de estas estrellas se estudian con más profundidad en la sección siguiente (sección A.3)

Dado el gran número de estrellas que han de ser analizadas, hemos realizado un criterio de selección. En primer lugar, todas las estrellas cercanas a los objetos principales de COROT han sido observadas en una campaña fotométrica de cuatro años de duración en el Observatorio de Sierra Nevada. Las estrellas cuyos resultados no fueron convincentes durante la campaña, fueron reobservadas y reanalizadas. Por último, hemos analizado las curvas de luz de Hipparcos y ASAS-3 de toda la muestra de estrellas Be, con el fin de complementar y completar el estudio realizado.

A.2.1 Observaciones y análisis de datos

Como hemos mencionado anteriormente, las curvas de luz que hemos analizado proceden de tres diferentes instrumentos. En primer lugar, realizamos observaciones en el Observatorio de Sierra Nevada (OSN, Granada) desde 2002 hasta 2006. El instrumento utilizado es un fotómetro de cuatro canales que nos permite observar simultáneamente a través de los filtros *uvby* de Strömgren . El método de la fotometría diferencial de tres estrellas es el empleado en las observaciones. Dos estrellas supuestamente constantes y una medida del cielo son observados por cada objeto que queremos observar. Un total de 22 estrellas fueron observadas durante un máximo de 10 días con una precisión de menos de 7 milésimas de magnitud en los filtros *vby* y de 10 milésimas en el filtro u en todos los casos.

En segundo lugar, hemos analizado las curvas de luz de todas las estrellas observadas por Hipparcos que se encuentran en los campos de asterosismología de COROT. Hubert y Floquet (1998) mostró que los datos obtenidos por Hipparcos son de gran utilidad para el estudio de la vari-

abilidad de una gran muestra de estrellas Be. Por último, hemos analizado las curvas de luz de todas las estrellas observadas por ASAS-3 en los campos de asterosismología de COROT, que contienen una mayor densidad de puntos, una mayor duración pero peor precisión que Hipparcos.

Para el análisis de períodos, hemos empleado el programa Period04 (Lenz y Breger 2005) que está diseñado especialmente para el análisis de series temporales con datos no igualmente espaciados. Este programa busca las frecuencias de una en una, calculando la transformada de Fourier y luego ajusta los parámetros de una función sinusoidal mediante mínimos cuadrados. El método es iterativo hasta que la frecuencia no es estadísticamente significativa. Además utilizamos un código no lineal de ajuste multiparamétrico que busca en un gran rango de frecuencias (Vanicek 1971). Este código es muy útil para los datos obtenidos en tierra (OSN y ASAS-3), los cuales están contaminados por "alias" de un día.

La precisión en la frecuencia es dada por la fórmula $1/T$, donde T representa la duración de las observaciones. En nuestro caso, hemos estimado 0.1 c d^{-1}, 0.001 c d^{-1}y 0.0006 c d^{-1}para los datos del OSN, Hipparcos y ASAS-3 respectivamente.

A.2.2 Discusión

Hemos analizado y caracterizado las curvas de luz de las 82 estrellas Be que se encuentran en los campos de asterosismología de COROT de las cuales 28 son variables y 27 son no variables. El resto de estrellas, o bien presentan variaciones de largo o medio período que no hemos podido modelizar adecuadamente, o bien las curvas de luz asociadas contienen pocos puntos y por tanto no se ha podido realizar el análisis de la variabilidad de corto período de estas estrellas. En la Tablas 2.4 y 2.5 (pág. 57) se muestra que los resultados obtenidos a partir de los tres instrumentos son compatibles en la mayoría de los casos. Hay que resaltar que hemos detectado múltiples periodos en cuatro estrellas, considerándolas de gran interés científico para un estudio más profundo, como el que realizará COROT.

Hemos investigado el grado de variabilidad de corto periodo de las estrellas Be, dependiendo de la temperatura. Hemos encontrado variabilidad de corto período en el 77% de las estrellas tempranas (B0-B3) y en el 26%

de las estrellas tardías (B4-B9). Estos resultados son compatibles con los obtenidos por Hubert y Floquet (1998) basándose en datos de Hipparcos con una muestra más grande. La diferencia de porcentajes puede deberse a que las amplitudes de la frecuencias asociadas a las estrellas Be tardías son teóricamente más pequeñas y por tanto más difícil de detectar.

Además hemos situado estas estrellas en el diagrama HR, observando que las estrellas variables caen dentro o cerca de las regiones de inestabilidad de las estrellas β Cephei o SPB, (mirar Fig. 2.29 en la pág. 61) sugiriendo que las estrellas Be pulsan de la misma forma que éstas. También se observa en la misma gráfica que la mayoría de las estrellas no variables están fuera de las regiones de inestabilidad.

Por último, presentamos una lista de estrellas Be que tienen una gran probabilidad de ser observadas por COROT. Siete de ocho de esas estrellas has sido consideradas variables en este trabajo. Además, HD 49330 presenta una frecuencia con amplitud variable, HD 50209 es probablemente bi-periódica, y HD 51193 es variable con una amplitud que cambia de noche a noche. Las observaciones obtenidas por el satélite COROT nos permitirán refinar la determinación de las frecuencias reales y probablemente descubrir muchas más.

A.3 Pulsaciones no radiales en las estrellas NW Ser y V1446 Aql

Las variaciones de corto periodo observadas en las curvas de luz y en los perfiles de líneas espectrales de las estrellas Be se atribuyen a la presencia de pulsaciones no radiales o de manchas o nubes alrededor de éstas. La detección de multiperiodicidad fotosférica y en particular, la detección de multiperiodicidad en las curvas de luz fotométricas, constituye una evidencia de la hipótesis de las pulsaciones no radiales. En esta sección se presenta un estudio en profundidad de dos estrellas Be -NW Ser y V1446 Aql- cuyas curvas de luz muestran una clara evidencia de multiperiodicidad.

NW Ser es una estrella brillante y extensivamente observada durante las últimas dos décadas. Varios autores han analizado los datos de Hipparcos, obteniendo los siguientes resultados: Hubert y Floquet (1998) detectaron variabilidad con un período de 0.488 días; Percy y colaboradores (1999) reanalizaron los mismos datos combinados con datos obtenidos en tierra, detectando un período de 0.46 días, junto con uno más largo de 5.5 días; finalmente, Aerts (2000) detectó dos períodos cercanos (0.475 y 0.406 días).

V1446 Aql fue observada como Be en las observaciones de prisma-objetivo realizado en el Monte Wilson. Aparece como variable irregular en el catálogo de Hipparcos, pero no se había detectado variabilidad de corto periodo.

A.3.1 Análisis de datos

Las curvas de luz de las dos estrellas obtenidas en el Observatorio de Sierra Nevada presentan una variación cuya amplitud cambia muy rápidamente. Esto sugiere la presencia de un fenómeno de interferencia entre frecuencias: cuando las frecuencias están en interferencia constructiva, la amplitud es mayor, mientras que cuando es destructiva, la amplitud es mucho menor, como se observa en la Fig.3.1 en la pág. 70. El análisis de frecuencias con los métodos descritos anteriormente confirma la presencia de hasta cuatro períodos en las dos curvas de luz. 1.197, 1.126, 3.304 y 1.412 c d^{-1}son

la frecuencias detectadas para la estrella NW Ser y 1.617, 2.783, 2.557 y 1.269 c d^{-1}para la estrella V1446 Aql.

A.3.2 Modelización de las pulsaciones

Con el fin de determinar si las frecuencias detectadas se predicen inestables, hemos realizado un estudio teórico preliminar. Los parámetros físicos de las estrellas han sido obtenidos del análisis de espectroscopía de alta resolución, teniendo en cuenta los efectos del "gravity darkening" y asumiendo una velocidad de rotación del 88% de su velocidad de rotura. Los tracks evolutivos se han calculado con CESAM, teniendo en cuenta los efectos de rotación.

Para el análisis de inestabilidad hemos utilizado el código GraCo, que está basado en las ecuaciones no adiabáticas de Unno y colaboradores (1989). Desafortunadamente, este código no tiene en cuenta los efectos de alta rotación requeridas para la mejor caracterización de estas estrellas. Hay que resaltar que la teoría perturbativa es válida solo para frecuencias de rotación mucho menor que las frecuencias de pulsación. En nuestro caso, la frecuencia de rotación es incluso más grande que las frecuencias de pulsación y por tanto se necesita una teoría no perturbativa.

Los modos inestables que el código predice en las dos estrellas son los modos g con $\ell = 2 - 3$. En el caso de NW Ser, los rangos de inestabilidad de β Cephei y SPB están muy cerca, sugiriendo que esta estrella es un pulsador híbrido. Este resultado es consistente con el hecho de que la posición de esta estrella en el diagrama HR cae en la región donde las dos inestabilidades se superponen. En el caso de la V1446 Aql, solo modos g con $\ell = 2 - 3$ se predicen teóricamente.

Además hemos empleado el método de identificación de modos fotométrico descrito en Garrido (2000), con el fin de determinar el grado ℓ de los modos de pulsación de las estrellas a partir de las observaciones. Calculamos las proporciones entre amplitudes para cada frecuencia y los comparamos con los que predicen los modelos teóricos para diferentes grados ℓ. En el caso de NW Ser, modos de pulsación con grado $\ell = 3$ son los más probables para las frecuencias 1.126 y 1.412 c d^{-1}, mientras que los grados $\ell = 1$ o 2 son los más probables para las frecuencias 1.197 y 3.304

c d^{-1}. En el caso de la V1446 Aql, todos los modos detectados parecen tener asociados dipolos y cuadrupolos.

Para confirmar estos resultados necesitamos observaciones espectroscópicas que puedan realizar una identificación de modos para objetos tan rápidos como estos.

Estos resultados, junto con la multiperiodicidad de dos estrellas Be observadas recientemente por el satélite MOST (Walker y colaboradores 2005a, b), apuntan hacia la interpretación de la variabilidad de corto período de las estrellas Be en términos de pulsaciones no radiales.

A.4 Estudio espectroscópico de la estrella NW Ser

En esta sección presentamos el estudio espectroscópico que hemos realizado en la estrella NW Ser. Como hemos comentado anteriormente, para la identificación de modos en una estrella con una velocidad de rotación tan alta como ésta es necesario un estudio espectroscópico en profundidad.

Las observaciones fueron realizadas en el año 2004 en el Observatoire de Haute Provence (OHP) en Francia y en el año 2005 en el David Dunlap Observatory (DDO) en Toronto. Un total de 26 y 64 espectros fueron obtenidos respectivamente, con una resolución de entre 10 000 y 20 000, y una señal-ruido de entre 100 y 500. Espectros adicionales fueron obtenidos por C. Buil para estudiar las variaciones de las líneas Hα y He I 6678. Por último, hemos analizado un espectro Échelle obtenido en el OHP con el espectrógrafo ELODIE.

La reducción ha sido realizada con el paquete de programas IRAF, usando las técnicas estándar para CCDs.

Para la determinación de los parámetros físicos de la estrella, teniendo en cuenta los efectos inducidos por la alta velocidad de rotación, hemos adoptado un método similar al descrito por Frémat y colaboradores (2006), pero esta vez, ha sido aplicado a espectros con mejor señal-ruido y promediados con las observaciones de 15 días obtenidas en el año 2005. El proceso se basa en el ajuste de los perfiles de línea del Hidrógeno y Helio con espectros teóricos obtenidos con el código FASTROT (Frémat y colaboradores 2005) y asumiendo diferentes valores de Ω/Ω_c. En la pág. 91 se muestra la lista de parámetros con el que se obtiene el mejor ajuste.

Hemos realizado un estudio de la variación de largo período en las líneas Hα y He I 6678 con el fin de estudiar el comportamiento del disco circunestelar. En 1999 no se observa emisión en la línea de Hα. Sin embargo, en 2001, 2002 y 2003 la línea Hα muestra emisión en las alas y una absorción ancha en el centro. Suponiendo que el disco circunestelar se mueve con velocidad kepleriana, entonces podemos estimar el radio donde la línea de emisión se forma a partir de la distancia entre los picos de emisión. Por tanto, vemos que en el año 2002 el radio donde se forma la

emisión está muy cerca del radio de la estrella y esto sugiere que justo antes de las observaciones probablemente hubo una eyección de materia. Además, el espectro de ese mismo año muestra una absorción más profunda, sugiriendo que la materia del disco ha aumentado. En 2003, la anchura equivalente de la emisión en la línea Hα es menor, lo que implicaría que la estrella está perdiendo el disco. En esta misma dirección observamos que la separación de los picos de emisión se hace más pequeña y por tanto el disco se está separando de la estrella. En 2004 la línea no muestra emisión alguna. No se detecta emisión en la línea He I 6678, aunque en 2002 se observa un aumento de la absorción, como ocurría en Hα, probablemente debido a la eyección de materia de la estrella al disco.

Además hemos investigado las variaciones de corto período en los perfiles de linea y en los parámetros espectrales (velocidad radial del centroide de la línea -*RV*-, la profundidad central -*CD*-, la velocidad de rotación observada -$V \sin i$- y la anchura a la media altura -*FWHM*-) Las líneas He I 4387, He I 4471, Mg II 4481 y Si III 4553 han sido observadas durante los dos años, mientras que la línea Hγ ha sido observada solo en el año 2005. Para el análisis de series temporales hemos empleado la transformada de Fourier + Clean y el ajuste de mínimos cuadrados aplicados a cada bin del perfil de línea.

Hemos detectado una frecuencia dominante en $f_1 = 1.35$ c d^{-1}tanto en el año 2004 como en el 2005. La potencia es mayor en las alas que en el centro, sugiriendo un modo de pulsación asociado de gravitación (modos g). Hemos detectado su primer harmónico ($2f_1 = 2.68$ c d^{-1}) en los dos años, aunque con mucha menos potencia. A partir de la pendiente de la velocidad de fase de la frecuencia y de su harmónico hemos podido realizar una identificación de modos preliminar, basándonos en las relaciones obtenidas por Telting y Schrijvers en 1997. En el caso de la frecuencia $f_1 = 1.35$ c d^{-1}, el análisis de todas las líneas dan como resultado un modo de pulsación de grado $\ell = 2 \pm 1$ y orden acimutal de $m = 1 \pm 2$. Otro procedimiento para hallar los parámetros de los modos de pulsación es el llamado Fourier Doppler Imaging. Este método estudia los cambios Doppler producidos por las perturbaciones de temperatura o de las velocidades de pulsación que son proyectados en diferentes longitudes de onda debido a la alta velocidad de rotación. Obtenemos un grado

$\ell \sim 2-3$ y un orden acimutal $m \sim 3$ para la frecuencia dominante. Para comprobar estos resultados, hemos generado una serie de modelos, calculando las variaciones del perfil de línea teóricos a partir de los parámetros físicos de la estrella. Mediante una comparación visual de los diagramas en gris de las variaciones observadas y las teóricas observamos que los modos de pulsación más probables asociados a la frecuencia dominante tienen parámetros $\ell \sim 2$ y $m = -1, -2, -3$.

Otra frecuencia $f_2 = 1.12$ c d^{-1}ha sido detectada en las variaciones del perfil de línea en las observaciones del 2005. Esta frecuencia representa un caso más complicado ya que la velocidad de fase no es muy convincente en la parte roja del espectro. Además, el análisis de los parámetros espectrales da como resultado frecuencias de largo período que corresponden con el alias de un día de la frecuencia f_2. Por otra parte, las variaciones de los parámetros espectrales no pueden ser descritos por una sola frecuencia, sugiriendo la presencia de múltiples períodos en la estrella. Más observaciones espectroscópicas son necesarias para confirmar f_2.

A.5 Búsqueda de estrellas Be en los campos de exoplanetas de COROT

Además de la observación de las estrellas Be brillantes en los campos de asterosismología por COROT, estamos interesados en la observación de estrellas débiles en los campos de exoplanetas. Nuestro objetivo es obtener series temporales fotométricas para poderlas estudiar con fines sismológicos. Este proyecto formará parte del Programa Adicional de COROT y ya ha sido aprobado por el comité científico de COROT.

Nuestra primera tarea es la detección de estrellas Be débiles en los campos de exoplanetas para los dos primeros apuntados ya seleccionados. En esta sección explicamos la técnica fotométrica que hemos desarrollado para detectar estrellas Be, describimos las observaciones realizadas con este propósito, y presentamos un lista de estrellas Be débiles en los campos de exoplanetas para los dos primeros apuntados ya seleccionados.

La detección de estrellas de emisión mediante CCD se basa en la observación a través de un filtro centrado en la línea Hα y en un filtro más ancho que contenga la misma línea. Comparando el color producido por la diferencia de estos dos con un índice de color que mida el continuo de Paschen podemos identificar las estrellas con emisión. Para seleccionar solo las estrellas de tipo B utilizamos el sistema fotométrico de filtros estrechos de Strömgren, ya que con ellos podemos distinguir entre una estrella azul enrojecida y una estrella intrínsecamente roja

A.5.1 Observaciones y reducción de datos

Las observaciones fueron realizadas en la Palma con la Cámara de Gran Campo (WFC) en el telescopio Isaac Newton (INT). Las estrellas de los campos de exoplanetas de los primeros dos apuntados largos fueron observados durante Agosto y Diciembre del 2005.

Hemos desarrollado un procedimiento de reducción de imágenes que nos permite obtener resultados fotométricos de una forma rápida y casi automática. En primer lugar se obtiene la fotometría de cada estrella con un ajuste de PSF con el programa DoPHOT. Al observar que la identi-

ficación de estrellas con este programa no era satisfactoria, pensamos en utilizar otro programa que diese mejores resultados. Así pues, el programa SExtractor identifica todas las estrellas de la imagen y las proporciona al programa DoPHOT para que halle las magnitudes. Por último, los programas de utilidades wcstools determinan las coordenadas ecuatoriales para cada estrella en las imágenes.

Para la determinación de la extinción atmosférica se observaron varios campos estándar entre dos y cinco veces a diferente masa de aire. Además hemos calculado las transformaciones al sistema estandar de Strömgren, obteniendo errores razonables de pocas centésimas (ver pág. 134).

A.5.2 Discusión

Hemos encontrado 43 estrellas Be en los dos primeros campos de exoplanetas que serán observados con COROT, 29 cerca de HD 49933 + HD 49434 y 14 cerca de HD 180642 + HD 181555 (Tabla 5.4 en la pág. 139). Se ha realizado una estimación de los tipos espectrales de cada estrella Be gracias a la observación con filtros Strömgren. Todas estas estrellas han sido propuestas para ser observadas por COROT, en el marco del Programa Adicional.

Además planeamos continuar con las observaciones para detectar estrellas Be débiles en los campos aún por decidir de COROT. El procedimiento desarrollado en esta sección nos permitirá obtener resultados de buena precisión de forma casi automática.

A.6 Estrellas Be multiperiódicas en la Nube Pequeña de Magallanes

El objetivo de esta sección es comprobar las técnicas de búsqueda de periodos en datos similares a los que COROT obtendrá. Con este fin, vamos a analizar las series temporales de MACHO (Alcock y colaboradores 1999). Aunque la precisión con estos datos es mucho menor que la esperada para los datos obtenidos por el satélite COROT, la duración de las curvas de luz de MACHO es suficiente para poder resolver frecuencias muy cercanas que produzcan fenómenos de interferencia ("beating").

Además, el análisis de las estrellas en la Nube Pequeña de Magallanes (NPM) amplía nuestro estudio pulsacional a estrellas Be con poca metalicidad. Teóricamente, las inestabilidades pulsacionales de las estrellas β Cep, SPB y Be dependen dramáticamente de la abundancia de metales, ya que el mecanismo de excitación de las pulsaciones es generado como resultado de la gran cantidad de transiciones en los iones del hierro. Pamyatnykh (1999) demostró que las inestabilidades de las β Cephei prácticamente desaparecen para metalicidades de $Z = 0.01$. El estudio de las Nubes Pequeña y Grande de Magallanes es especialmente interesante ya que sus metalicidades son 0.004 y 0.008 respectivamente.

Una gran muestra de estrellas B y Be en las Nubes de Magallanes ha sido observada por Martayan (2005) con el espectrógrafo multi-objeto GIRAFFE en el telescopio ESO/VLT. Martayan y colaboradores (2006) presentaron un análisis preliminar de las curvas de MACHO de 13 estrellas Be en la NPM. Emplearon métodos como el PDM y FT + CLEAN para la búsqueda de periodos. En esta sección presentamos los resultados obtenidos al aplicar nuestras técnicas de búsqueda de determinación de períodos con el fin de compararlas con los métodos empleados por Martayan y colaboradores (2006) y eventualmente refinar su análisis y detectar nuevas frecuencias.

A.6.1 Discusión

Hemos detectado multiperiodicidad en 9 estrellas de la NPM. Trabajos realizados previamente en la búsqueda de múltiples periodos dieron resultados negativos (Balona 1992; Baade y colaboradores 2002). Balona concluyó que la variación de corto periodo de las estrellas Be de las NPM se producía por modulación rotacional, al no detectar multiperiodicidad en ninguna de las estrellas observadas.

La detección fotométrica de multiperiodicidad en nuestras estrellas demuestra claramente que son estrellas pulsantes. Los modelos teóricos actuales no predicen la presencia de modos inestables en estrellas masivas para metalicidades tan pequeñas. Sin embargo otros resultados observacionales van en el sentido contrario:

- Kolaczkowski y colaboradores (2004) detectaron varias estrellas β Cephei y SPB en la Nube Grande de Magallanes (NGM). Sin embargo, la metalicidad en la NGM es apenas menor que la metalicidad dada por Panyatnykh (1999) para la presencia de pulsaciones.

- Recientemente, con la ayuda de los proyectos fotométricos OGLE y MACHO, Fabrycky en 2005 y Schmidtke y colaboradores en 2004 detectaron múltiples periodos en binarias de rayos X (binarias Be/X) en la NPM. Sin embargo, las binarias Be/X son sistemas en los que la estrella primaria ha sido enriquecida químicamente por la transferencia de materia de su compañera. Por tanto, hasta que no se determinen las abundancias químicas de los sistemas binarios y se prueben que son similares a los de la NPM, estos resultados no constituyen una prueba en contra de los actuales modelos de pulsación.

- Nuestros resultados proporcionan una prueba mas contundente en contra de las predicciones de los modelos actuales. La metalicidad de la NPM ($Z = 0.004$) es significativamente menor que el límite de 0.01. Por otra parte, las estrellas que hemos estudiado no tienen ningún indicio de binariedad y en ningún caso se sospecha que su metalicidad debe ser significativamente diferente de la media de la NPM.

Por tanto, nuestros resultados apuntan hacia la necesidad de nuevos modelos o de una mejora en la determinación de la opacidades.

A.7 Conclusiones

El objetivo principal de nuestro proyecto es el estudio de las características pulsaciones de las estrellas Be usando datos de la misión espacial COROT. El trabajo presentado en esta tesis incluye la selección y el estudio de muestras de estrellas Be que han sido propuestas al comité científico de COROT. Las dos muestras que hemos elaborado han sido aceptadas y serán definitivamente observadas. Cinco estrellas han sido ya seleccionadas en los campos de asterosismología de los dos primeros apuntados. Por tanto se ha conseguido el primer objetivo satisfactoriamente.

A.7.1 Trabajos futuros

La primera estrella Be será observada en el comienzo del año 2007, y por tanto, la continuación de esta tesis es clara: empezar a analizar los datos de las estrellas Be observadas por COROT. Estos nuevos datos nos permitirán realizar un estudio en profundidad de las características pulsacionales de las estrellas Be y nos permitirá resolver interrogantes que han surgido en esta tesis con mucho más detalle.

Además, el seguimiento de varios temas presentados en esta tesis son los siguientes:

- Hemos realizado nuevas observaciones espectroscópicas de la estrella NW Ser en el verano del año 2006. El estudio de estos nuevos datos nos permitirán refinar la determinación de los modos de pulsación.
- Continuaremos nuestro programa de identificación de nuevas estrellas Be en los campos de exoplanetas en los sucesivos apuntados de COROT. Gracias a haber desarrollado una técnica automática para la reducción de los datos, podemos avanzar con esta tarea de una forma más rápida y eficiente.
- Nuestro grupo está implicado en el estudio de las estrellas B y Be con el satélite KEPLER. La misión KEPLER está dedicada a la detección de planetas terrestres mediante el método de los tránsitos

y además ofrecerá un programa adicional para obtener series temporales con propósitos científicos diferentes. Está previsto empezar observaciones fotométricas en el campo de KEPLER con el objetivo de identificar estrellas B y Be con las técnicas descritas anteriormente.

List of Figures

List of Tables